1-1-1984

Determination of the interdiffusion coefficient in the Fe-Ni and Fe-Ni-P systems below 900Â°C.

Douglas Clarke Dean

DETERMINATION OF THE INTERDIFFUSION COEFFICIENT IN THE Fe-Ni AND Fe-Ni-P SYSTEMS BELOW 900°C

by

Douglas Clarke Dean III

A Thesis

presented to the Graduate Committee

of Lehigh University

in candidacy for degree of

Master of Science

in

Metallurgy and Materials Engineering

Lehigh University

Bethlehem, PA

1984

This thesis is accepted and approved in partial fulfillment of the requirements for the degree of Master of Science.

15 October, 1984

Professor in Charge

Department Chairman

ACKNOWLEDGMENTS

Support from NSF Grant #EAR 821-2531 is acknowledged. The technical support of Drs. Goldstein, Narayan, Baumann and Michael along with will-be Drs. Merchant, Robino, Reuter and Vecchio is appreciated.

TABLE OF CONTENTS

LIST OF TABLES

LIST OF TABLES (cont'd.)

LIST OF FIGURES

LIST OF FIGURES (cont'd.)

LIST OF FIGURES (cont'd.)

LIST OF FIGURES (cont'd.)

ABSTRACT

The volume diffusivity of Ni between 925°C and 610°C in γ Fe-Ni and Fe-Ni-P alloys and between 855°C and 554°C in α Fe-Ni and Fe-Ni-P alloys was measured. An analytical electron microscope with a spatial resolution of 5nm was used to measure the chemical diffusion gradient perpendicular to the diffusion couple interface in a TEM thin foil. Typically this concentration gradient was measured over a 1 μm to 2 μm diffusion distance. This small diffusion zone permits short diffusion times and ensures that only effects of volume diffusion are measured.

An error in $\tilde{D}$ of ±15% results from the Boltzman Matano analysis for concentration gradients of 1 μm or more. In binary γ Fe-Ni, the $\tilde{D}$ values determined between 911°C and 610°C, follow the extrapolated curve of Goldstein et al. (1965) from above 1000°C. The $\tilde{D}$ values from ternary γ Fe-Ni-P couples with a nominal 0.2 wt% P show a progressive increase over the binary γ values. This increase goes from zero at 932°C to a factor of 10 at and below 650°C. This increase can be explained by the model of Helfmeier (1974).

In binary α Fe-Ni, the values of $\tilde{D}$ are discontinuous about the Curie temperature (770°C) where the structure changes from a paramagnetic state to a ferromagnetic state. In the paramagnetic state, the α binary value of $\tilde{D}$ at 853°C follows previous studies. However in the ferromagnetic state the $\tilde{D}$ values are up to a factor of 20 lower than previously determined by tracer diffusion. This discrepancy in binary ferromagnetic values between studies may be explained by a thermodynamic factor equal to 0.01 in Darken's equation.

In ternary α Fe-Ni-P, the values of $\tilde{D}$ are continuous about the Curie temperature. This suggests that the effect of P on the diffusivity of Ni in α Fe-Ni is not affected by the magnetic transformation. In the ferromagnetic state, the effect of P on the diffusivity of Ni is similar to the observed increase in $\tilde{D}$ with P content in γ Fe-Ni. This effect is again explained by the model of Helfmeier (1974).

INTRODUCTION

The Widmanstatten structure observed in iron meteorites is the result of a diffusion controlled phase transformation in the Fe-Ni-P system below 850°C. This geometric, two phase structure is comprised of ferrite, a Ni poor phase in a plate morphology with a specific crystallographic orientation relation to the parent austenite, the Ni rich phase (Goldstein and Axon, 1973).

The width of the ferrite plates can be used to delineate the cooling rate of a meteorite. Some controversy exists however in the literature over the value of these cooling rates (Wasson and Willis, 1978; Goldstein and Short, 1967; Narayan, 1984). Since Ni diffusion in the austenite determines the rate of the Widmanstatten transformation, this uncertainty in the value of the cooling rate is in part caused by the lack of accurate Ni volume diffusivity data below 850°C (Million et al., 1981).

The reason for this lack of data is two-fold: first, the diffusivity is extremely low in the system, necessitating up to 10^4 years for a single atom jump to occur at room temperature, and second, grain boundary diffusion is thought to predominate below 900°C (Goldstein et al., 1964).

The recent advent of analytical electron microscopy (AEM) offers the opportunity to overcome both of these problems by generating quantitative chemical analysis on a nanometric scale. Therefore, shorter diffusion times are possible and volume diffusion can be measured away from any grain boundary (Narayan and Goldstein, 1983).

The purpose of this study is to generate Ni volume diffusion coefficients with the aid of AEM in austenite and ferrite in the Fe-Ni and Fe-Ni-P systems for temperatures below 900°C.

BACKGROUND

BINARY DIFFUSION

Interdiffusion Coefficients

Fick's second fundamental law describes solid state diffusion (Shewmon, 1963) as

$$\frac{\partial C}{\partial t} = \frac{\partial}{\partial X} \tilde{D} \frac{\partial C}{\partial X} \qquad (1)$$

where

t = time for diffusion

C = concentration

X = distance

$\tilde{D}$ = interdiffusion coefficient

Boltzman, followed by Matano further developed Ficks second law to account for the variation of the diffusion parameter as a function of composition. The Boltzmann-Matano analysis as it is known defines

$$\tilde{D} = \frac{-1}{2t} \frac{\partial X}{\partial c} \int_{c=0}^{c=1} x \, dC \qquad (2)$$

where

C = composition

t = time for diffusion

x = diffusion distance from the Matano interface, with

$$\int_{c=0}^{c=1} x \, dC = 0 \quad \text{at the Matano interface}$$

The Matano interface is defined as the cross section through which there have been equal total fluxes of the two atomic forms A and B (Reed-Hill, 1973).

The parameter $\tilde{D}$ in Eqn. (2) is termed the interdiffusion coefficient and it represents the rate at which an element diffuses into a medium under specified temperature and pressure.

Tracer Diffusion

Radioactive tracers serve to study impurity or self diffusion in metals and alloys. The tracer diffusion coefficient, resulting from these studies, D*, can be related to the interdiffusion diffusion coefficient through Darken's equation (Darken, 1949):

$$\tilde{D} = F(D_A^* N_B + D_B^* N_A) \tag{3}$$

where F is the thermodynamic factor and is defined as

$$F = 1 + \frac{d \ln \gamma_A}{d \ln N_A} = 1 + \frac{d \ln \gamma_B}{d \ln N_B} \tag{4}$$

where γ_A, γ_B = the activity coefficients of A and B respectively.

N_A, N_B = mole fraction of A and B respectively.

The thermodynamic factor, F approaches 1 in an ideal solution and therefore,

$$\tilde{D} = D_A^* N_B + D_B^* N_A \qquad \text{for an ideal solution,} \qquad (5)$$

In the limiting case, $\tilde{D} = D_A^*$ in pure B. In other words, $\tilde{D}$ corresponds to the impurity diffusion coefficient of A in B.

Diffusivity as a Function of Temperature

Tracer and chemical diffusion coefficients D can be described as a function of temperature by the equation

$$D = D_o \exp(-Q/RT) \qquad (6)$$

where R is the universal gas constant, T the temperature (Kelvin), Q is the activation energy and D_o is the frequency factor. Q and D_o may vary with composition but are independent of temperature (Reed Hill, 1973). This equation is most often used to extrapolate the diffusion coefficient over a specified range of temperature, and composition.

Grain Boundary Diffusion

For grain boundary diffusion, the boundary is thought of as a thin layer of high diffusivity material sandwiched between large volumes of low diffusivity material (Fisher, 1950). The diffusion equations are altered to take into account the width of the grain boundary. Grain boundary diffusion is a two directional process with diffusion occurring down the boundary as well as perpendicular to the boundary into the matrix. The volume diffusivity is always lower than the grain boundary diffusivity.

TERNARY DIFFUSION

As seen above only one interdiffusion coefficient is necessary to characterize binary alloys. Ternary systems present a more complex problem than binary systems since four interdiffusion coefficients are necessary to completely describe their diffusion (Vignes and Sabatier, 1969).

In ternary systems (alloy A-B-C)

$$J_B = -D^A_{BB} \frac{\partial C_B}{\partial X} - D^A_{BC} \frac{\partial C_C}{\partial X} \tag{7}$$

$$J_C = -D^A_{CB} \frac{\partial C_B}{\partial X} - D^A_{CC} \frac{\partial C_C}{\partial X} \tag{8}$$

where element A is the solvent of the system. The value of D^A_{BC} is the diffusion coefficient of element B affected by element C in the solvent A. The coefficients D^A_{BB} and D^A_{CC} are termed major coefficients and D^A_{BC} and D^A_{CB} are termed minor or cross diffusion coefficients (Heyward, 1973).

In limiting cases where the cross diffusion term is negligible compared to the major coefficient term, $\tilde{D}$, the interdiffusion coefficient in a binary A-B alloy, is directly proportional to D^A_{BB}.

PREVIOUS WORK

The diffusion coefficients of Fe and Ni in the Fe-Ni and Fe-Ni-P systems have been determined previously at high temperatures between 1400°C and 1000°C, see Appendix 1 for references in γ.

Binary Diffusion in Austenite

One reason for the extensive work in the binary system is that Fe-Ni forms a continuous solid solution above 912°C (Million, et al., 1981). This indicates that it is potentially an ideal solution and that Darken's equation, Eq. (3), should be verified for the thermodynamic factor, F, approximately equal to 1.

Million (1981) did an extensive survey of the Fe-Ni diffusion literature in the γ field and found that Eq. (5) is verified at 1250°C. However below 1000°C the experimental values show considerable deviation from this equation (i.e., F deviates from unity), particularly at higher Ni content (Ni > 50 weight %) as seen in Fig. 1a. This trend can be inversely related to the phase diagram data where a minimum in the liquidus and solidus curves is observed at Ni_3Fe as shown in Fig. 1b.

The data for low nickel concentration between 5% Ni and 30% Ni however, shows little variation from an ideal solution at 1100°C and 1250°C (Fig. 1a). Therefore the Ni interdiffusion coefficient tends towards the Ni tracer diffusion coefficient at low Ni concentrations above 1100°C.

Table 1a through c lists the activation energy and frequency factor for the chemical and tracer diffusion coefficients in Fe-Ni for various Ni composition ranges. Recalling Eqn. 5, the interdiffusion coefficient $\tilde{D}$ in pure Fe is compatible with the Ni tracer diffusion coefficient D^* in pure Fe. Values of $\tilde{D}$ and D^* vs. temperature for each set of data in Table 1 are plotted in Figs. 2a through f. It is worth noting that even though the variation of the diffusion coefficient with Ni content is well documented, only Goldstein (1964) and Zemskiy's (1976) equations take this variation into account in their values of D_o and Q. As seen in Figs. 2a and b there is considerable spread in the extrapolated interdiffusion coefficients down to 600°C for 10% and 20% Ni alloys. A value for the diffusivity at 600°C can be chosen anywhere between 10^{-18} cm^2/sec and 10^{-16} cm^2/sec, or within a two orders of magnitude range. This large range is also observed in Fig. 2f where the extrapolated Ni tracer diffusivities are plotted along with the extrapolated interdiffusion coefficients for 10% Ni.

Binary Diffusion in Ferrite

The diffusivity of Ni in α Fe-Ni, has been measured by Borg and Lai, (1963) and Hirano et al. (1961) using tracer diffusion, D^*_{Ni} in αFe. Their results are summarized in Table 2 and Figure 3. Figure 3 also includes additional interdiffusion data from Goldstein et al. (1964). The values of D_o and Q are not given as a function of Ni content, for this variation is clearly negligible when considering the small compositional range of Ni within the ferrite phase field.

Figure 3 shows the extent of data correlation. Both investigations report an abrupt transition in the diffusivity at 770°C, the Curie temperature, where the ferritic Fe-Ni changes from the paramagnetic to the ferromagnetic state. Hirano et al. originally gave values for D_o and Q in the ferromagnetic state while Moren and Goldstein (1978) derived these values from Borg and Lai's data. Wasson and Willis (1978) used Hirano's values and Moren and Goldstein (1978, 1979) used Borg and Lai's values to estimate the cooling rates of iron meteorites in ferromagnetic ferrite. A substantial conflict also exists in the cooling rate determination from the two groups. More data below 700°C are needed to determine the correct α phase diffusivities.

Although values for the thermodynamic factor in Darken's Eq. (4) have not been worked out, by comparing Goldstein values of $\tilde{D}$ with Borg and Lai's values of D^*, it appears that $\tilde{D} = D^*$ in α. It is also important to note that the diffusion coefficient in α is always 1 to 2 orders of magnitude greater than in γ. This difference is explained by the open, bcc structure of α which forms less of a barrier to atom movement than the more densely packed, fcc structure of the γ phase.

Ternary Diffusion

Heyward and Goldstein's (1973) determination of the diffusivity of Ni in γ Fe-Ni-P between 1100°C to 900°C is the only known study in the literature. This following section reports their results.

Heyward and Goldstein found that the ratio of the cross diffusion coefficient and the major diffusion coefficient with

respect to Ni, $D^{Fe}_{NiP}/D^{Fe}_{NiNi}$, is less than 0.01 in α and less than 0.04 in γ. Therefore the interdiffusion coefficient $\tilde{D}$ can be directly related to the Ni major coefficient D^{Fe}_{NiNi}. This means that $\tilde{D}$ adequately describes the flux of Ni in Fe-Ni-P. The values of D^{Fe}_{NiNi} do however vary with Ni and P content.

The principal result of Heyward and Goldstein's study is that small additions of P ($\leq$0.25 wt % in austenite) increases the diffusivity of Ni in Fe-Ni-P alloys by an order of magnitude compared to the binary Fe-Ni at 900°C. This increase is consistent with the fact that P lowers the melting point of Fe-Ni α and γ in the ternary as well as the binary system.

Most recently, Helfmeier (1974) studied the influence of the solute As on the diffusion of Cu in Ni. Since As and P are in the same column in the periodic table, elements VI, P is expected to act similarly to As. Also Cu and Ni form fcc solid solutions similar to Fe and Ni. Therefore, a correlation between Helfmeier's study and the present study appears possible. Helfmeier observed an increase in Cu diffusivity with the addition of As. He explained the observed increase in Cu diffusivity by a positive bonding force between As and vacancies in the Ni matrix which causes an apparent decrease in the equilibrium number of vacancies. To compensate, additional vacancies are created in the Ni structure, thereby increasing the substitutional diffusion of Cu in the matrix. Possibly, a positive bonding force between P and vacancies in the Fe-Ni matrix causes the diffusivity of Ni to increase. We will be looking for such an effect in our experimental study.

It is interesting to compare the Ni diffusivity values to those obtained by Romig and Goldstein (1981) in Fe-Ni and Fe-Ni-P, α_2 martensitic alloys. In α_2 alloys, the increase in diffusivity due to P is small compared to the increase in ferrite and austenite.

Matsuyama et al. (1984) have also measured P tracer diffusion coefficients in ferritic Fe-Ni-P alloys between 825°C and 770°C. Heyward and Goldstein found that the ratio of the P cross diffusion coefficient to the Ni major coefficient D^{Fe}_{PNi}/D^{Fe}_{PP} is less than 0.03 in α and less than 0.05 in γ. Therefore the tracer diffusion coefficient of D^{*}_{P} in Fe of Matsuyama et al. can be compared to the major interdiffusion coefficient, D^{Fe}_{PP}, of Heyward and Goldstein. It is however important to note that Heyward and Goldstein measured D^{Fe}_{PP} between 1200°C and 900°C, so only a comparison between extrapolated diffusivity values from these two studies is possible. In Fig. 4, the values of Heyward and Goldstein and Matsuyama et al. are compared to the binary Fe-P tracer diffusion coefficients of Gruzin and Mural (1964) determined between 900°C and 800°C. The values of D_o and Q from each study are given in Table 3. Although the slope of these curves are different, the extrapolated values for the tracer diffusion and interdiffusion coefficients from each study are within a factor of 10 of each other. It is important to note that the diffusivity of P is an order of magnitude greater than the Ni diffusivity in α and two orders of magnitude greater than the Ni diffusivity in γ. Since the difference in P composition between end members in this study is small, no P diffusion gradient is expected at the bond interface of the ternary couples.

Grain Boundary Diffusion

Grain boundary diffusion is a problem in measuring volume diffusion in austenitic Fe-Ni below 1000°C (Goldstein et al., 1965) as seen in Fig. 2a. The results of four known studies of grain boundary and volume diffusion in Fe-Ni are summarized in Table 4. All four studies report values for D_{vol} and D_{GB} as a function of temperature. The grain boundary width has also been assumed to be $\delta = 5 \times 10^{-8}$ cm in all four studies.

At a given temperature the measured or effective diffusivity, D_{eff}, is the sum of the volume diffusivity and the grain boundary diffusivity. D_{eff} can be expressed by (Glitz et al., 1979)

$$D_{eff} = D_{vol} + D_{GB} \cdot N \cdot \delta \qquad (9)$$

where D_{vol} = volume diffusivity

D_{GB} = grain boundary diffusivity

N = number of grain boundaries per unit length (cm)

δ = width of grain boundary region

The deviation between D_{eff} and D_{vol} indicates the influence of grain boundary diffusivity at a given temperature. The greater the ratio D_{eff}/D_{vol}, the greater the effect of D_{GB} (since N and δ are constant in Eq. (9)). Only Hanatate et al. (1978) between 1287°C and 1153°C and Krishtal et al. (1967) between 1200°C and 1000°C reported average grain sizes. Therefore D_{eff} can only be calculated for the D_{vol} and D_{GB} values of Hanatate et al. and Krishtal et al. The average grain size was 10 mm in both studies, so N = 10 in both

cases. Hanatate et al.'s and Krishtal et al.'s extrapolations of D_{eff} and D_{vol} as a function of temperature, T, are given in Fig. 5a and Fig. 5b, respectively. These extrapolations show that D_{GB} has an effect on D_{eff} below 1100°C. This effect is verified in Fig. 6 where the ratio of D_{eff}/D_{vol} is plotted as a function of temperature. The influence of D_{GB} becomes marked only below 1000°C, where D_{eff} is approximately two times greater than D_{vol}. As seen in Fig. 6, the predicted overall effect of D_{GB} below 700°C according to Krishtal et al. is much less than that of Hanatate et al. Hanatate et al. (1978) explain the discrepancy between two D_{eff}/D_{vol} curves by the lack of accurate experimental procedures on the part of Krishtal et al. Therefore the temperature at which grain boundary diffusion becomes predominant in D_{eff} in Krishtal et al.'s study appears to be low.

In summary, grain boundary diffusion becomes the controlling mechanism for diffusion below 1000°C in austenitic Fe-Ni with an average grain size of 10 mm or less. Hanatate's results are consistent with Goldstein et al.'s measurements on the effect of grain boundary diffusion below 1000°C.

Meteorites

The meteoritic Widmanstatten structure formed by a nucleation and diffusion controlled growth process that is slow even on a geological time scale. Ferrite (kamacite) preferentially nucleates along the octahedral planes of the parent austenite (taenite) phase. The Widmanstatten pattern is developed when individual plates or bands of ferrite thicken by solid state diffusion and eventually touch one another (Buchwald, 1973).

If one measures a Ni concentration profile from one ferrite plate to another across the austenite matrix using electron probe microanalysis (EPMA), a surprisingly large Ni variation is observed (Goldstein and Axon, 1973), as seen in Fig. 7. The Ni concentration variation is related to the Fe-Ni phase diagram at low temperatures. This variation clearly indicates that meteoritic Widmanstatten pattern has not equilibrated even though it has cooled over a very long time period. The sharp Ni gradient at the α, γ interface in Fig. 7 is due to the slow diffusivity of Ni in austenite below 800°C.

An interesting aspect of this non-equilibrium structure is that a cooling rate can be associated with the Ni variation in γ. Using various approaches (Wasson and Willis, 1978; Moren and Goldstein, 1979), computer programs have been generated to estimate these cooling rates. The accuracy of each estimation however is totally dependent on the accuracy of the determination of the volume diffusion coefficient of Ni in Fe at compositions close to the two phase $\alpha + \gamma$ solvus lines below 800°C.

As noted earlier, in the single phase austenite region of binary Fe-Ni, the extrapolated values of $\tilde{D}$ from previous investigations fall within a range of two orders of magnitude at 600°C, as seen in Fig. 2f. Since the value for $\tilde{D}$ can be chosen anywhere within this range, a tremendous spread could exist in the cooling rate estimations. Obviously, the volume diffusion coefficient $\tilde{D}_{Ni}$ needs to be determined with greater accuracy in the γ phase at compositions close to the $\gamma/\alpha + \gamma$ phase boundary.

In binary ferrite, the values of $\tilde{D}$ are either extrapolated from Borg and Lai's (1963) or Hirano et al.'s (1961) tracer diffusion study. All these values however assume that $D^* = \tilde{D}_{Ni}$ or that the thermodynamic factor F is equal to unity in the ferromagnetic state. This fact however remains to be documented since only one data point of Goldstein et al. is available in the ferromagnetic state, as shown in Fig. 3.

Though iron meteorites are composed largely of Fe-Ni, they also possess an array of trace elements (Buchwald, 1973). One of these solute elements, phosphorous, at small concentrations ($< 1\%$) significantly increases the diffusivity of Ni in Fe-Ni (Heyward and Goldstein, 1973). Therefore, in order to obtain accurate diffusivity values for meteorites, the effect of P must also be taken into account. This study investigates the diffusivity of Ni in ternary Fe-Ni-P alloys at and below 700°C.

ANALYTICAL ELECTRON MICROSCOPY

Quantification

Quantification of x-ray results is accomplished through the use of the ratio method of Cliff and Lorimer (1974);

$$\frac{C_A}{C_B} = k_{AB} \frac{I_A}{I_B} \qquad (10)$$

where C_A and C_B are the weight % of elements A and B in the analysed volume, I_A and I_B are the characteristic x-ray intensities of the analyzed volume of A and B above background and k_{AB} is the

proportionality factor, or Cliff-Lorimer factor. This factor is independent of composition.

This study uses a k_{NiFe} factor of 1.21 ± 0.06 determined by Wood et al. (1982). Reuter et al. (1984) obtained a value for k_{NiFe} of 1.23 ± 0.04 using the same intrumentation as Wood et al. (1983) and this study. Reuter's k_{NiFe} value is within the experimental error of Wood's k_{NiFe} value.

The Cliff-Lorimer equation assumes that absorption and fluorescence corrections are negligible. These assumptions however must be verified for the Fe-Ni alloys used in this study.

Fluorescence Correction

The characteristic K_α peak of Fe is fluoresced by the K_α peak of Ni in Fe-Ni alloys. Williams (1984) calculated the intensity enhancement of the K_α Fe peak for a 100 nm thick specimen of composition 5 wt% Fe, 95 wt% Ni, using the following equation developed by Nockolds et al. (1980) for a binary A-B alloy

$$\frac{I_A^*}{I_A} = c_B \cdot \omega_B \cdot \frac{R_A - 1}{R_A} \cdot \frac{A_A}{A_B} \left(\frac{\mu}{\rho}\right)_A^B \cdot \frac{U_B \ln U_B}{U_A \ln U_A} \cdot \frac{\rho t}{2} \cdot \left(0.923 - \ln \left(\frac{\mu}{\rho}\right)_{SPEC}^B \rho t\right) \cdot \sec \alpha \qquad (11)$$

where I_A^* = intensity of x-rays from element A due to fluorescence

I_A = generated intensity not including fluorescence

R_A = absorption edge jump ratio

ω_B = fluorescence yield of element B

c_B = weight fraction of element B

$A_{A(B)}$ = atomic weight of element A (or B)

$\left(\mu/\rho\right)_A^B$ = mass absorption coefficient of B in A

$\mu/\rho\,{}^{B}_{SPEC}$ = mass absorption coefficient of B in specimen

$U_{A(B)}$ = overvoltage of A (or B)

α = tilt angle

ρ = density of sample

t = sample thickness

Williams' calculated intensity of the K_α Fe peak was found to be enhanced by 8.9% over the generated intensity, I_A.

Since this study used alloys with less than 30 wt% Ni, the enhancement of the intensity in the K_αFe peak was much less than the 8.9% calculated for the 100 nm thick sample. Although fluorescence increases with specimen thickness in Eqn. 11, the percent enhancement in intensity of the Fe K_α peak was less than 4% for all alloys in this study, even when considering the range of possible specimen thicknesses. Since the uncertainty in k_{NiFe} factor determination (±5%) is larger than the maximum fluorescence effect, the fluorescence correction is ignored in this study.

Absorption Correction

Table 5 and Fig. 8 were generated using the expression for the x-ray absorption correction given by Goldstein et al. (1977)

$$k^{*}_{AB} = (k_{AB}) \frac{(\mu/\rho)^{A}_{SPEC}}{(\mu/\rho)^{B}_{SPEC}} \cdot \frac{1-\exp-\{(\mu/\rho)^{B}_{SPEC} \operatorname{cosec} \alpha\ (\rho t)\}}{1-\exp-\{(\mu/\rho)^{A}_{SPEC} \operatorname{cosec} \alpha\ (\rho t)\}} \qquad (12)$$

where k^{*}_{AB} = absorption corrected value of k_{AB}

k_{AB} = absolute value of Cliff-Lorimer factor

$\mu/\rho \,{}^{A(B)}_{SPEC}$ = mass absorption coefficient for x-rays from elements A (or B) in the specimen

α = take off angle (20°)

ρ = density of specimen

t = foil thickness

The percent absorption correction is simply the ratio k^{*}_{AB}/k_{AB} (x 100).

The desired accuracy of the data in this study is ±5% given the error in k factor determination. As seen in Table 5, a 5% absorption correction in a 2% Ni-Fe alloy is necessary at a thickness of 142 nm. In a 27.5 wt% Ni alloy, this 5% correction becomes necessary at a thickness of 194 nm.

Optimum Beam Size

A focused beam on a thin foil generates x-rays from within the beam-specimen interaction region. Elastic and inelastic scattering of incident electrons in the sample cause this interaction volume to increase with increasing foil thickness (Williams, 1984) as seen in Fig. 9. Since point analyses at fixed intervals will be obtained in this study, it is important to determine the spatial resolution of each data point in order to avoid sampling the same region. The diameter of the x-ray generation volume or the spatial resolution of the probe according to Reed (1982) is $\sqrt{d^2 + b^2}$ where d = initial beam size and b = beam broadening within the sample. This beam broadening can be expressed by (Goldstein et al. 1977):

$$b = 625\ (\rho/A)^{1/2}\ (Z/E_o)\ t^{3/2} \qquad (13)$$

with t = specimen thickness

E_o = incident beam energy

and the sample composition parameters

ρ = density of the foil,

Z = atomic number and

A = the atomic weight.

Other formulations of b give similar results (Michael, 1984). It is important to know the value of b in determining the optimum beam size for a given spot analysis interval, in order to keep within the spatial resolution of the probe. Table 6 gives the beam broadening b and values of $(d^2 + b^2)^{\frac{1}{2}}$ as a function of thickness.

Beam Convolution

Beam spreading has a marked effect on the accuracy of concentration curves when the composition of the sample changes over a distance equivalent to the spatial resolution of the probe. The diffusion distance in 600°C binary austenite couples is expected to be less than 0.5 μm or 500 nm. Since the concentration gradient varies over 5 wt% Ni, on the average, a 1 wt% Ni variation will occur every 100 nm in the diffusion zone. Given a maximum total beam size $(d^2 + b^2)^{\frac{1}{2}}$ value of 50 nm from Table 6, the Ni composition variation within the spatial resolution of the probe may be significant. Therefore it may be necessary to use a beam convolution program to take into account the composition variation within the X-ray source size. Convolution programs have been developed for AEM concentration profiles by Doig and Flewitt (1980) and Michael (1984). Michael's program, modified for a concentration gradient, is used in this study.

Quantification Accuracy

The accuracy of AEM quantification is limited by the error in the experimental determination of k_{NiFe} and by the counting statistics in both the Fe K_α peak and the Ni K_α peak. As seen previously, the error in k_{NiFe} using Wood's value was ± 5%. The error in the peak intensities can be calculated using Romig and Goldstein's (1980) equation for the percent error evaluated at a 99% confidence level:

$$\% \text{ error} = \pm \frac{3\sqrt{N}}{N} \times 100 \qquad (14)$$

where N corresponds to the counts above background in a given characteristic x-ray peak. The percent error decreases with increasing counts, N. Therefore greater accuracy is achieved through longer count times and/or increased probe current. Since probe current is proportional to the probe size to the 8/3 power (Goldstein et al., 1981), larger probe sizes may be necessary to improve accuracy.

Unfortunately increasing the probe size decreases the spatial resolution of the microscope. Other factors must also be considered if prolonged count times are used. One of these is beam contamination on the specimen which increases in thickness over time and absorbs specific x-rays emitted from these specimens. More important is specimen drift in the microscope, which causes the chemical analyses to be taken over a line as opposed to a point (Williams, 1984). The optimum x-ray counting time is therefore a compromise between the spatial resolution of the probe and the

intensity obtained in the individual characteristic x-ray peaks.

A LaB_6 electron source has more probe current than a W filament as seen in Fig. 10 (Zaluzec, 1979). Enhanced peak intensities of Fe and Ni are therefore achieved in this study by using a LaB_6 electron source.

Another way of obtaining increased peak intensities for a given electron probe size is to use thicker samples. However both x-ray absorption and x-ray resolution will be compromised. For example the specimen thickness must be under 200 nm in the analyzed volume, in order to remain within a 5% absorption correction as seen in Table 5.

EXPERIMENTAL PROCEDURE

Choice of Diffusion Couples

The principle objective of this study is to measure the Ni interdiffusion coefficients, $\tilde{D}_{Ni}$, in the α and γ phases of the Fe-Ni and Fe-Ni-P systems below 900°C. In addition, in the γ phase the objective is to measure the diffusivities as close to the two phase $\alpha + \gamma$ boundary as possible. To obtain these $\alpha + \gamma$ interdiffusion coefficients, diffusion couples were prepared and heat treated at the desired temperatures for specific times in order to develop the necessary diffusion gradients. These gradients were measured across the bond interface using AEM.

As seen in Fig. 11, the Fe-Ni phase diagram (Romig and Goldstein, 1980) was used to help select the end member compositions of the binary diffusion couples. A 5% Ni variation between end members in the γ phase was chosen (see end member compositions A and B on Fig. 11). Since the two phase $\alpha + \gamma$ boundary varies with temperature, the composition of the γ phase diffusion couple was adjusted accordingly.

The choice of ternary diffusion couple compositions is inherently more complex. Figure 12 shows the general outline of the various fields for the Fe-Ni-P system with the nomenclature proposed by Moren and Goldstein (1978). The α, $\alpha + \gamma$ and γ fields are those given in the binary diagram. The α + Ph, $\alpha + \gamma$ + Ph and γ + Ph fields include the phosphide compound $(FeNi)_3P$. In the three letter codes used in the figure, the first letter A or G is for the alpha or gamma phase. The second letter U or L is for the upper and lower

point (P content), the lower point being on the Ni axis and the third letter N or P refers to Ni or P. Narayan (1983) using Romig and Goldstein's (1981) Fe-Ni-P phase diagram data below 700°C, developed a least squares polynomial fit for the eight variables needed to define the α, $\alpha+\gamma$ and γ phase regions. Figures 13a through 13e show the calculated ternary isotherms from 800°C to 600°C. The compositions for the ternary α and γ couples are also shown (a-b for α, c-d for γ). A 5% difference was preserved between all the γ end member compositions. A constant 0.2 wt% P was chosen for the Fe-Ni-P ternary alloys. Since the binary and ternary couples diffused at a given temperature had the same end member Ni content, a direct comparison between binary and ternary diffusion coefficients could be made.

Below 700°C in the phase, the 0.2 wt% P present in the ternary Fe-Ni-P alloys exceeds the solid solubility limit of P in γ. Therefore phosphides, termed Ph on the isotherms in Figs. 13d and e should be present in these γ diffusion couples.

Raw Materials

Pure iron and nickel rods (99.999+), five millimeters in diameter and one hundred and fifty millimeters long were purchased from Johnson Matthey Chemicals Limited. A manufacturers' analysis of these metals is given in Table 7. The phosphorus used in the ternary alloys came from two sources. First, a homogeneous iron-nickel phosphorus alloy rod of composition 10 wt% Ni, 0.92 wt% P, balance Fe was provided by R. Sellamuthu. This master alloy was used to make up all the ternary austenitic alloys. Second, 99.99%

pure iron phosphorus powder, mostly FeP but containing approximately 20% Fe_3P, was used to create an iron 1.0 wt% phosphorus master alloy. This master alloy was used to make up the Fe-0.2 wt% P alloy and other ternary ferritic alloys.

Melting

The pure and master alloy rods were sectioned on a diamond saw and ground to the required weight within a precision of ± 0.005 grams. The total weight of an alloy averaged 7 grams. All sections were ultrasonically cleaned in acetone and placed in alumina crucibles with the lowest melting point metal on top. The crucibles were then placed inside the high frequency (H.F.) furnace as shown in Fig. 14. A graphite susceptor acted as the heating element for the initial melt. From 3 minutes prior to start up and until the melt was quenched, this set up was continually flushed out with argon to prevent oxidation. A Lepel 30 kW induction furnace was used to melt the alloys. The crucible containing the sectioned metal was slowly heated up to the melting point of the samples to avoid it's cracking. The molten metal was held for two minutes for the purpose of mixing. After this, the sample crucible was slowly cooled through the mushy zone to prevent coring, followed by a fast water quench to form a single phase alloy.

The 28 gram Fe-1 wt% P master alloy was melted using the same procedure only in a larger set up. The FeP powder was added when the Fe rod was molten. To prevent excess P sublimation, the powder was wrapped in a pure Fe foil.

All the alloys were then surface ground to remove surface

oxides, cleaned, dried and remelted. Remelting was important because the graphite susceptor tended to hinder thorough mixing during the initial melt. The same procedures as in the initial melting were used, the only difference being the set up used in remelting. This set up is described in detail by A. Romig (1980) and seen in Fig. 15.

Homogenization

The alloys were again ground on a SiC belt to remove surface oxidation, loosely wrapped in tantalum foil and vacuum sealed down to a pressure of 50 millitorrs of Hg inside fused quartz tubing. The alloys were then homogenized in a Marshall horizontal tube furnace at 1100°C for 7 to 10 days. The Fe-Ni-P alloys were homogenized at 1000°C for 1 week. All samples were quenched by breaking the ampules in water. A section approximately 2 mm thick was cut off each alloy using a diamond saw, mounted in lucite, ground and polished through 1 μm diamond.

Homogeneity was checked using a JEOL 733 superprobe (EPMA). Pure iron and nickel standards were used. A section of the Lombard meteorite containing a $(FeNi)_3P$ phosphide of composition 15.5 wt% P was used as the P standard (Heyward, 1973). Twenty points within the range of 100±2 wt% (weight percent) were taken at random on the sample. The correction factors for atomic number, absorption and fluorescence were previously determined by Narayan (1984). An Apple computer program was used to determine each sample's range of homogeniety $\pm W_{1-\alpha}$ for a given confidence level $1-\alpha$. $W_{1-\alpha}$ is defined as (Goldstein, 1979):

$$W_{1-\alpha} = \pm C\left(\frac{t^{1-\alpha}_{n-1}}{\sqrt{n}}\right)\left(\frac{S_c}{N}\right) \qquad (15)$$

where C = true weight fraction of the element of interest

$t^{1-\alpha}_{n-1}$ = student t value for $1-\alpha$ confidence level

n = number of observations

S_c = standard deviation of the measured counts

N = mean of counts

If the absolute value of $W_{1-\alpha}$ falls between 0 and 1 then the sample is considered homogeneous. If the alloy was outside the range of homogeneity (i.e., $W_{1-\alpha} > 1$) or if the sample had excessive porosity, it was either remelted and rehomogenized or it was discarded. The analyses of the resulting alloys used in this study are given in Table 8.

Diffusion Couple Preparation

The object of diffusion couple preparation was to make the samples as flat as possible to ensure proper bonding. Homogeneous alloys of desired end member compositions were cut with a diamond saw into three mm wide samples. Samples constituting the end members of a diffusion couple were mounted together in a thin layer of lucite. They were ground flat and polished through 1 μm alumina on a wheel. The mount was then placed face down on a surface grinder with a 60 grit abrasive wheel. The back of the mount was ground down until the sample's back face was parallel to its front face. The samples were then broken out of the mount, cleaned in acetone and remounted. The front surface was ground on 320 grit

paper to remove any contamination due to the grinding wheel's lubricant. The samples were polished through 1 μm diamond on a glass plate. Once again they were broken out of the mount, cleaned in acetone and carefully checked for any traces of lucite which could contaminate the bond interface with carbon. Each sample was individually repolished with 1 μm diamond on a glass plate before ultrasonic cleaning in ethanol for 10 minutes. The samples were then squirted with methanol to prevent staining and dried with a hand dryer. After a quick blast with freon to remove any surface dust, two samples were immediately bonded together in a stainless steel picture frame clamp, a schematic of which is shown in Fig. 16. The pressure applied by the screw in the stainless steel picture frame was sufficient to depress surface asperities thereby increasing the quality of the bond (Garmong et al., 1975). Also, the clamps ensured a small compressive force at the diffusion temperature because the stainless steel's coefficient of expansion is lower than that of the Fe-Ni alloys. Careful specimen preparation along with applying proper pressure with the clamp resulted in a successful bond 90% of the time.

Heat Treatment

The diffusion couples inside their picture frame were individually vacuum sealed in fused quartz tubing. Tantalum strips acting as oxygen getters were also included. The ampules were then placed inside small Marshall tube furnaces equipped with self-tuning, current-adjustable-type Leeds & Northrup controllers and

power packs. The uniform hot zone was 4 cm long at 700°C. An external platinum-10% platinum rhodium thermocouple resting on the sealed quartz tube right above the diffusion couple continually monitored the diffusion temperature. The temperature variation was at most ± 3°C. If the diffusion time was longer than one week, the samples were diffused at temperature for 24 hours, quenched and removed from the clamp. Two couples diffused at the same temperature for the same period of time, were then vacuum sealed together along with tantalum strips inside fused quartz, reinserted in the diffusion furnace and allowed to diffuse for the appropriate amount of time. The diffusion times and temperatures for all couples are given in Table 9. The four couples diffused by Narayan (1984) are also included in Table 9. Once the heat treatment was over, the specimens were quenched by breaking the quartz tubes in water. The couples diffused for less than a week were released from their diffusion clamps at this point. Upon releasing the couples, the strength of the diffusion bond was tested by hand prying. If the couple did not break apart, the bond was considered good.

Transmission Electron Microscopy (TEM)

A side of the couple perpendicular to the interface was filed flat and glued on an aluminum stub using one part graphite for conductivity mixed with one part Duco cement. After two hours drying time, the sample was electro-spark-discharge machined with the interface parallel to the brass electrode. A schematic of the TEM preparation technique is given in Fig. 17.

The resulting 3 mm diameter cylinder was carefully checked for

any discontinuities at the interface's surface. If any were found, the discontinuities were hand filed. The cylinder was then glued to a metal support, in this case a steel charpy bar, and disks up to 2 mm thick were sawed off using a diamond blade as seen in Fig. 17. Experience proved that these precautions were necessary for stresses due to the diamond wheel were sufficient to cause the bond interface to tear apart. This was particularly true if a) too thin a slice was taken, b) no support was given to the cylinder or c) if cracks, or discontinuities, acting as stress concentrators, were present at the interface.

The 3 mm disks were ground down to a thickness of about 80 μm on 600 grit paper, using ethanol as the wetting agent. After proper cleaning and drying, the specimens were electro-jet polished with the Struers Tenupol instrument (105 volts using the bath of 2 percent perchloric acid in ethanol, cooled to under -20°C). In nearly all cases, the thin area did not end up at the bond interface. The sample was subsequently ion milled in a Commonwealth or a Gatan ion beam thinner until the thin area was present at the interface. The thinning rate was optimal when the ion thinners were run at 6 kv with a current of 2 mA. in a 2×10^{-4} Torr vacuum or better.

Analytical Electron Microscopy (AEM)

All analytical electron microscopy (AEM) work was conducted on a Philips 400T transmission electron microscope (TEM) equipped with an EDAX x-ray detector and a Tracor Northern 2000 X-ray analyzer. Beam alignment, magnetic correction and specimen height adjustments

were made in the TEM mode. Then using selective area diffraction patterns, the sample was checked for possible oxidation. If contamination was present, the sample was "dusted off" in the ion beam thinner for 30 minutes.

After the TEM adjustments, the instrument was switched over to scanning transmission electron microscope (STEM) mode. The STEM silicon backscatter detector was used to image the sample. Although secondary electron and backscatter imaging of the interface were tried, the only proven way to locate the interface was by collecting x-ray spectra in the Energy Dispersive Spectrometer (EDS) to quantify the end member compositions. Once an appropriate magnification, which encompassed both end member compositions on the STEM screen was chosen, a STEM microanalysis trace was taken as seen in Fig. 18. The step size across the diffusion gradient varied from 4×10^{-5} cm (400 nm) to 5×10^{-6} cm (50 nm). The sample was adjusted for specimen drift whenever necessary. Three to four traces at different locations in the thin area were taken across the interface on each sample. Figure 19 shows four composition traces taken across a F20N-F25N binary couple diffused at 650°C for 121 days.

RESULTS

For each couple a Matano analysis of the best fit concentration gradient profile was conducted using well established procedures (Reed-Hill, 1973). $\tilde{D}$ was evaluated (Eq. (2)) at the Matano interface which corresponds to approximately the midpoint composition in each diffusion couple. The values of $\tilde{D}$ as a function of temperature are given in Tables 10a) and b).

Examples of composition versus distance profiles for the ternary austenite couple F25NP-F30NP diffused at 650°C, the binary austenite couple F5N-F10N diffused at 911°C and the binary ferrite couple F-F2N diffused at 654°C are shown in Figs. 19 through 21. In addition, a comparison of composition versus diffusion distance profiles for a ternary austenite couple, F25NP-F30NP, and a binary austenite couple, F25N-F30N, diffused in the same furnace at 610°C for 62 days is shown in Fig. 22.

DISCUSSION

AEM PARAMETERS

Although AEM traces were taken over a small distance ($\leq$ 3 μm), the foil thickness was not constant. The bond interface was in fact preferentially thinned during electrojet polishing. The end member regions were consequently thicker than the diffusion zone where concentration profiles were measured. Contamination spot measurements (Lorimer et al., 1976) in these end member regions of a concentration profile were used to calculate the maximum sample thickness. The end member regions were thinner than 150 nm.

Absorption Correction

Since 150 nm was the maximum specimen thickness in analyzed areas of the sample, the calculated absorption correction, using Eq. (12), was always less than 5% (Table 5). This absorption correction is smaller than the error in Wood's k_{NiFe} factor determination. Therefore, no absorption correction was applied in this study.

Optimum Beam Size

Beam broadening, using Eq. (11), was calculated previously as a function of specimen thickness and was reported in Table 6. The effect of Ni variation on beam broadening (Table 6) is negligible since Fe and Ni are neighboring elements in the periodic table of elements. Also, P had no effect on beam broadening since the P content was less than 0.3 wt% in the alloys. A probe size of 20 nm was used in this study to optimize x-ray intensities in the analyzed volume. Spot analyses were taken as close as 50 nm apart in γ couples diffused at 650°C and 610°C as well as in the α couple

diffused at 550°C. Referring to Table 6, beam overlapping would occur in these couples in thicknesses greater than 200 nm. Since thickness measurements were less than 150 nm, beam overlapping did not occur in the samples analyzed in this study.

Beam Convolution

The lack of agreement between a calculated diffusion profile and a measured profile using AEM may be due to beam broadening. Beam broadening has the greatest effect on the diffusivity values in samples with the smallest diffusion distance because the composition changes significantly over distances smaller than the probe size. The worst case of a short profile is in the F25N-F30N couple diffused at 610°C (Fig. 22). Michael's (1984) beam convolution program was used to evaluate the effect of beam broadening on the concentration gradient during AEM. A simulated F25N-F30N couple was used as an example in Michael's program.

The electron probe is described as a Gaussian that broadens as it traverses the specimen. The probe is assumed to remain Gaussian. In order to maintain a constant number of electrons in the foil, this Gaussian shape must broaden with thickness.

The intensity distribution in the electron probe is expressed as:

$$I(x,y,t) = \frac{I_e}{\pi(2\sigma^2 + \beta t^3)} \exp\left(\frac{-(x^2 + y^2)}{2\sigma^2 + \beta t^3}\right) \qquad (16)$$

where t = thickness

I_e = total electron flux

σ = description of probe size

x,y = distances normal to the beam in the foil

β = scattering parameter

According to Michael, the value of σ is equal to the beam diameter of the Gaussian at full width half maximum (FWHM) divided by 2.35. Michael (1984) found that equations for β in the literature were all similar. His program uses Reed's (1982) equation for β since it is the most conservative estimate

$$\beta = 9.8 \times 10^{10} \left(\frac{Z}{E}\right)^2 \rho/A \qquad (17)$$

The convolution of the beam intensity distribution and the concentration distribution in the specimen is

$$\int_0^t \left(\int_{-y}^{y} \left(\int_{-x}^{x} I(x,y,t)\, C(x)\, dx \right) dy \right) dt \qquad (18)$$

where $I(x,y,t)$ = the beam intensity at position x,y and t

$c(x)$ = the Grube solution to the concentration profile, where

$$C(x) = \frac{C(1)+C(0)}{2} + \frac{(C(1)-C(0))}{2} \operatorname{erf}\left(\frac{X}{2\sqrt{DT}}\right) \qquad (19)$$

C(1) and C(0) = the end member compositions. In this example of diffusion couple F25N-F30N,

C(0) = 25 wt% Ni and

C(1) = 30 wt% Ni

X = diffusion distance

$\tilde{D}$ = interdiffusion coefficient, in this case $\tilde{D} = 4.10^{-18}$ cm^2/sec for couple F25N-F30N

T = time, in this case T = 5.6×10^6 sec.

A beam size of $(d^2 + b^2)^{\frac{1}{2}}$ from Reed (1980) was evaluated through the thickness of the sample to duplicate the actual beam broadening in the sample. An initial probe size of d = 10 nm was used in the program. This value of d corresponds to the probe size used in the actual F25N-F30N couple analysis. A specimen thickness of 150 nm was chosen to provide a conservative estimate of the effect of spatial resolution. This value overestimated the thickness of the sample where the actual concentration profiles were generated. The calculated Grube solution for various assumed diffusivities is shown in Fig. 23. The effect of beam convolution is shown in Fig. 24. Beam broadening of over 10% of the total concentration profile has a surprisingly small effect on the experimental concentration profile. Only in the vicinity of the end member compositions where a more rapid change of slope is observed, is the beam broadening important (Fig. 24). This effect necessitates further explanation.

The deconvoluted profile is the average of the composition variation along the calculated Grube solution. This average composition remains unchanged in the constant slope portion of the concentration gradient. Therefore, beam broadening only has an effect in the vicinity of the end members where a less rapid change of slope is observed. The spatial resolution of 32 nm in Fig. 24 represents the beam size at the thickest part of the sample. The majority of the intensity distribution however is generated in the upper half of the sample where the spatial resolution is better than 19 nm, according to Eq. 13. Therefore the 32 nm beam size shown in

Fig. 24 is an overestimation of the spatial resolution achieved during analysis in the sample.

Michael's (1984) program was also used to convolute a more representative diffusion gradient obtained in this study than F25N-F30N. The ternary F25NP-F30NP couple diffused at 610°C for 2 months was used as an example. This couple's 1 μm diffusion distance was similar to that of other couples in this study (see Figs. 19 through 21). The program used the same input parameters as described above for the deconvolution of the F25N-F30N couple. For F25NP-F30NP, the couple's end member compositions were 25 wt% Ni and 30 wt% Ni and $\tilde{D} = 4 \times 10^{-17}$ cm^2/sec. The calculated Grube solution along with the convoluted profile are shown in Fig. 25. The effect of deconvolution resulted in less than a ±6% error in the $\tilde{D}$ value. Since a given error of ±10% exists from the uncertainties in the determination of $\tilde{D}$ using the Matano analysis, the effect of deconvolution on D can be ignored.

Counting Statistics

Count times were limited to between 90 and 120 seconds due to specimen drift in the microscope. The specimen location with respect to a reference marker on the STEM screen was checked after every point analysis. If the specimen had visibly drifted during the analysis, it was readjusted with respect to the reference marker.

The number of x-ray counts in the characteristic K_α x-ray peaks of Ni and Fe for a 90 to 120 seconds counting time varied with sample composition and thickness. In the F10N-F15N couple diffused

at 700°C, approximately 10,000 counts in the Ni K_α peak and 90,000 counts in the Fe K_α peak were measured at each analysis point in the 10 wt% end member. A calculated error of ±4% using Romig and Goldstein's Eq. (12) for a 99% confidence level is calculated for each point. The error per point for all the samples analyzed in this study varied from 2% to 7%. These counting rate errors when added to the ±5% variation in k_{NiFe} given by Wood et al. (1984), resulted in an overall error per point of ±7% to ±12%.

The Ni variation across a typical diffusion gradient was 5 wt% (Table 9). Therefore the error per analysis point spanned up to one third of the total Ni concentration gradient. This large error per point is illustrated in Figure 19 for couple, F20NP-F25NP, diffused at 650°C. Based on an average error per point of ±7%, the error bars span 1.5 wt% Ni.

Fortunately, the error analysis using Romig and Goldstein's approach overestimates the innaccuracies in our present data. First, at least 3 traces were taken at different locations along the interface; therefore 3 times the amount of counts in each individual point was accumulated along the diffusion gradient. Data from multiple traces reduces the counting statistics error by approximately 50%. Second, only relative Ni variation between two well characterized, homogeneous end-members (Table 8) was measured. Any error in the k_{NiFe} determination can be ignored since an internal calibration standard is present. This causes the overall error in the concentration gradient to be reduced to between ±2% and ±6%. The error in Fig. 19 for example is reduced from ±7% per point

to a ±2% error in the best fit profile for the F20NP-F25NP couple. Using the limits of the ±2% error in the best fit profile, the shortest and longest diffusion gradients for F20NP-F25NP were determined. Matano analyses of these gradients revealed that their resulting values of $\tilde{D}$ were within 20% of one another. Therefore the error in $\tilde{D}$ resulting from a ±2% error in the best fit concentration profile through the diffusion gradient is ±10%.

It is important to note that only a 0.4 μm diffusion zone was measured for the F25N-F30N couple diffused at 610°C for 2 months. This diffusion zone was less than half the diffusion length of the other couples. This small diffusion zone in the F25N-F30N couple resulted in a poor best fit profile since relatively little composition data could be generated in the steep concentration gradient, note Fig. 23. A Matano analysis of this couple was not warranted due to the inaccuracy in the best fit profile. In order to measure the interdiffusion coefficient of F25N-F30N, Grube solutions were calculated using Eqn. (19) for the shortest and the longest possible diffusion zones. The Grube solutions estimated $\tilde{D} \simeq 6 \times 10^{-18} cm^2/sec$ for the longest diffusion zone and $\tilde{D} \simeq 2 \times 10^{-18} cm^2/sec$ for the shortest diffusion zone. These two values represent the limits of the possible $\tilde{D}$ values for F25N-F30N as seen in Fig. 23. The error in D from this couple was ±50 to 100%.

The minimum mass fraction (MMF) of an element A that can be detected (Joy and Maher, 1977), can be expressed by:

$$MMF = C_A (3)\sqrt{2I_b^A} / [I_A - I_b^A] \qquad (20)$$

where C_A = known concentration of element A; in this study the wt% P $\simeq$ 0.2.

I_b^A = total number of counts from the background continuum of element A; in this study $I_b^A \simeq 100$.

I_A = total number of x-ray counts from element A; in this study $I_A \simeq 200$.

The MMF value of P in α or γ Fe-Ni was 0.08 wt% in this study. Since P contents were greater than 0.10 wt% in the diffusion couple end members (Table 8), the P K_α peak was detected during AEM analysis in all the ternary couples studied. However, since the counting statistics error resulting from a poor peak to background ratio accounted for an error of ±0.08 wt%, a quantitative study of the P concentration gradients could not be made.

MEASUREMENTS OF $\tilde{D}$

Errors in the measurements of the interdiffusion coefficients were discussed in the previous section. The best fit profile due to counting statistics of ±2% typically resulted in an error of ±10% for the $\tilde{D}$ values evaluated by Matano analyses. The use of the Boltzmann-Matano analysis itself results in a ±10% error in $\tilde{D}$ due to inaccuracies in the measurement of the slope of the concentration gradient at the Matano interface and the determination of the exact area under the concentration gradient. In addition, a typical error of ±6% in $\tilde{D}$, due to beam spreading was measured.

The total error in $\tilde{D}$ is given by the expression

$$\text{Error in } \tilde{D} = (E_S^2 + E_M^2 + E_C^2)^{\frac{1}{2}} \qquad (21)$$

where

E_S = error in counting statistics

E_M = error in Matano analysis

E_C = error due to beam convolution

Using typical values of 10% for E_S, 10% for E_M and 6% for E_C, the average error in $\tilde{D}$ values (Table 10) is estimated at 15%. It is important to point out that the error in 610°C binary austenite couple F25N-F30N determined by Grube solution was ±100%. Therefore the total error in $\tilde{D}$ evaluated using Eqn. 21 is ±101%.

Binary Couples in Austenite

In binary γ , Fig. 26, the experimental values of the interdiffusion coefficients, $\tilde{D}$, follow the extrapolated curve of Goldstein et al. (1964) for $\tilde{D}$. In order to correlate the extrapolated values of $\tilde{D}$ from Goldstein et al. with the present experimental $\tilde{D}$ values, the value of $\tilde{D}$ was adjusted to match the average Ni content in the diffusion couple at each temperature. This adjustment caused C_{Ni} to be increased from 7.5 at% at 900°C to 27.5 at % at 600°C. Since the diffusivity of Ni increases with Ni content in Fe-Ni (Goldstein et al., 1964), the extrapolated curve of Goldstein et al. in Fig. 26 has an upward trend with decreasing temperature. Goldstein et al.'s curve is the lowest extrapolated curve of the previous investigators (note Fig. 2f). The following material discusses the lack of agreement with other studies.

As seen in Fig. 2e, the diffusion values for eight tracer and microprobe studies in Fe-Ni austenite for low Ni concentrations are reported between approximately 1200°C and 1000°C. The correlation

between the diffusivity curves from all these studies was not good. A factor of three separated the high $\tilde{D}$ value of Ustad and Sorum (1973) from the low $\tilde{D}$ value of Goldstein et al. (1964) at a given temperature. Experimental errors are usually within ±10% relative. The disagreement is increased when the diffusivity curves are extrapolated to lower temperatures. The discrepancy between diffusion coefficients at 600°C is greater than an order of magnitude as seen in Fig. 2f. The inaccuracies in choosing the best fit D_o and Q values for a given set of diffusion data above 1000°C could in part account for spread in the extrapolated diffusion values down to 600°C. These inaccuracies in D_o and Q were also compounded by the experimental error in determining the values of D and by the fact that in all eight studies, five or less experimental values of D were used to determine D_o and Q.

Ustad and Sorum (1973) and Ganessan et al. (1984) based their D_o and Q values in part on data below 1000°C. As seen in Fig. 5, grain boundary diffusion becomes predominant below approximately 1000°C. Goldstein et al. (1964) and Ustad and Sorum (1973) also reported grain boundary problems occurring around 1000°C. Grain boundary diffusion has the effect of decreasing the value of Q in the diffusivity equation (Fig. 5). This decrease in Q value caused the apparent, extrapolated volume diffusivity values, $\tilde{D}$, to be greater than their actual value below 900°C. Therefore the discrepancy between extrapolated values of $\tilde{D}$ below 900°C in binary austenite can be explained by experimental inaccuracies in determining the best fit D_o and Q values at 900°C and above.

The fact that the present data followed Goldstein et al.'s extrapolated curve as opposed to Ustad and Sorum's is an indication that Goldstein's diffusivity data, as claimed, avoided grain boundary diffusion. Therefore Goldstein et al.'s choice of D_o and Q for volume diffusivity is more accurate than that of other workers.

Ternary Couples in Austenite

It is important to note that the F20NP-F25NP couple diffused at 650°C and the F25NP-F30NP couple diffused at 600°C, contained wt% P in excess of the saturation limit at the diffusion temperature (Fig. 13d and 13e). From Doan and Goldstein (1970), $(FeNi)_3P$ phosphides of composition ~15.5 wt%P should precipitate in these ternary diffusion couples. No phosphides were found either in TEM studies or by use of the EDS detector to identify P K_α, in the matrix of these ternary couples. Erhart and Paju (1983) claim P segregates towards grain boundaries in austenitic Fe alloys. Therefore, it might be expected that phosphide precipitation ought to occur at the grain boundaries in the F20NP-F25NP and F25NP-F30NP couples. Again no phosphides were found in a grain boundary diffusion study of F20NP-F25NP.

At 900°C, Heyward and Goldstein reported a value of 1.12×10^{-13} cm^2/sec for the Ni major diffusion coefficient, D^{Fe}_{NiNi}, with a P content of 0.25 wt%, while an extrapolated value of the interdiffusion coefficient of 2.7×10^{-14} cm^2/sec at 900°C was obtained from this study. Also Heyward and Goldstein found that the ternary Ni diffusion coefficient was up to an order of magnitude higher than the binary diffusivity between 1200°C and 900°C. It is important to

point out that Heyward and Goldstein measured the major diffusion coefficient of Ni in Fe-Ni-P, i.e., D^{Fe}_{NiNi}. This major diffusion coefficient is a more accurate value of the actual diffusivity of Ni than the interdiffusion coefficient $\tilde{D}$. The value of $\tilde{D}$ is only equal to D^{Fe}_{NiNi} in Fe-Ni-P when the P concentration is zero. Since P is present in this study, the discrepancy in the values of D^{Fe}_{NiNi} and $\tilde{D}$ at 900°C may simply be an indication that $\tilde{D}$ is not equal to D^{Fe}_{NiNi} at low P concentrations.

Figure 27 shows that the ternary diffusion coefficients progressively increase over the binary diffusion coefficients with decreasing temperature. The average Ni content in the ternary couples used in this study also increases with decreasing diffusion temperature (Table 8b)). Heyward and Goldstein (1973) studied the effect of Ni concentration on the diffusivity of Ni in Fe-Ni-P alloys between 1200°C and 900°C. By varying the Ni content from 6 wt% to 12 wt%, Heyward and Goldstein determined that the diffusivity of Ni is increased by a factor of 1.7 at any given temperature. Since the Ni content of the ternary couples used in this study increases with decreasing temperature, this effect might in part explain the increase in Ni ternary diffusion coefficient with decreasing temperature.

Comparison between Ternary and Binary Diffusivity in γ.

Fig. 28 compares the ternary and binary γ data obtained in this study. At a given diffusion temperature, the average Ni content in the ternary couple is equivalent to the average Ni content in the binary couple (Tables 8 and 9). The experimental diffusivity values

however increase over the binary values with decreasing temperature (Fig. 28). Since this increase in ternary diffusivities cannot be explained by an increase in the average Ni content as discussed in the previous section, one must examine the effect of P contents in the ternary alloys.

The largest P variation between end members of the ternary couples was 0.1 wt% (F20NP-F25NP couple diffused at 650°C). Since the extrapolated P diffusivity is over an order of magnitude greater than the extrapolated Ni diffusivity in Fe-Ni-P below 900°C (Matsuyama et al., 1984; Heyward and Goldstein, 1973), P has most likely homogenized in the interface region of all the ternary couples in this study.

The average P content in all the couples varied between 0.14 wt% and 0.21 wt%. Since the average P content of the ternary couples is approximately the same, the increase in the ternary Ni diffusivity over the binary Ni diffusivities, seen in Fig. 28, is not due to the variation in average P content between couples.

Another reason for the variation in ternary and binary Ni diffusivities may be due to the decreasing solubility of P with decreasing temperature. At high temperatures, 925°C and 875°C, the P solubility limit is above 1.6 wt% P. Therefore the diffusion couples with a P content between 0.1 wt% and 0.2 wt% are far below the solubility limit of P. The corresponding increase in Ni diffusivity of the ternary couples is small (less than 2 times at 875°C, no measurable increase at 925°C). On the other hand, at 650°C and 600°C, where the solubility limit of P is below 0.2 wt% P,

the increase in Ni diffusivity of the ternary couples is an order of magnitude. Therefore it appears that the increase in Ni diffusivity in austenitic Fe-Ni-P depends on the ratio of the P composition in the alloy to the P saturation limit in γ. Table 11 lists the ratio of $\tilde{D}$ ternary to $\tilde{D}$ binary and the ratio of the P alloy content in the diffusion couple to the P solubility limit at several diffusion temperatures. This data is plotted in Figure 29. The ratio of $\tilde{D}_{ternary}$ to $\tilde{D}_{binary}$ increases from zero at P compositions far below the saturation limit (925°C), to more than an order of magnitude increase at and above the P saturation limit (650°C).

The increase in diffusivity of Ni as the P content increases may be explained with the vacancy model proposed by Helfmeier (1974). According to the model the P atoms in the matrix form a positive binding force with vacancies in the Fe-Ni matrix. This causes the equilibrium vacancy concentration to be increased in the matrix and thereby increasing the substitutional diffusion of Ni in the matrix. As P increases towards the saturation limit in γ, the binding force increases, more vacancies are tied up in the matrix, and the diffusivity of Ni is increased. Above the P saturation limit however, the amount of P soluble in the matrix remains constant. Consequently the vacancy concentration in the matrix should not vary when the wt% P in an alloy exceeds the solubility limit and the ratio of $\tilde{D}_{ternary}/\tilde{D}_{binary}$ should remain constant.

This solute solubility effect is observed in this study in the 650°C and 600°C couples (note Table 11 and Figure 29). In the 650°C couple, the wt% P in the end members is 1.2 times the solubility

limit while in the 600°C couple, the wt% P in the end members is approximately double the wt% P soluble in the matrix. As shown in Table 11 and Figure 29, the ratio of $\tilde{D}_{ternary}/\tilde{D}_{binary}$ does not vary between the 650°C and 600°C. Therefore it appears Helfmeier's model of solute-vacancy interaction may be applied in γ Fe-Ni.

It is also interesting to compare the one Cu-Ni-Sb data point from Helfmeier (1974) to the Ni diffusivity data. Helfmeier observed that the diffusivity of Cu in Ni-1.7 at% Sb (ratio of at% Sb in the alloy to at% Sb soluble in the alloy $\simeq$ 0.25) is increased by a factor of 3 over the diffusivity of Cu in pure Ni. This increase in diffusivity due to the addition of an element VI in an fcc matrix is in agreement with this study. In this study the effect of P at this solubility ratio on the ratio of $\tilde{D}_{ternary}$ to $\tilde{D}_{binary}$ is a factor of 2.5

Hoshino et al. (1982) also observed that between 872°C and 732°C, small additions of Sb (wt% Sb alloy/wt% Sb soluble $\lesssim$ 0.2) in pure Cu resulted in up to a factor of 10 increase in Cu self diffusion. The interesting point is that Hoshino observed that the diffusivity ratio between Cu-Sb and Cu increased with increasing Sb content. The same trend in diffusivity vs. solute content is observed in this study.

Binary Couples in Ferrite

In binary α, above the Curie temperature of 770°C and in the paramagnetic state, the two values of $\tilde{D}$ determined by EPMA at 850°C and 805°C agree with the tracer diffusivity values of Borg and Lai with a factor of two (Fig. 30). At the Curie temperature, approxi-

mately 770°C, where the α Fe-Ni changes from paramagnetic state to a ferromagnetic state, a discontinuity in the slope and value of the diffusivity of Ni is observed. A similar effect was observed in Borg and Lai and Hirano et al.'s studies. However, the interdiffusion data in the ferromagnetic state (≤ 700°C) in this study are much lower than that determined by Borg and Lai and Hirano et al. This discrepancy can be explained by Darken's Eq. (6). Hirano et al. (1961) and Borg and Lai (1963) used tracer diffusion to measure D^*. As seen in Eq. (4), the thermodynamic factor F relates the interdiffusion coefficient $\tilde{D}$ to the tracer coefficient D^*. Therefore, it is estimated from the data of this study that in the paramagnetic state, F = 1 so $\tilde{D} = D^*$. In the ferromagnetic state F appears to be between 0.05 and 0.1. Hirano et al. (1961) used α Fe single crystals so that an increase in Ni diffusivity due to grain boundary diffusion cannot be considered. The tracer measurement technique employed by Hirano et al. (1961) and Borg and Lai (1963) consists of sectioning off finite sections of the solvent (α Fe) and measuring the solute radioactivity (Ni^*_{63}) in that section. In the ferromagnetic state, the diffusion distance for both studies was ≤ 5 μm and D^* was determined using less than eight radioactivity measurements. The present data is considered more accurate because it used over 15 concentration measurements of Ni to determine $\tilde{D}$.

Ternary Couples in Ferrite

In the paramagnetic state, at 850°C and 800°C, the extrapolated major diffusion coefficient D^{Fe}_{NiNi} of Heyward and Goldstein (1973) is

an order of magnitude higher than this study's interdiffusion coefficient, $\tilde{D}$, determined by EPMA. This difference between the values of D^{Fe}_{NiNi} and $\tilde{D}$ is also seen in γ. It is explained by the fact that D^{Fe}_{NiNi} and $\tilde{D}$ can only be compared when the P concentration is zero.

The linearity in $\tilde{D}$ values between 850°C and 600°C in the diffusivity of Ni in ternary α-Fe-Ni-P (Fig. 30) is contrary to the observed effect in binary α Fe-Ni where a marked discontinuity exists between $\tilde{D}$ values in the paramagnetic state and ferromagnetic state. The effect of P on the magnetic transformation needs to be further investigated.

In α-Fe, the Curie temperature of pure α Fe decreases linearly with increasing P content. This decrease is from 770°C in pure α Fe down to 735°C in α Fe-1 wt% P. Similarly, the Curie temperature of pure α Fe decreases with increasing Ni content, from 770°C down to approximately 740°C in Fe-6 wt% Ni (Metals Handbook, 1973). The Curie temperature of the α Fe-Ni-P alloys in this study are however not known. It is possible that the combined effect of Ni and P may decrease the Curie temperature sufficiently so that a discontinuity in $\tilde{D}$ ternary is not observed. Bruggeman and Roberts (1975) measured the diffusivity of Fe in Sb- αFe and pure α Fe between 900°C and 700°C. At 850°C, Bruggeman and Roberts observed an increase of 10% to 20% in the diffusivity of Fe in Sb- αFe compared to αFe. This increase is small and within the error limits of $\tilde{D}$ in this study (see section on experimental error in $\tilde{D}$). The ratios of wt% solute in the alloy to wt solute soluble are small (less than 0.1) in both

Bruggeman and Roberts (1975) and in this study. At 805°C in this study, the diffusivity of Ni in Fe-Ni-P is within ±15% of the diffusivity of Ni in binary Fe-Ni, which is in agreement with Bruggeman and Roberts (1975). However at 850°C the ternary diffusivity is one third that of the binary diffusivity (Fig. 30).

P has a tendency to increase the diffusivity of Ni in Fe-Ni. The fact that the diffusivity in ternary paramagnetic Fe-Ni decreases over the diffusivity in binary paramagnetic by a factor of 3.2 at 850°C with an addition of 0.2 wt% P therefore needs to be explained. P may decrease the Curie temperature of Fe-Ni to below 600°C. This decrease in Curie temperature could explain the sudden discontinuity in diffusivity observed between 600°C and 554°C in α Fe-Ni-P. An alternative explanation is that the influence of P on the diffusivity of Ni in α Fe-Ni may not be affected by a change in magnetic state in the matrix. A study of the Curie temperature in Fe-Ni-P is necessary to determine which explanation is correct.

In the ferromagnetic state, all the binary and ternary couples used the same 2 wt% Ni variation between diffusion couple end members (Table 9a and b). Since the same alloys were used as end members, there was no variation in wt% P between ternary couples diffused at different temperatures. Therefore, any variation between the ternary and binary interdiffusion coefficients in this study is independent of compositional variations in the alloys.

As seen in Fig. 30, the ternary interdiffusion coefficient decreases linearly with temperature between 700°C and 600°C. At 560°C however, the value of $\tilde{D}$ is increased over the value of $\tilde{D}$ measured at 600°C.

The amount of P present in the alloy with respect to the solubility limit of P in ferrite is the critical factor in determining the increase in the diffusivity of Ni in α Fe. Table 12 lists the ratio of the measured ternary to binary diffusivities and the ratio of P content to P solubility limit as a function of temperature. Figure 31 shows the relationship between the ratio of ternary to binary diffusion coefficients to the ratio of P content to P solubility limit. Between 700°C and 600°C, the diffusivity of Ni in α Fe-Ni-P compared to α Fe-Ni increases to over a factor of 10. At 560°C as the P content approaches the P solubility limit, the increase in diffusivity of Ni in α Fe-Ni-P compared to the diffusivity of Ni in α Fe-Ni is almost two orders of magnitude (as seen in Fig. 31). No other study was found which examined the diffusivity effects of a solute VI element on a bcc metal near the solute solubility limit.

GRAIN BOUNDARY DIFFUSION

The smallest grain size at the bond interface in the diffusion couples in this study was measured optically $\sim$ 1 mm. Since the diffusion zones in the γ and ferromagnetic α were < 3 μm wide, concentration profiles were readily measured away from grain boundary affected areas.

Grain boundaries act as short circuit paths for the transport of Ni across the interface. Therefore near a grain boundary there will be a depletion of Ni in the high wt% Ni side of the band interface or an enrichment of Ni on the low wt% Ni side. The

spatial resolution of the probe (< 50 nm, Table 6) was sufficient to detect any distortion in the Ni concentration gradient due to grain boundary diffusion. An example of grain boundary distortion in the Ni concentration gradient is shown in Fig. 32 for the F25NP-F30NP couple diffused at 650°C. The volume diffusion concentration gradient of this couple is given in Fig. 19.)

Given the grain size of the diffusion couples at the bond interface and the spatial resolution capabilities of AEM, the resulting best fit profiles for all the diffusion couples in this study reflect only volume diffusion effects.

METEORITES

Narayan (1984) recently evaluated the cooling rates of various Fe meteorites based on the assumption that the addition of 0.2 wt% P in γ Fe-Ni causes the diffusivity of Ni to consistently increase by an order of magnitude. This is not the actual case since the increase in diffusivity is related to the solubility of P in the matrix. However Widmanstatten growth occurs at or below ~650°C, where the P content exceeds the γ solubility limit. In this temperature range the ratio of $\tilde{D}_{Ni}$ ternary to $\tilde{D}_{Ni}$ binary is essentially 10 (note Fig. 29). Therefore the assumption used by Narayan is supported by the results of this study.

The cooling rates in α meteorites of Wasson and Willis (1978) and Moren and Goldstein (1978) also need to be reevaluated since they were based on Hirano et al. (1961) and Borg and Lai's (1963) binary tracer diffusivities. These tracer diffusivity values are an order of magnitude higher than the interdiffusion coefficients

determined in this study. Also the ternary α interdiffusion coefficient varies as a function of the P solubility limit in α .

CONCLUSIONS

AEM with spatial resolution on the order of 10 nm was used to measure the interdiffusion coefficients $\tilde{D}$ in the Fe-Ni and Fe-Ni-P systems between 925°C and 610°C in γ and between 850°C and 550°C in α. The use of AEM insured only effects of volume diffusion were measured.

1) The accuracy of the $\tilde{D}$ values is ±15% for diffusion distances of 1 μm long or more. The accuracy of $\tilde{D}$ decreases to ±100% for diffusion distances less than 0.5 μm.
2) Beam convolution of AEM profiles due to beam broadening resulted in an error of ±6% in $\tilde{D}$ values for diffusion distances of 1 μm or more.
3) The values of $\tilde{D}$ in binary γ determined between 910°C and 610°C follow the extrapolated $\tilde{D}$ curve from Goldstein et al. (1964).
4) The values of $\tilde{D}$ in ternary γ Fe-Ni-P show a progressive increase over the $\tilde{D}$ values in binary γ Fe-Ni between 932°C and 610°C. This increase goes from zero at 932°C to a factor of 10 below 650°C. The increase in diffusivity is related to the ratio of the amount of P in the alloy to the amount of P soluble in the alloy. The closer the wt% P in the alloy is to the P solubility limit, the greater the increase in diffusivity. At and above the P solubility limit, the increase in diffusivity in γ Fe-Ni appears to level off at an order of magnitude. The effect of P on the diffusivity of Ni in Fe-Ni-P can be explained by the

model of Helmeier (1974).

5) In paramagnetic binary α Fe-Ni, the $\tilde{D}$ values determined by EPMA at 853°C and 805°C in this study are in agreement with previous studies by Borg and Lai (1963) and Hirano et al. (1961).

6) In ferromagnetic binary α Fe-Ni, the $\tilde{D}$ values determined between 700°C and 554°C are 1 to 2 orders of magnitude lower than previously determined by tracer diffusion.

7) In paramagnetic ternary α Fe-Ni-P, the interdiffusion coefficient values determined at 844°C is less than the paramagnetic binary α Fe-Ni value.

8) In paramagnetic and ferromagnetic ternary α Fe-Ni-P, and $\tilde{D}$ values determined between 844°C and 600°C decrease linearly with temperature and no change in D_o and Q was observed. However between 600°C and 563°C, the diffusivity of Ni in α Fe-Ni-P actually increases.

9) The increase in diffusivity of ferromagnetic ternary α Fe-Ni-P over the diffusivity of ferromagnetic binary α Fe-Ni can be related to the ratio of the wt% P in the alloy to the wt% P soluble in the matrix. This increase in diffusivity in α Fe-Ni due to P is much greater than the increase in diffusivity in γ Fe-Ni due to P.

TABLE 1a)

Values of D_o and Q for Chemical Volume Diffusion Coefficient in Binary Fe-Ni Austenite

Reference	Temp. Range	wt% Ni Range	D_o (cm^2/sec)	Q (cal/mole)
Wells & Mehl* (1941)	1450°C-1050°C	4, (0.03% C)	0.44±0.11	67,700±750
		14, (0.03% C)	0.51±0.12	67,300±750
Balakir et al.+ (1974)	950°C-750°C	25	0.33	60,000
Ganessan et al.+ (1984)	1100°C-950°C	10	2.85×10^{3}	83,700
		20	2.32×10^{2}	76,700
Ustad & Sorum+ (1973)	1426°C-705°C	10	0.2	63,200
		20	0.2	63,000
Goldstein et al.+ (1965)	1300°C-1000°C	0 to 50	$e^{(0.051\ C_{Ni}+1.15)}$▲	$(76{,}400-11.6\ C_{Ni})$▲

Values of D_o and Q for intrinsic diffusion coefficient in binary Fe-Ni austenite using microprobe, note $\tilde{D} = C_{Ni}\ D_{Ni} + (1-C_{Ni})\ D_{Fe}$ where C_{Ni}=weight fraction Ni

Reference	Temp. Range	wt% Ni Range		D_o (cm^2/sec)	Q (cal/mole)
Badia & Vignes+	1360°C-1136°C	32	D_{Fe}	3.6	68,500
			D_{Ni}	1.6	72,500

*chemical analysis of sectioned material +microprobe analysis ▲C_{Ni} = atomic percent Ni

TABLE 1b)

Values of D_o and Q for Tracer Diffusion of Ni^{*}_{63} in Fe-Ni Alloys in the Ni Composition Range of 0 wt% to 5 wt%

Reference	Temp. Range	wt% Ni Range	D_o (cm^2/sec)	Q (cal/mole
Frantsevich et al. (1969)	1400°C-1000°C	2	1.1	59,000
		4	1.4	58,000
Hancock & Leak (1967)	1500°C-1300°C	0.2-0.5	1.09	69,300
		2.3	0.6	67,300
Henry & Cizeron (1978)	1240°C-920°C	0	5×10^{-3}	55,000
		5	1.5×10^{-2}	57,600
Lange et al. (1964)	1130°C-940°C	0	0.44	66,600
Hanatate et al. (1978)	1287°C-1153°C	0	1.09	70,911
MacEwan et al. (1959)	1400°C-1152°C	5.8	2.11	73,500
Zemskiy et al. (1976)	1100°C-800°C	5	$8.92 \times 10^{-3} \times e^{(18.3(N-0.38)^2)}$	$(63.6-64\ N+63\ N^2)^{*} \times 10^3$

* N = mole fraction Ni in alloy

TABLE 1c)

Values of D_o and Q for Tracer Diffusion in Fe-Ni Alloys with 15-20 wt% Ni

Reference	Temp. Range	wt% Ni Range	D_o (cm^2/sec)	Q (cal/mole)
Hancock & Leak (1967	1500°C-1300°C	19.34	0.4	65,400
Henry & Cizeron (1978)	1240°C-920°C	15	0.27	64,600
		20	0.8	67,300
MacEwan et al. (1959)	1400°C-1152°C	14.8	5	75,600

TABLE 2

Values of D_o and Q for Volume Diffusion Coefficient in Binary Ferrite Fe-Ni $D=D_o \exp(-Q/RT)$

Reference	Measurement Method	Temp. Range	D_o (cm^2/sec)	Q (cal/mole)
Borg & Lai (1963)	Residual tracer	a) 900°C-800°C paramagnetic	9.9	61,900
		b) below 680°C* ferromagnetic	10.5*	64,300*
Hirano et al. (1961)	Residual tracer	a) above 800°C paramagnetic	1.3	56,000
		b) below 680°C ferromagnetic	1.4	58,700

*= values of D_o and Q reported by Moren and Goldstein (1978) from Borg & Lai's data.

TABLE 3

Values of D_o and Q in Ferritic Fe-P and Fe-Ni-P Alloys

Reference	Temp. Range	wt% Ni	wt% P	D_o (cm^2/sec)	Q (cal/mole)
Heyward & Goldstein[+] (1973)	1200°C-900°C	0.5	1.2	2.72	52,200
Gruzin & Mural[*] (1963)	900°C-800°C	0	0	1.58	52,300
Matsuyama, et al.[*] (1984)	825°C-770°C	1	0.07	598	66,000
Matsuyama, et al.[*]	825°C-770°C	0	0.08	376	66,000

[+]Values of D_o and Q based on D_{PP}^{Fe} determined by EPMA.

[*]Values of D_o and Q based on D_P^* determined by residual tracer.

TABLE 4

Values of D_o and Q for Volume and Grain Boundary Diffusion Determined by Tracer Analysis in Fe and Fe-Ni Austenite

Reference	Temp. Range	% Ni in Fe	Volume		Grain Boundary	
			D_o (cm^2/sec)	Q cal/mole	D_o (cm^3/sec)	Q cal/mole
Lange et al. (1964)	1130°C-940°C	0	0.44	66,600	3.8×10^{-7}	36,400
Hanatate et al. (1978)	1287°C-1153°C	0	1.1	70,100	1.2×10^{-6}	42,100
Zemskiy et al. (1976)	1100°C-800°C	5	0.08	60,200	2.5×10^{-9}	24,600

Values of D_o and Q for Volume and Grain Boundary Diffusion Determined by Microprobe Analysis in Fe-Ni Austenite

Reference	Temp. Range	% Ni Range	Volume		Grain Boundary	
			D_o (cm^2/sec)	Q cal/mole	D_o (cm^3/sec)	Q cal/mole
Krishtal et al.	1200°C-1000°C	0-100	1.25	67,700	2.5×10^{-6}	44,500

NOTE: The grain boundary width is included in D_o values for grain boundaries given above. This grain boundary width is estimated at $\delta = 5 \times 10^{-8}$ cm in all four studies.

TABLE 5

Percent Absorption Correction in k_{AB} Factor as a Function of Specimen Thickness in Fe-2% Ni and Fe-27.5% Ni Alloys

Specimen Thickness	Percent Absorption Correction Fe-2% Ni	Fe-27.5% Ni
1 nm	1%	1%
86 nm	3%	-
117 nm	-	3%
142 nm	5%	-
194 nm	-	5%
282 nm	10%	-
384 nm	-	10%

TABLE 6

Beam Broadening b and Total Beam Size $(d^2+b^2)^{\frac{1}{2}}$ as a Function of Specimen Thickness in Fe-Ni α and γ Alloys.

Thickness	Beam Size in Fe-Ni		Total beam size $\sqrt{d^2+b^2}$ for given initial beam size	
	Ferrite α (1 wt% Ni)	Austenite γ (27.5 wt% Ni)	d = 10 nm	d = 20 nm
50 nm	5.6 nm	5.7 nm	11.5 nm	20.8 nm
100 nm	16 nm	16.3 nm	19.1 nm	25.8 nm
150 nm	29.5 nm	30.1 nm	31.7 nm	36.1 nm
200 nm	45.5 nm	46.5 nm	46.6 nm	50.6 nm

TABLE 7

The Purity of the Raw Materials Used to Make Up the Alloys*

	Si	Cu	Fe	Mn	Mg	C
Fe	5	2	solvent	5	2	70
Ni	<1	2	15	-	<1	9

*values in ppm

TABLE 8

Diffusion Couple End Member Compositions Determined by EPMA

Binary Alloys

Designation	Desired Composition	Actual Composition wt%
F1N	1% Ni	0.97±0.01
F2N	2% Ni	2.02±0.02
F5N	5% Ni	5.04±0.14
F10N	10% Ni	9.95±0.15
F15N	15% Ni	15.02±0.04
F20N	20% Ni	19.73±0.15
F25N	25% Ni	24.53±0.38
F30N	30% Ni	29.57±0.45

Ternary Alloys

Designation	Desired Composition	Actual Composition (wt%) Ni	P
FP	0.2% P	-	0.26±0.05
F1NP	1% Ni, 0.2% P	0.98±0.02	0.28±0.05
F2NP	2% Ni, 0.2% P	1.9 ±0.07	0.30±0.05
F5NP	5% Ni, 0.2% P	4.86±0.02	0.18±0.02
F10NP	10% Ni, 0.2% P	9.9 ±0.05	0.12±0.01
F15NP	15% Ni, 0.2% P	14.03±0.13	0.16±0.03
F20NP	20% Ni, 0.2% P	19.92±0.37	0.12±0.04
F25NP	25% Ni, 0.2% P	24.7 ±0.30	0.22±0.03
F30NP	30% Ni, 0.2% P	29.95±0.50	0.23±0.05

TABLES 9 a) - d)

Diffusion Couple Heat Treatments, Experimental Temperatures and Times

TABLE 9a)

Binary Austenite

End Member Designations	Diffusion Temperature	Diffusion Time
F5N - F10N	911°C ± 1°C	22 hrs + 53 mins
F5N - F10N	851°C ± 1°C	42 hrs + 10 mins
F10N - F15N	802°C*	72 hrs
F10N - F15N	757°C*	24 days
F15N - F20N	704°C ± 1°C	40 days
F20N - F25N	650°C ± 2°C	121 days
F25N - F30N	610°C ± 2°C	62 days

*Heat treatments by Narayan (1983)

TABLE 9 b)

Ternary Austenite

End Member Designation	Diffusion Temperature	Diffusion Time
F5NP - F10NP	932°C ± 1°C	34 hrs + 50 mins
F5NP - F10NP	875°C	14 hrs + 35 mins
F10NP - F15NP	805°C*	26 hrs
F10NP - F15NP	750°C*	7 days
F15NP - F20NP	705°C ± 2°C	32 days
F20NP - F25NP	650°C ± 2°C	121 days
F25NP - F30NP	610°C ± 2°C	62 days

*Heat treatments by Narayan (1983)

TABLE 9 c)

Binary Ferrite

End Member Designation	Diffusion Temperature	Diffusion Time
F - F1N	853°C ± 1°C	30 hr + 45 mins
F - F1N	805°C ± 2°C	31 hrs
F - F2N	705°C ± 1°C	5 hrs + 40 mins
F - F2N	654°C ± 1°C	36 hrs
F - F2N	604°C ± 1°C	5 days
F - F2N	554°C ± 3°C	33 days + 6 hrs

TABLE 9 d)

Ternary Ferrite

End Member Designation	Diffusion Temperature	Diffusion Time
FP - F1NP	844°C ± 1°C	24 hrs + 30 mins
FP - F1NP	800°C ± 1°C	24 hrs + 30 mins
FP - F2NP	704°C ± 1°C	6 hrs + 20 mins
FP - F2NP	654°C ± 3°C	35 hrs + 45 mins
FP - F2NP	600°C ± 1°C	6 days + 17 hrs
FP - F2NP	563°C ± 2°C	31 days

TABLE 10 a)

Experimental Values of $\tilde{D}_{Ni}$ for Austenite

Binary Couples		Ternary Couples	
Temperature	$\tilde{D}$ (cm^2/sec)	Temperature	$\tilde{D}$ (cm^2/sec)
911°C	2.7×10^{-14}	932°C	4.7×10^{-14}
851°C	4.4×10^{-15}	875°C	1.7×10^{-14}
802°C	3.7×10^{-15}*	805°C	9.6×10^{-15}*
757°C	2.7×10^{-16}*	750°C	2.0×10^{-15}*
704°C	1.6×10^{-16}	705°C	6.0×10^{-16}
650°C	1.2×10^{-17}	650°C	1.4×10^{-16}
610°C	4.0×10^{-18}	610°C	4.0×10^{-17}

*Values reported by Narayan and Goldstein (1984)

TABLE 10 b)

Experimental Values of $\tilde{D}$ for Ferrite

Binary Couples		Ternary Couples	
Temperature	$\tilde{D}$ (cm^2/sec)	Temperature	$\tilde{D}$ (cm^2/sec)
853°C*	9.0×10^{-12}	844°C*	2.8×10^{-12}
805°C*	1.5×10^{-12}	800°C*	1.7×10^{-12}
705°C	1.1×10^{-14}	704°C	6.0×10^{-14}
654°C	3.3×10^{-16}	654°C	6.0×10^{-15}
604°C	6.8×10^{-17}	600°C	5.5×10^{-16}
554°C	1.1×10^{-17}	563°C	1.0×10^{-15}

*Diffusion gradients measured by EPMA

TABLE 11

Ratio of the Experimental Ternary Interdiffusion Coefficient to the Binary Interdiffusion Coefficient as a Function of the Ratio of the Average Phosphorus Content in the Diffusion Couple to the Phosphorus Solubility Limit at a Given Temperature in Austenite. Note wt% Ni is the same in both the ternary and binary couple.

Temperature (Approximate)	$\tilde{D}_{Ternary}/\tilde{D}_{Binary}$	wt% P_{Alloy}/wt% $P_{Soluble}$ (x 10^2)
923°C	1^+	15
875°C	1.5^+	18
805°C	2.5^+	30
750°C	7^+	37
705°C	3	51
650°C	11	121
610°C	10	183

$^+\tilde{D}_{Binary}$ is extrapolated

TABLE 12

Ratio of the Experimental Ternary Interdiffusion Coefficient to the Extrapolated or Experimental Binary Interdiffusion Coefficient as a Function of the Ratio of the Average Phosphorus Content in the Couple to the Phosphorus Solubility Limit at a Given Temperature in Ferrite. Note wt% Ni is Constant.

Temperature	$\tilde{D}_{Ternary}/\tilde{D}_{Binary}$	wt% P_{Alloy}/wt% $P_{Soluble}$ (x 10^2)
705°C	5	31
654°C	18	41
602°C	8	62
563°C	90+	82

+ $\tilde{D}_{Binary}$ is extrapolated

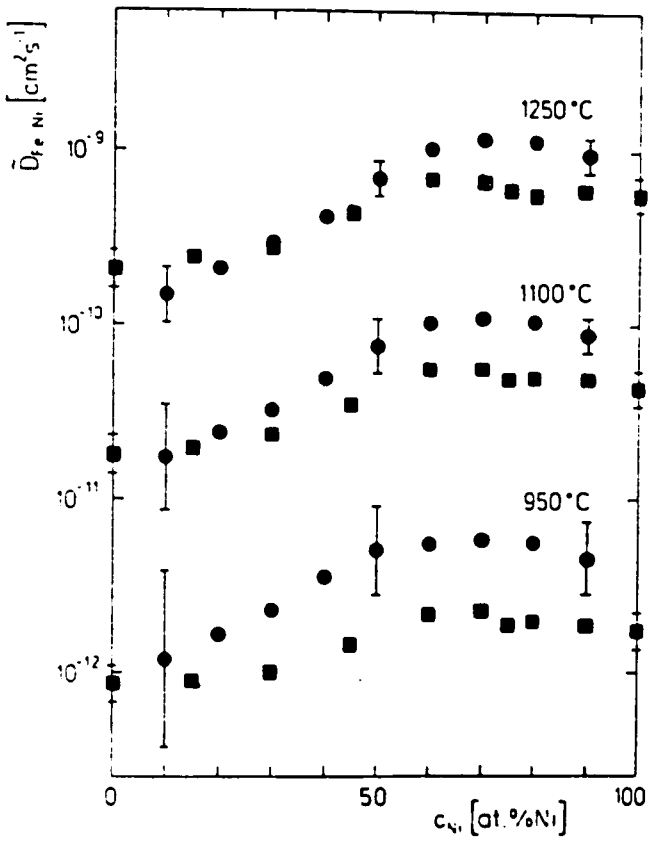

Fig. 1a: Concentration dependence of the interdiffusion coefficient in the Fe-Ni system: ● experimental values, ■ values calculated from self diffusion and thermodynamic data. Reference Million et al. (1981).

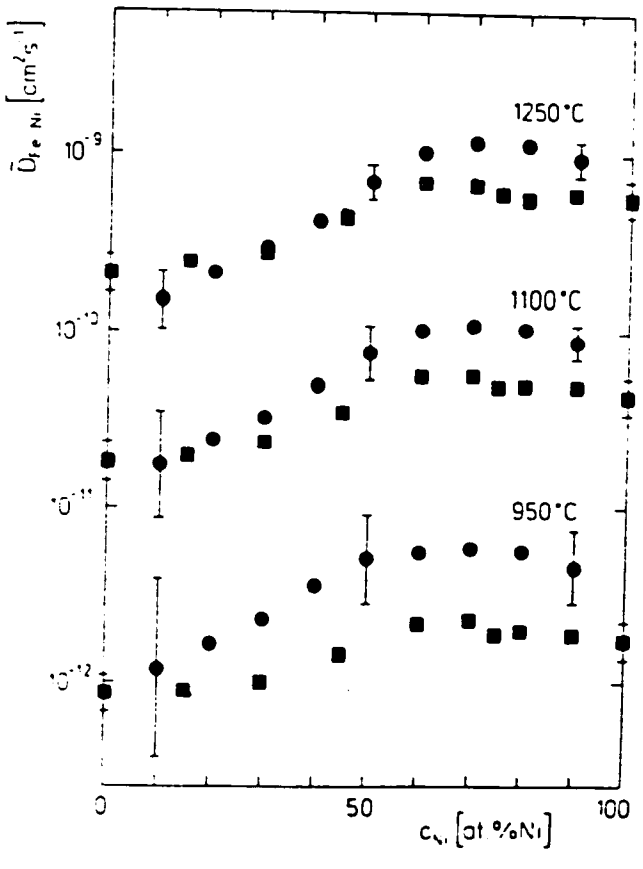

Fig. 1a: Concentration dependence of the interdiffusion coefficient in the Fe-Ni system: ● experimental values, ■ values calculated from self diffusion and thermodynamic data. Reference Million et al. (1981).

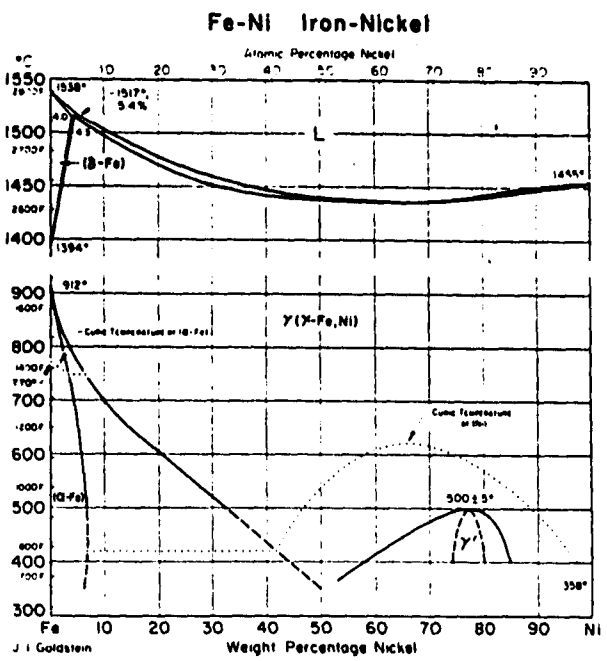

Fig. 1b: Fe-Ni phase diagram, reference Metals Handbook, volume 8 (1978).

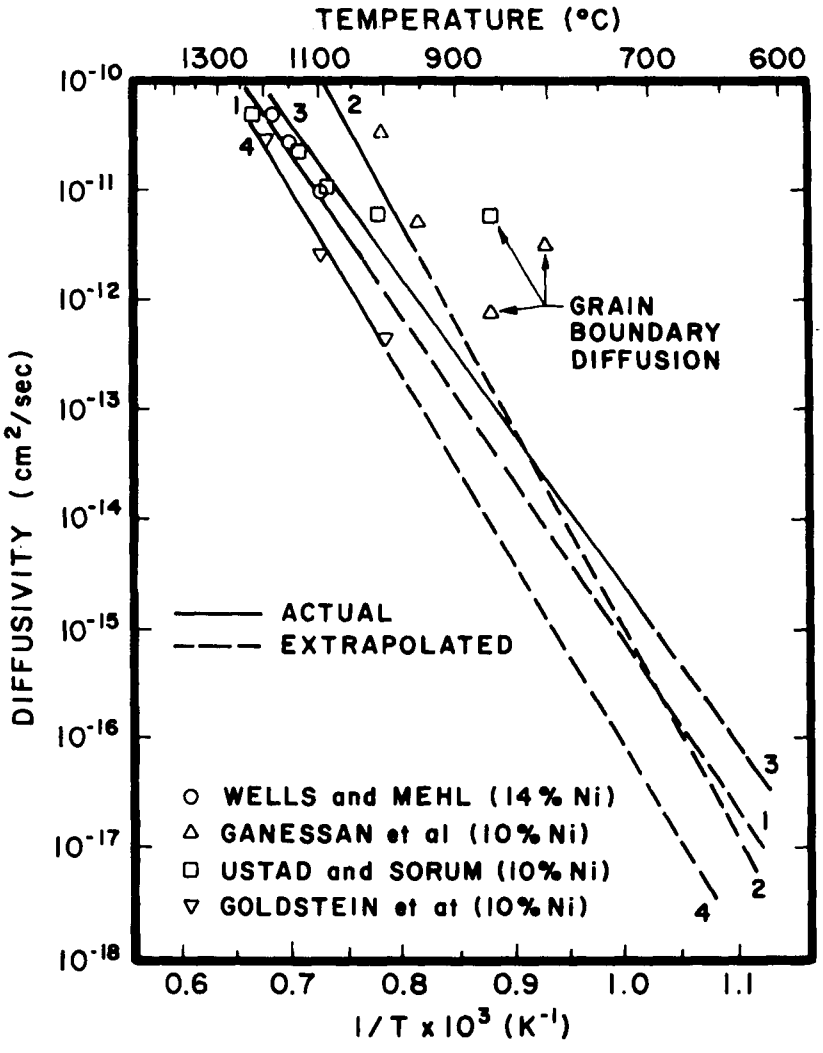

Fig. 2a: Interdiffusion coefficient values and extrapolations versus temperature obtained by EPMA+analysis for Fe-10% Ni. 1-Wells and Mehl (1941), range (1450°C-1050°C); 2-Ganessan et al. (1984) range (1100°C-950°C); 3-Ustad and Sorum (1973) range (1426°C-705°C); 4-Goldstein et al. (1964) range (1300°C-1000°C).

+Wells and Mehl determined $\tilde{D}$ by wet chemical analysis

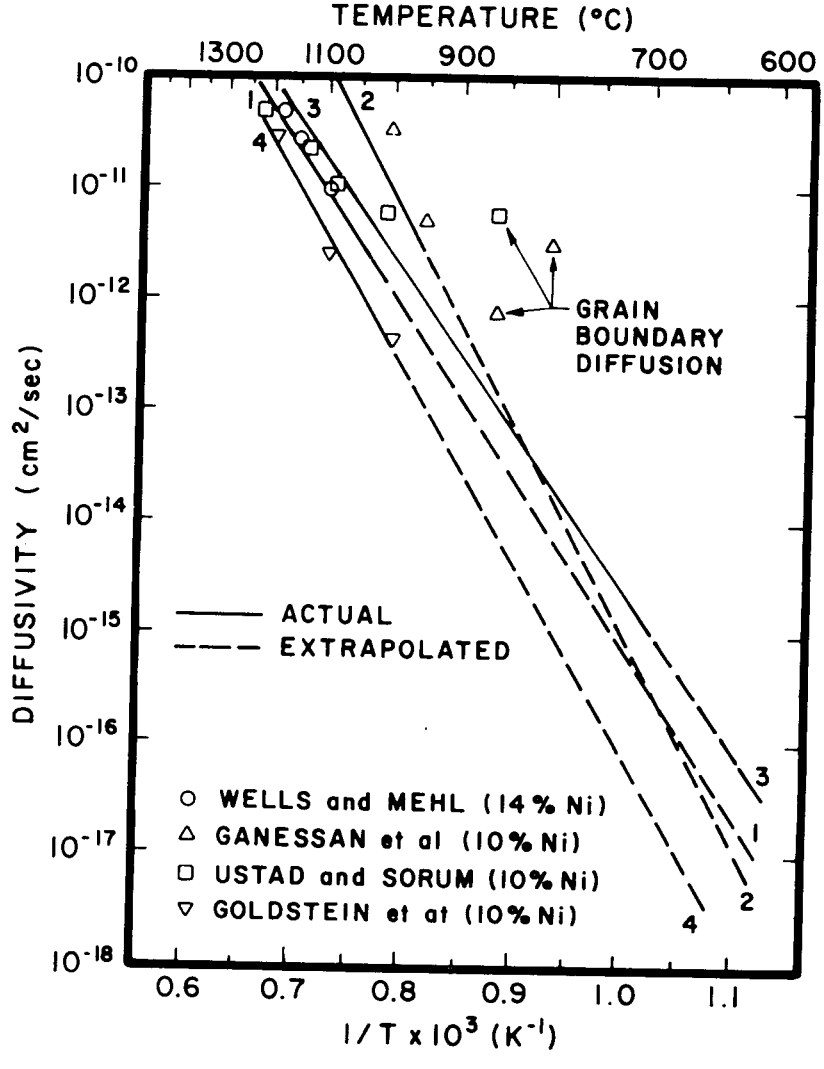

Fig. 2a: Interdiffusion coefficient values and extrapolations versus temperature obtained by EPMA+analysis for Fe-10% Ni. 1-Wells and Mehl (1941), range (1450°C-1050°C); 2-Ganessan et al. (1984) range (1100°C-950°C); 3-Ustad and Sorum (1973) range (1426°C-705°C); 4-Goldstein et al. (1964) range (1300°C-1000°C).

+Wells and Mehl determined $\tilde{D}$ by wet chemical analysis

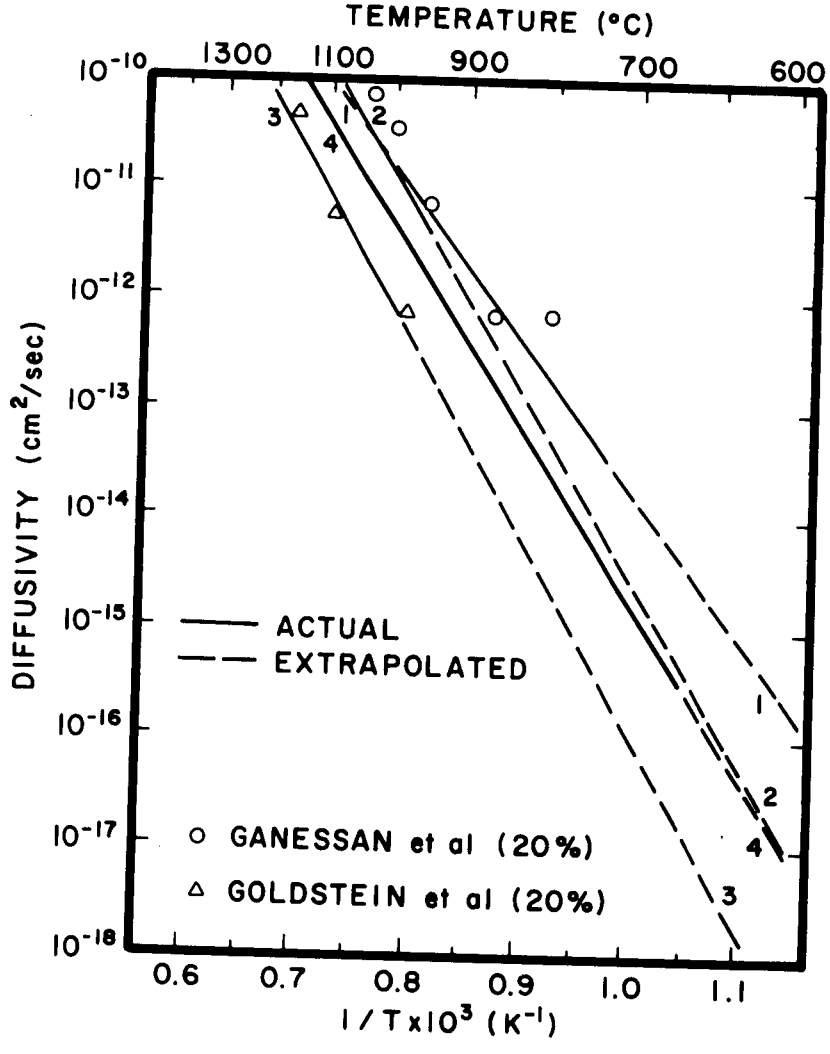

Fig. 2b: Interdiffusion coefficient values and extrapolations versus temperature obtained by EPMA for Fe-20% Ni: 1-Balakir et al. (1967) range (950°C-750°C); 2-Ganessan et al. (1984) range (1100°C-950°C; 3-Goldstein et al. (1964) range (1300°C-1000°C; 4-Ustad and Sorum (1973) range (1426°C-705°C).

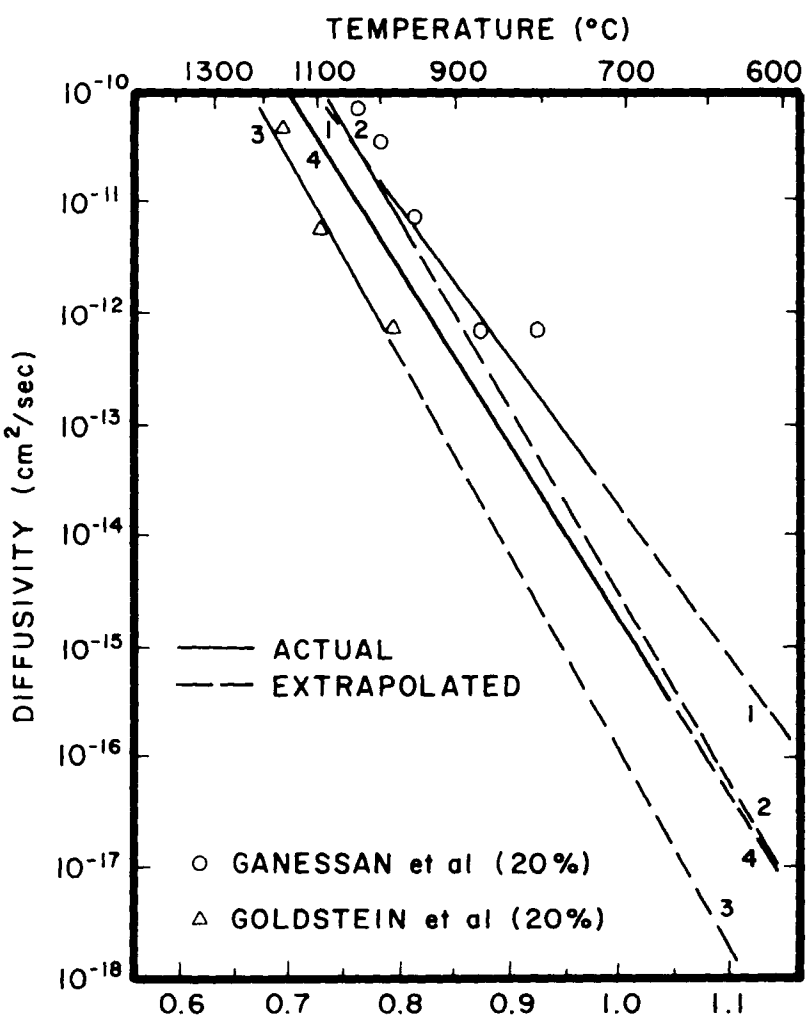

Fig. 2b: Interdiffusion coefficient values and extrapolations versus temperature obtained by EPMA for Fe-20% Ni: 1-Balakir et al. (1967) range (950°C-750°C); 2-Ganessan et al. (1984) range (1100°C-950°C; 3-Goldstein et al. (1964) range (1300°C-1000°C; 4-Ustad and Sorum (1973) range (1426°C-705°C).

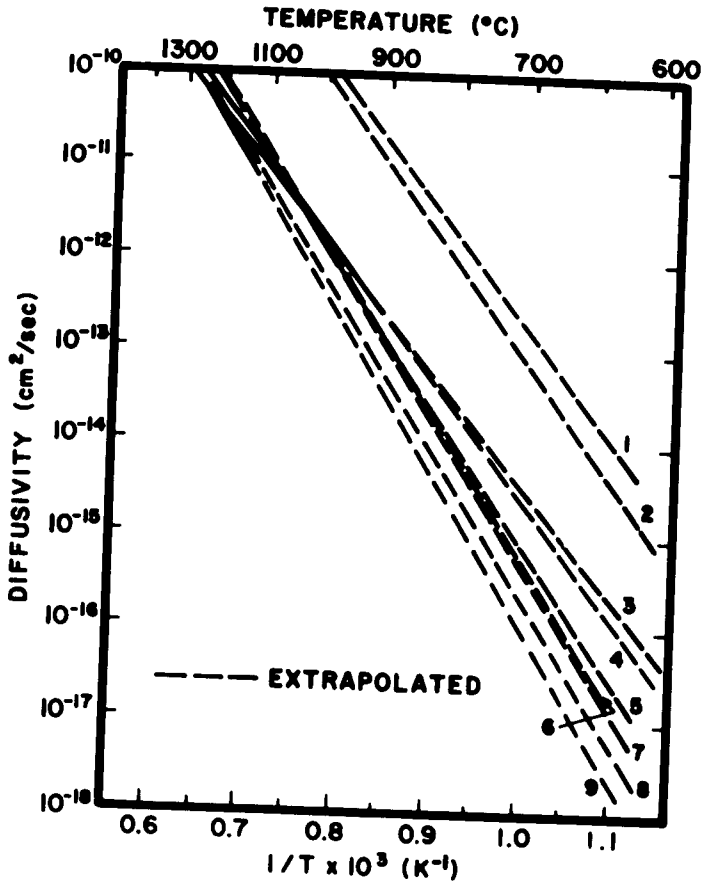

Fig. 2c: Tracer diffusion coefficient values and extrapolations versus temperature of D^{*}_{Ni} for Fe-Ni alloys in the range of 0 wt% Ni to 5 wt% Ni:
1-Frantsevich (1969) range (1400°C-1000°C), 2 wt% Ni;
2-Frantsevich (1969), 4.4 wt% Ni;
3-Henry & Cizeron (1978), range (1240°-920°C), 0 wt% Ni;
4-Henry & Cizeron (1978), 5 wt% Ni;
5-Lange et al. (1964), range (1130°C-940°C), 0 wt% Ni;
6-Hancock & Leak (1967) range (1500°C-1300°C), 0.2-0.5 wt% Ni;
7-Hancock & Leak (1967), 2-3 wt% Ni;
8-Hanatate et al. (1978), range (1287°C-1153°C), 0 wt% Ni;
9-MacEwan et al. (1959), range 1400°C-1152°C), 5 wt% Ni.

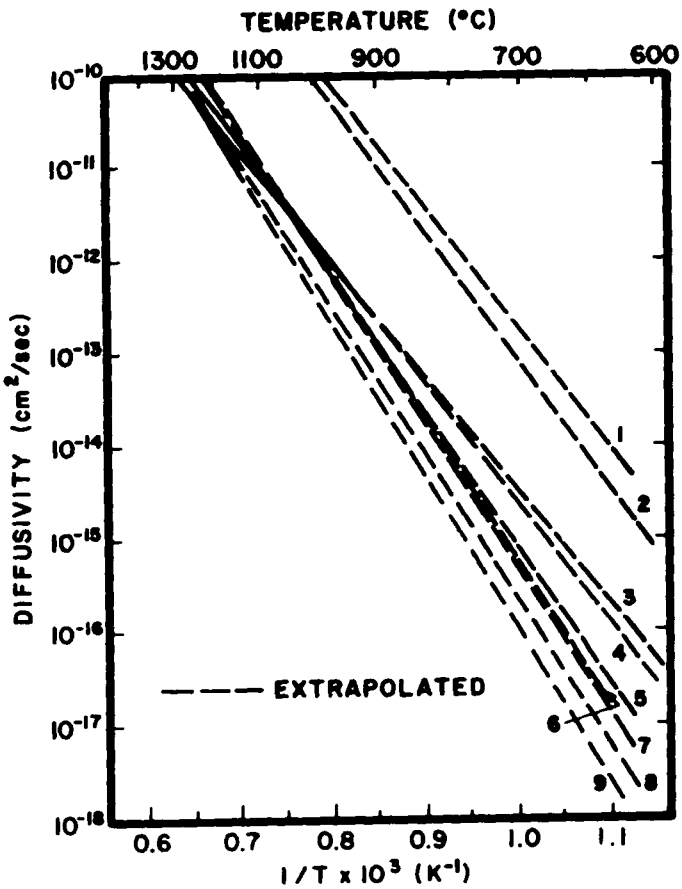

Fig. 2c: Tracer diffusion coefficient values and extrapolations versus temperature of D^{*}_{Ni} for Fe-Ni alloys in the range of 0 wt% Ni to 5 wt% Ni:
1-Frantsevich (1969) range (1400°C-1000°C), 2 wt% Ni;
2-Frantsevich (1969), 4.4 wt% Ni;
3-Henry & Cizeron (1978), range (1240°-920°C), 0 wt% Ni;
4-Henry & Cizeron (1978), 5 wt% Ni;
5-Lange et al. (1964), range (1130°C-940°C), 0 wt% Ni;
6-Hancock & Leak (1967) range (1500°C-1300°C), 0.2-0.5 wt% Ni;
7-Hancock & Leak (1967), 2-3 wt% Ni;
8-Hanatate et al. (1978), range (1287°C-1153°C), 0 wt% Ni;
9-MacEwan et al. (1959), range 1400°C-1152°C), 5 wt% Ni.

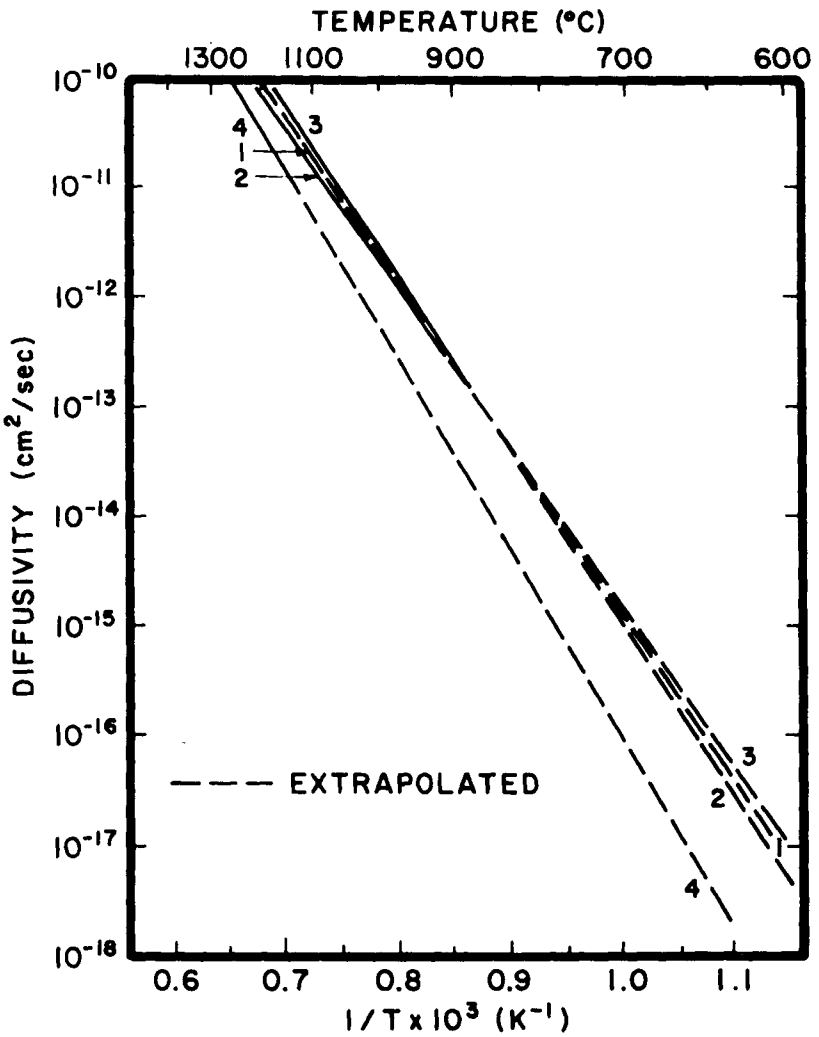

Fig. 2d: Tracer diffusion coefficient values and extrapolation versus temperature of D^{*}_{Ni} for Fe-Ni alloys in the range of 15-20 wt% Ni:
1-Hancock & Leak (1967), range (1500°C-1300°C), 20 wt% Ni;
2-Henry & Cizeron (1978), range (1240°C-920°C), 15 wt% Ni;
3-Henry & Cizeron (1978), 20 wt% Ni;
4-MacEwan et al. (1959), range (1400°C-1152°C), 14.8 wt% Ni.

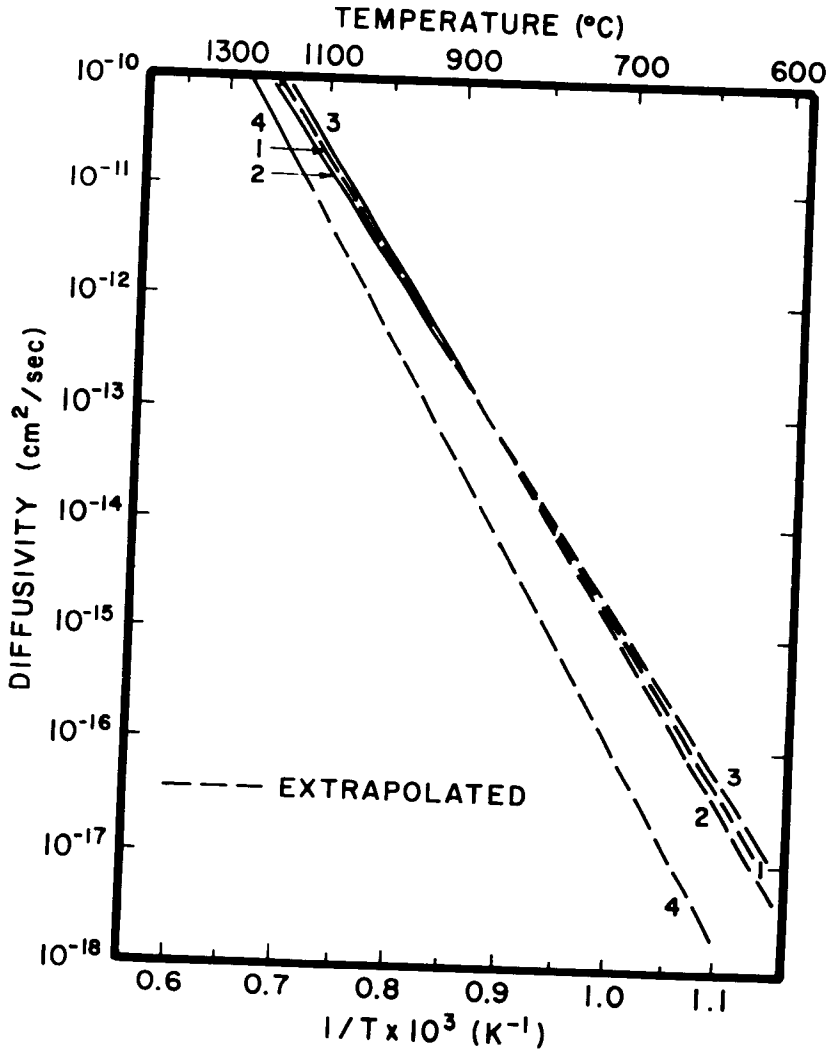

Fig. 2d: Tracer diffusion coefficient values and extrapolation versus temperature of D^{*}_{Ni} for Fe-Ni alloys in the range of 15-20 wt% Ni:
1-Hancock & Leak (1967), range (1500°C-1300°C), 20 wt% Ni;
2-Henry & Cizeron (1978), range (1240°C-920°C), 15 wt% Ni;
3-Henry & Cizeron (1978), 20 wt% Ni;
4-MacEwan et al. (1959), range (1400°C-1152°C), 14.8 wt% Ni.

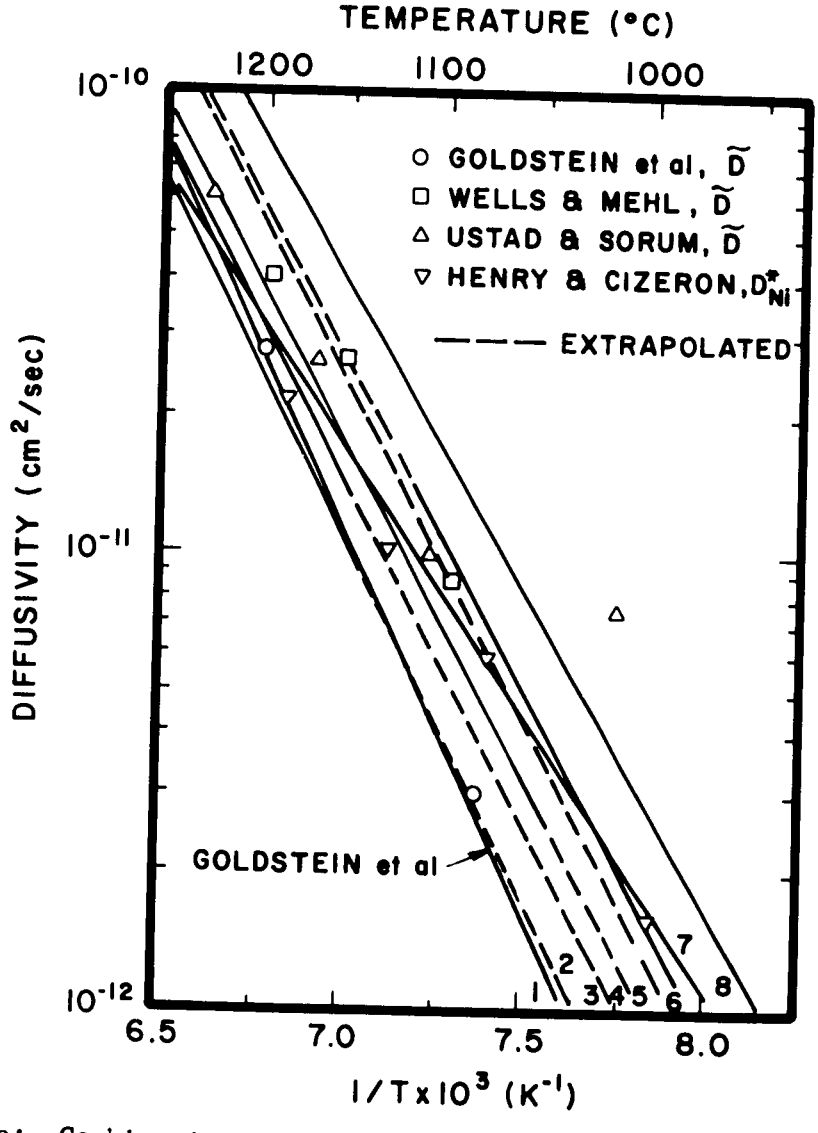

Fig. 2e: Combination of Fig. 2a of Fe-10% Ni interdiffusion coefficients and Fig. 2c of tracer diffusion coefficients in Fe-Ni (5 wt% < Ni) versus temperature in range of 1200°C to 950°C.

1) Goldstein et al. (1965), microprobe, range=1300°C-1000°C
2) MacEwan et al. (1959), tracer, range=1400°C-1152°C
3) Hanatate et al. (1978), tracer, range=1287°C-1158°C
4) Wells and Mehl (1941), chemical, range=1450°C-1050°C
5) Hancock and Leak (1967), tracer, range=1500°C-1300°C
6) Lange et al. (1964), tracer, range=1130°C-940°C
7) Henry and Cizeron (1978), tracer, range=1240°C-920°C
8) Ustad and Sorum (1973), microprobe, range 1426°C-705°C

Note Frantsevich et al. and Ganessan et al. studies are left out because they differed significantly from rest of studies.

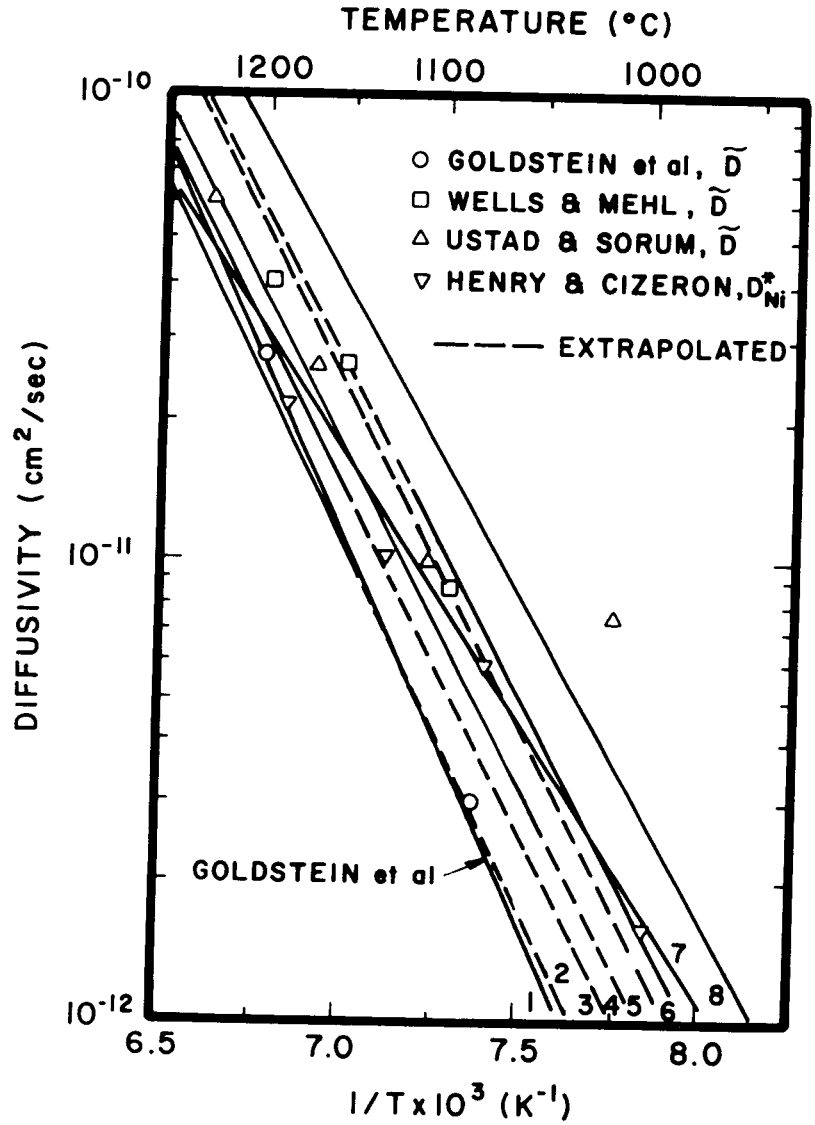

Fig. 2e: Combination of Fig. 2a of Fe-10% Ni interdiffusion coefficients and Fig. 2c of tracer diffusion coefficients in Fe-Ni (5 wt% < Ni) versus temperature in range of 1200°C to 950°C.

1) Goldstein et al. (1965), microprobe, range=1300°C-1000°C
2) MacEwan et al. (1959), tracer, range=1400°C-1152°C
3) Hanatate et al. (1978), tracer, range=1287°C-1158°C
4) Wells and Mehl (1941), chemical, range=1450°C-1050°C
5) Hancock and Leak (1967), tracer, range=1500°C-1300°C
6) Lange et al. (1964), tracer, range=1130°C-940°C
7) Henry and Cizeron (1978), tracer, range=1240°C-920°C
8) Ustad and Sorum (1973), microprobe, range 1426°C-705°C

Note Frantsevich et al. and Ganessan et al. studies are left out because they differed significantly from rest of studies.

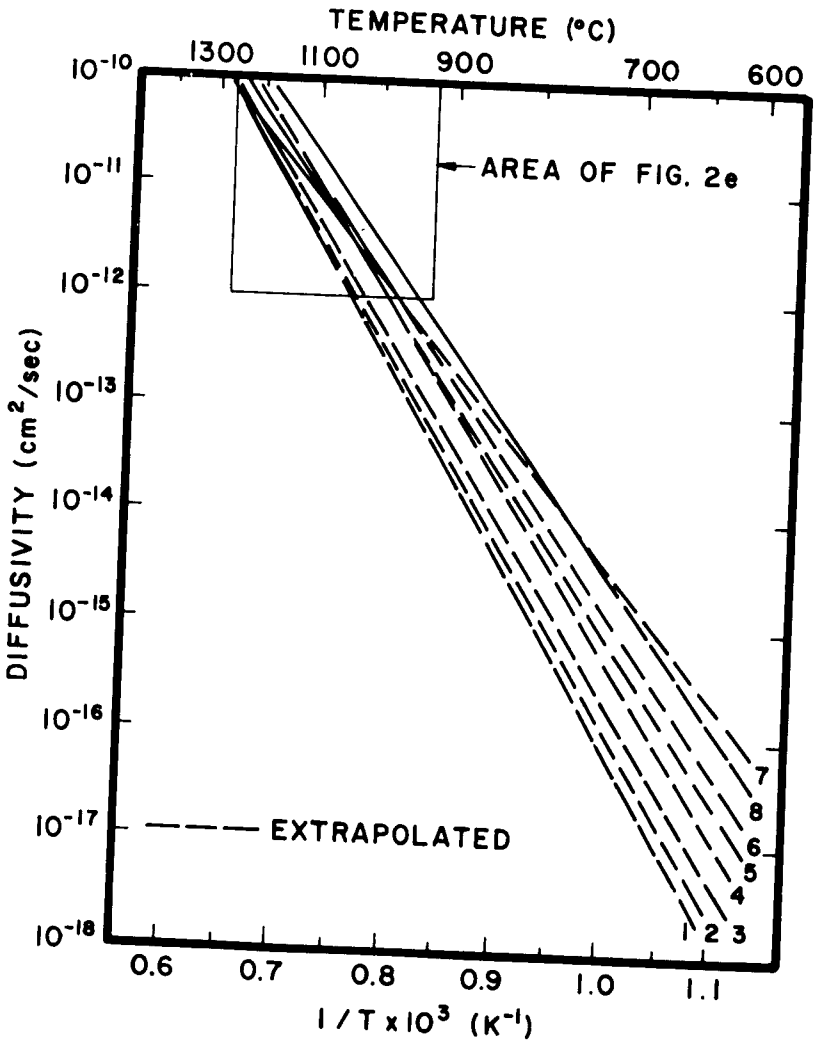

Fig. 2f: Extrapolation of curve in Fig. 2e down to 600°C, references 1-8 listed in Fig. 2e.

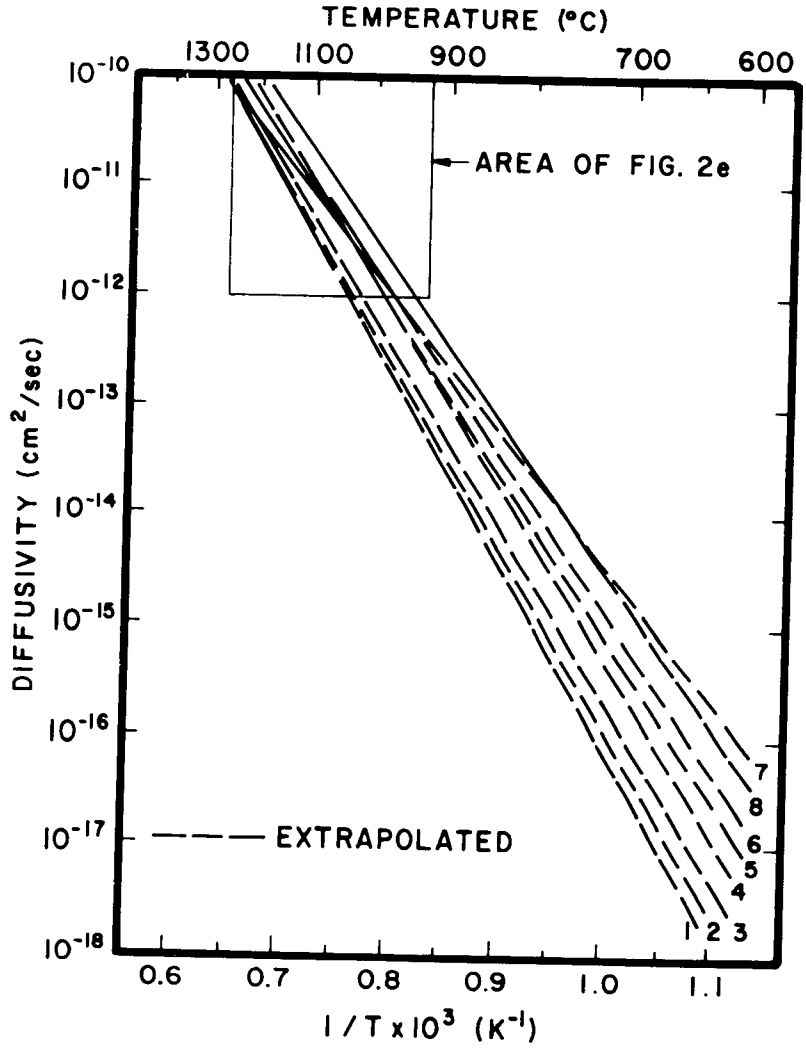

Fig. 2f: Extrapolation of curve in Fig. 2e down to 600°C, references 1-8 listed in Fig. 2e.

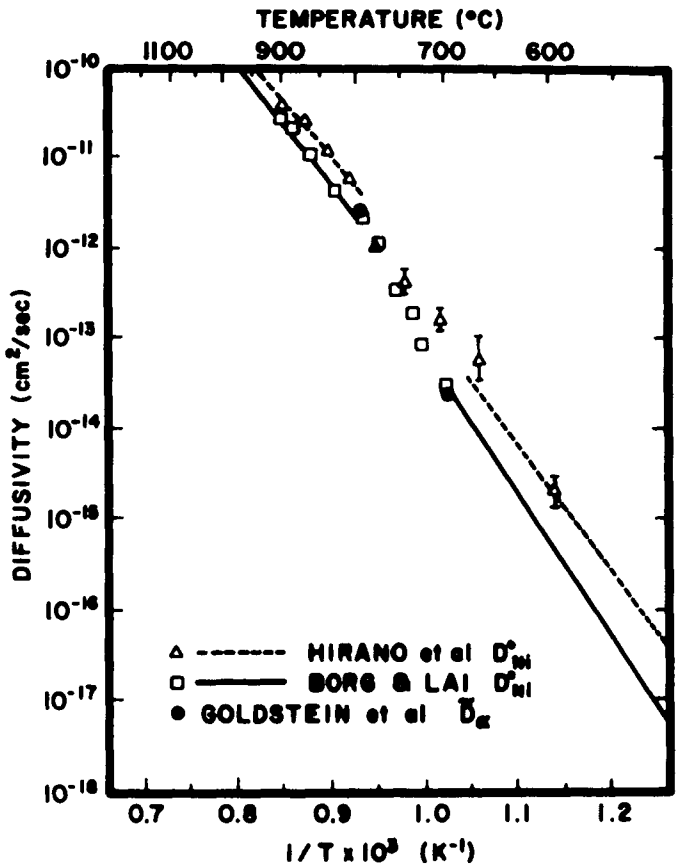

Fig. 3: Binary Fe-Ni ferrite diffusivity data as a function of temperature:
1-Hirano et al. (1961); △
2-Borg and Lai (1963); □
3-Goldstein et al. (1964). ●

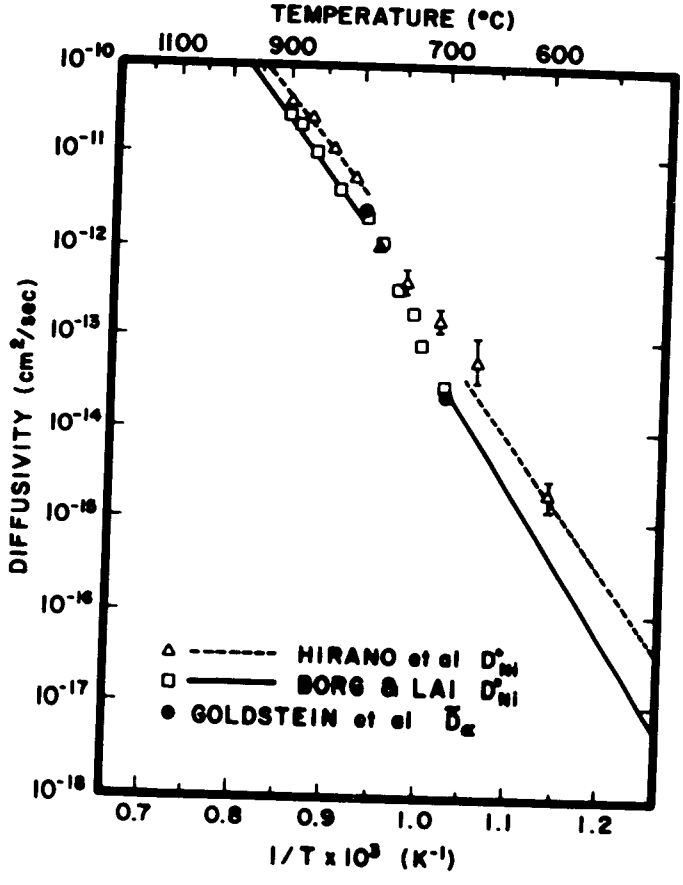

Fig. 3: Binary Fe-Ni ferrite diffusivity data as a function of temperature:
1-Hirano et al. (1961); △
2-Borg and Lai (1963); □
3-Goldstein et al. (1964). ●

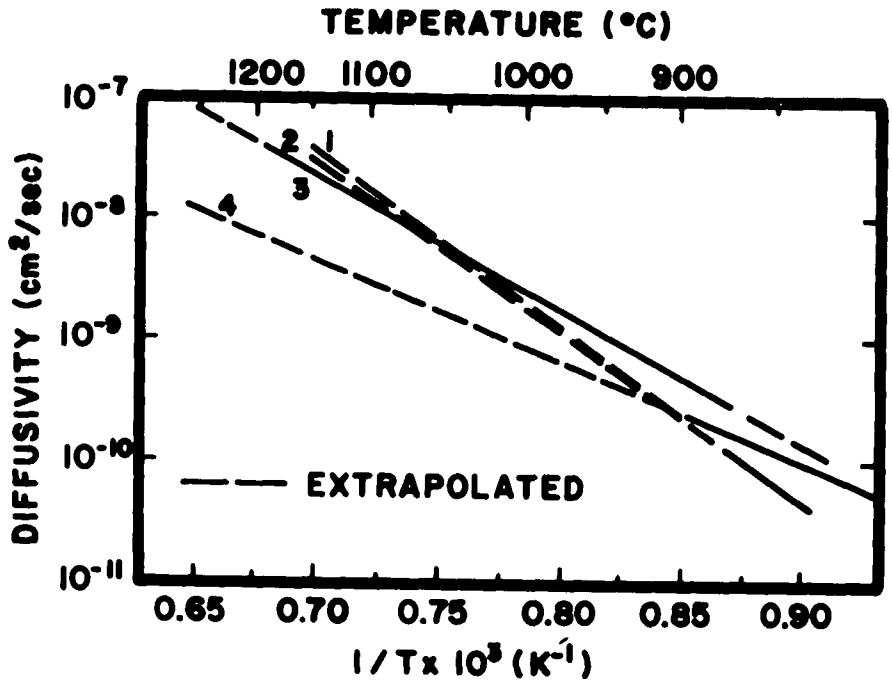

Fig. 4: Extrapolated and experimental tracer and interdiffusion coefficients of P in binary Fe-P and ternary Fe-Ni-P (Ni=1 wt%) alloys determined by tracer and microprobe studies.

1. Matsuyama et al. (1984), tracer study= ternary alloy, range (825°C-770°C).
2. Matsuyama et al. (1984), tracer study=binary alloy, experimental range (825°C-770°C).
3. Heyward and Goldstein (1973), microprobe study=ternary alloy, experimental range (1200°C-900°C).
4. Gruzin and Mural (1963), tracer study=binary alloy, experimental range (900°C-806°C).

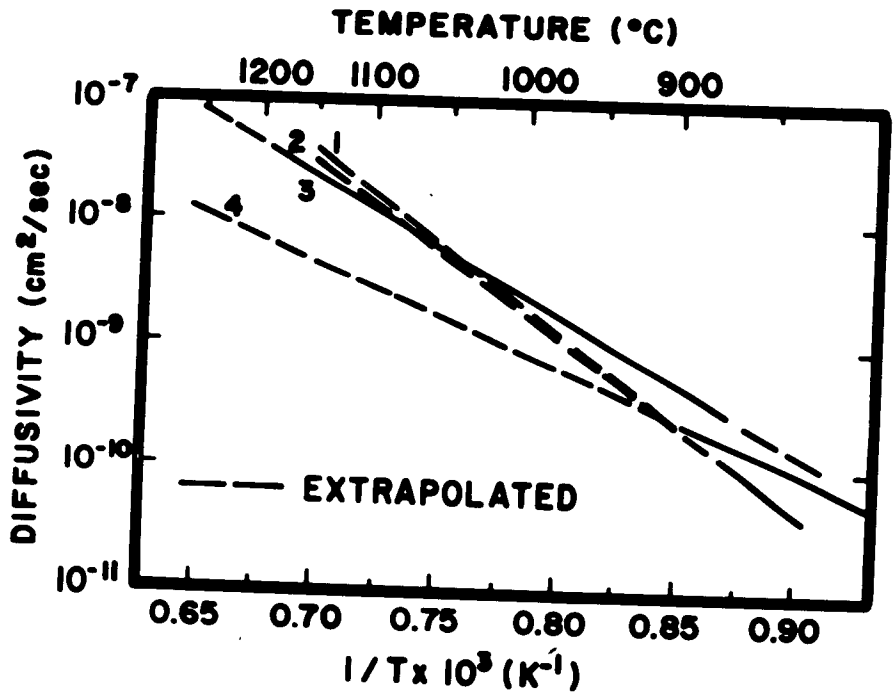

Fig. 4: Extrapolated and experimental tracer and interdiffusion coefficients of P in binary Fe-P and ternary Fe-Ni-P (Ni=1 wt%) alloys determined by tracer and microprobe studies.

1. Matsuyama et al. (1984), tracer study= ternary alloy, range (825°C-770°C).
2. Matsuyama et al. (1984), tracer study=binary alloy, experimental range (825°C-770°C).
3. Heyward and Goldstein (1973), microprobe study=ternary alloy, experimental range (1200°C-900°C).
4. Gruzin and Mural (1963), tracer study=binary alloy, experimental range (900°C-806°C).

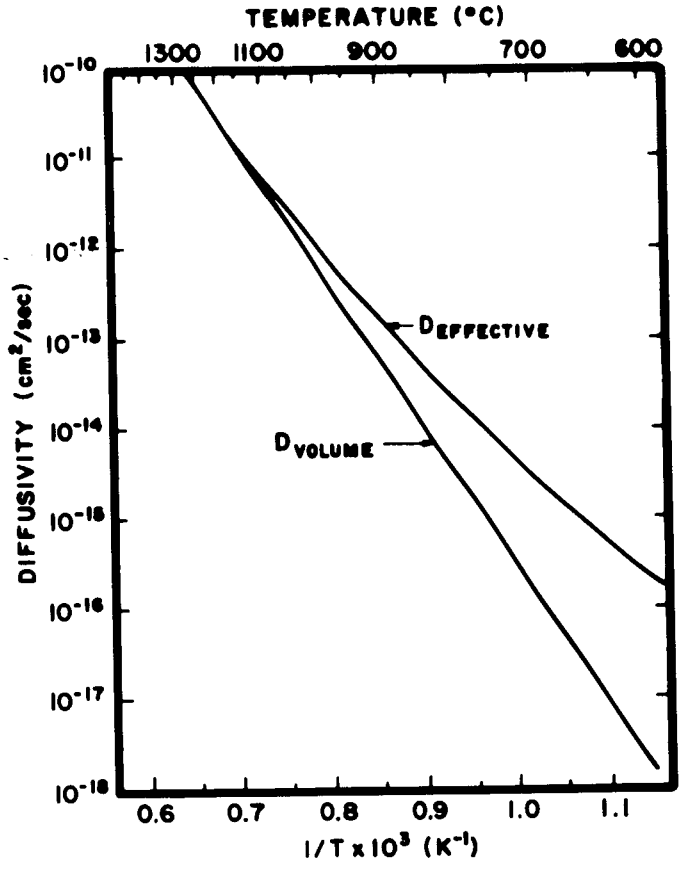

Fig. 5a: Plot of $\tilde{D}_{eff}$ and $\tilde{D}_{vol}$ versus temperature from Hanatate et al. (1978). Experimental range 1287°C-1153°C. D_o and Q values of D_{vol} and D_{GB} are given in Table 4.

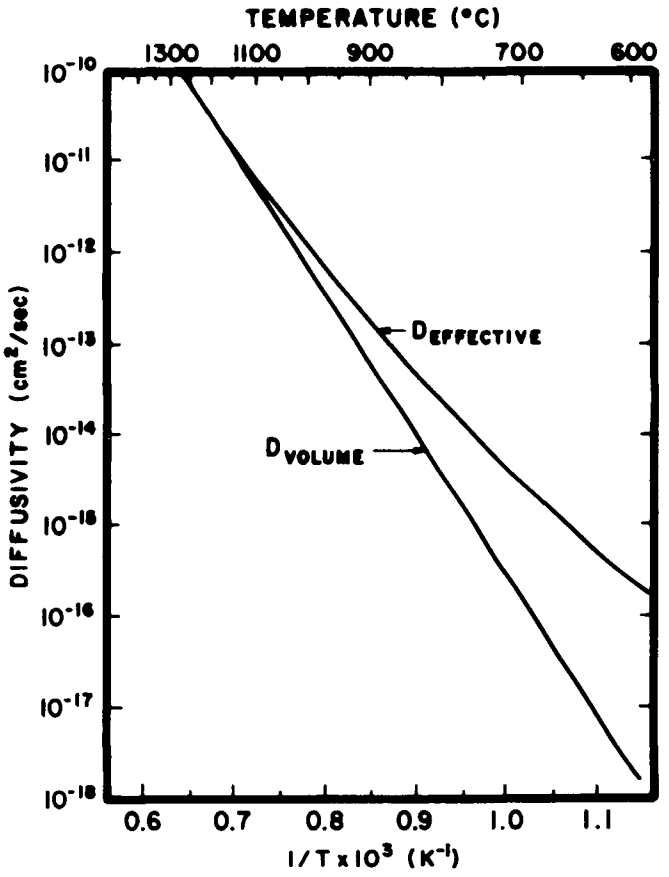

Fig. 5a: Plot of $\tilde{D}_{eff}$ and $\tilde{D}_{vol}$ versus temperature from Hanatate et al. (1978). Experimental range 1287°C-1153°C. D_o and Q values of D_{vol} and D_{GB} are given in Table 4.

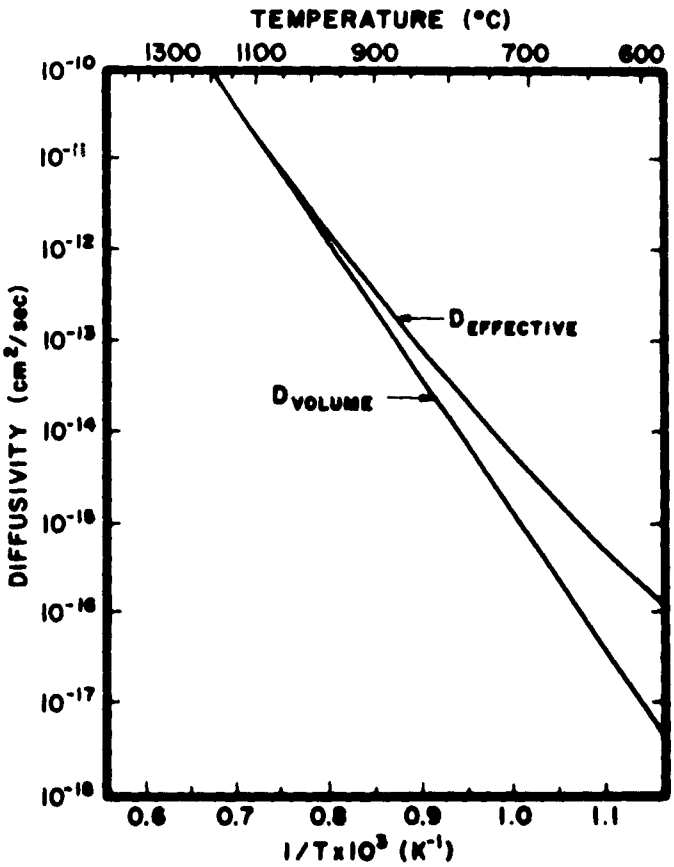

Fig. 5b: Plot of $\tilde{D}_{eff}$ and $\tilde{D}_{vol}$ versus temperature from Krishtal et al. (1967). Experimental range 1200°C-1000°C. D_o and Q values given in Table 4.

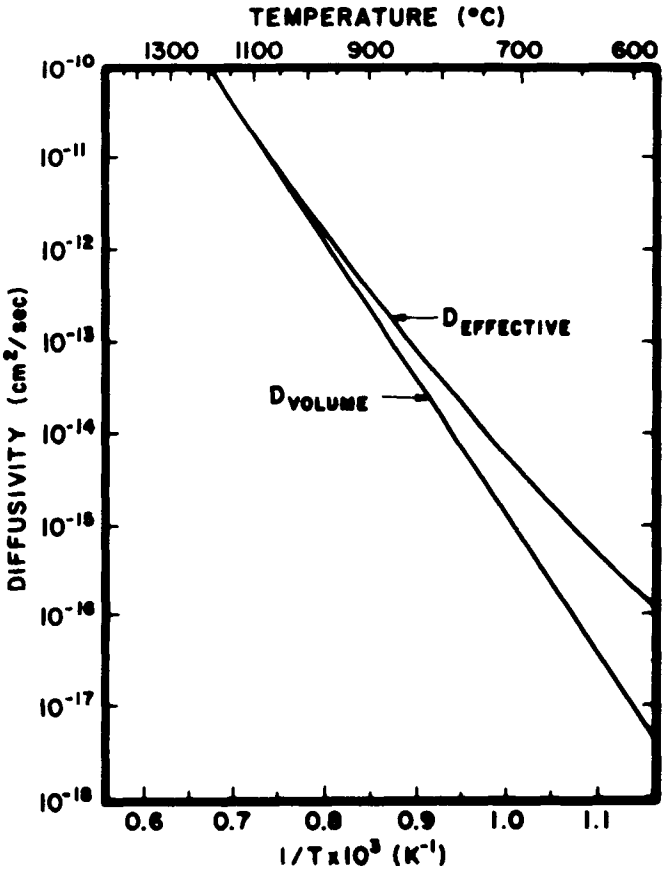

Fig. 5b: Plot of $\tilde{D}_{eff}$ and $\tilde{D}_{vol}$ versus temperature from Krishtal et al. (1967). Experimental range 1200°C-1000°C. D_o and Q values given in Table 4.

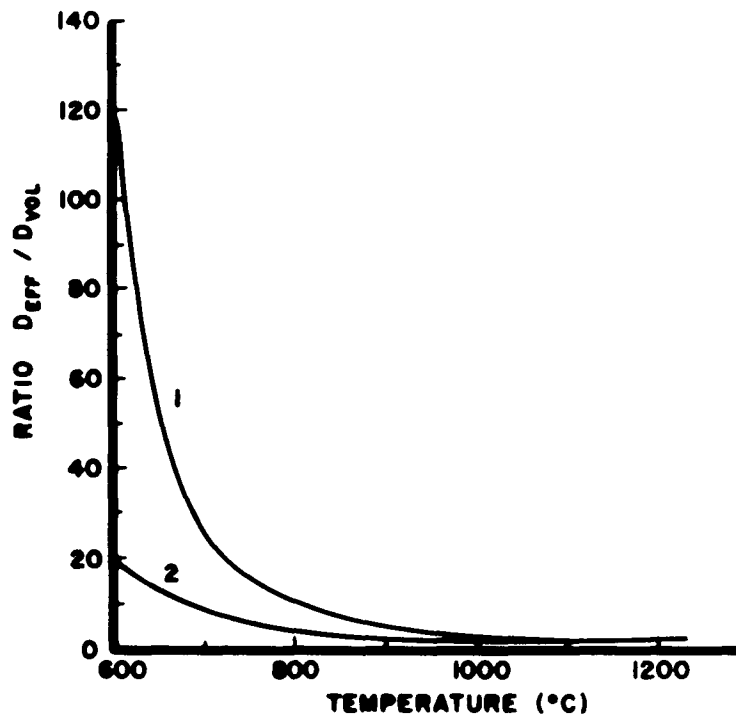

Fig. 6: Ratio of D_{eff}/D_{vol} versus temperature for Fe-Ni diffusion from 1) Hanatate et al. (1978) (Fig. 5a) and 2) Krishtal et al. (1967) (Fig. 5b).

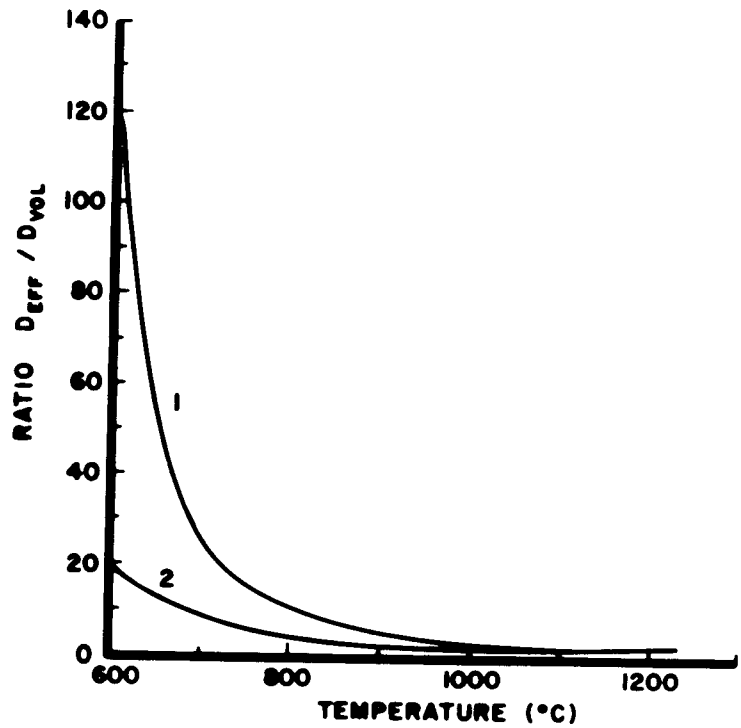

Fig. 6: Ratio of D_{eff}/D_{vol} versus temperature for Fe-Ni diffusion from 1) Hanatate et al. (1978) (Fig. 5a) and 2) Krishtal et al. (1967) (Fig. 5b).

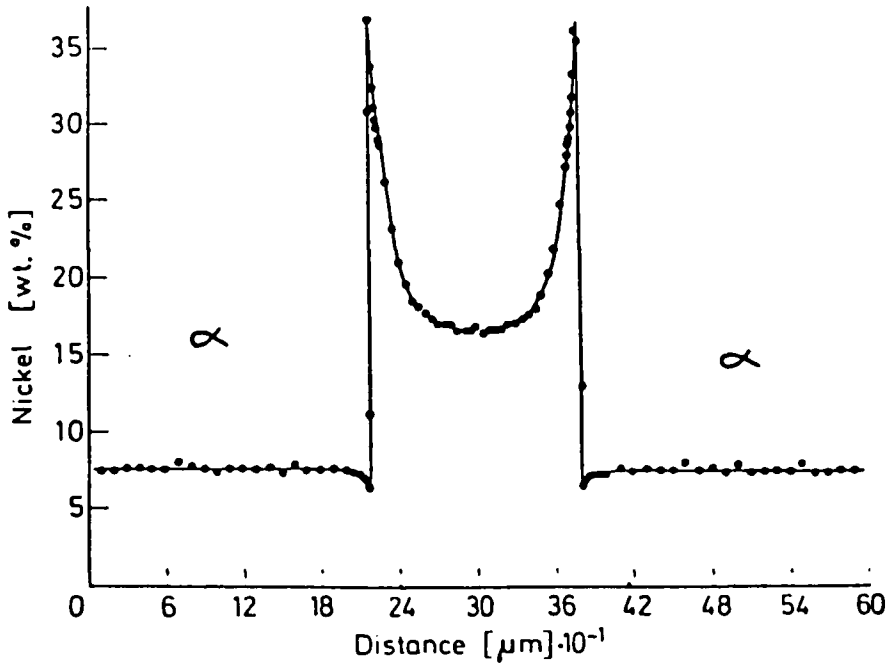

Fig. 7: Concentration gradient of Ni in the Grant meteorite, taken with electron microprobe across a ferrite-austenite-ferrite area. Note the Ni buildup above the bulk composition, C_o = 9.4 wt% Ni at the α-γ interface. Reference Goldstein and Axon (1973).

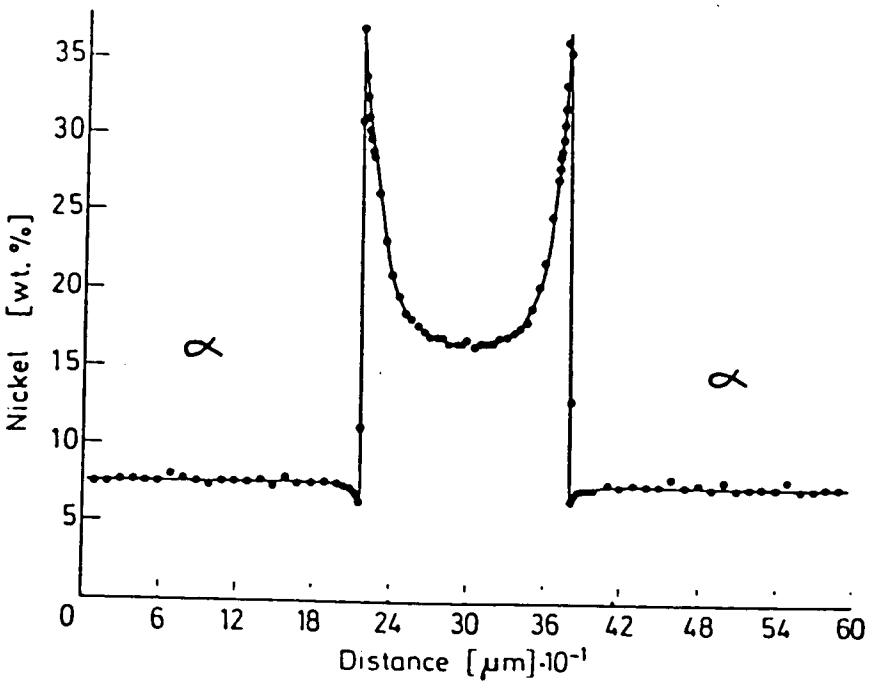

Fig. 7: Concentration gradient of Ni in the Grant meteorite, taken with electron microprobe across a ferrite-austenite-ferrite area. Note the Ni buildup above the bulk composition, C_o = 9.4 wt% Ni at the α-γ interface. Reference Goldstein and Axon (1973).

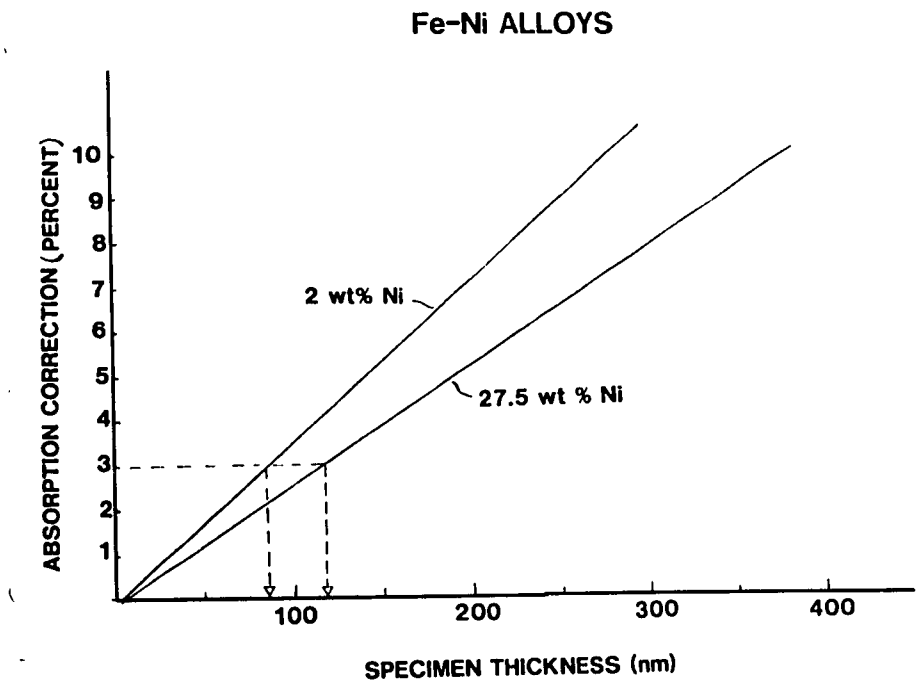

Fig. 8: Percent absorption correction as a function of specimen thickness in Fe-2 wt% Ni and Fe-27.5 wt% Ni alloys.

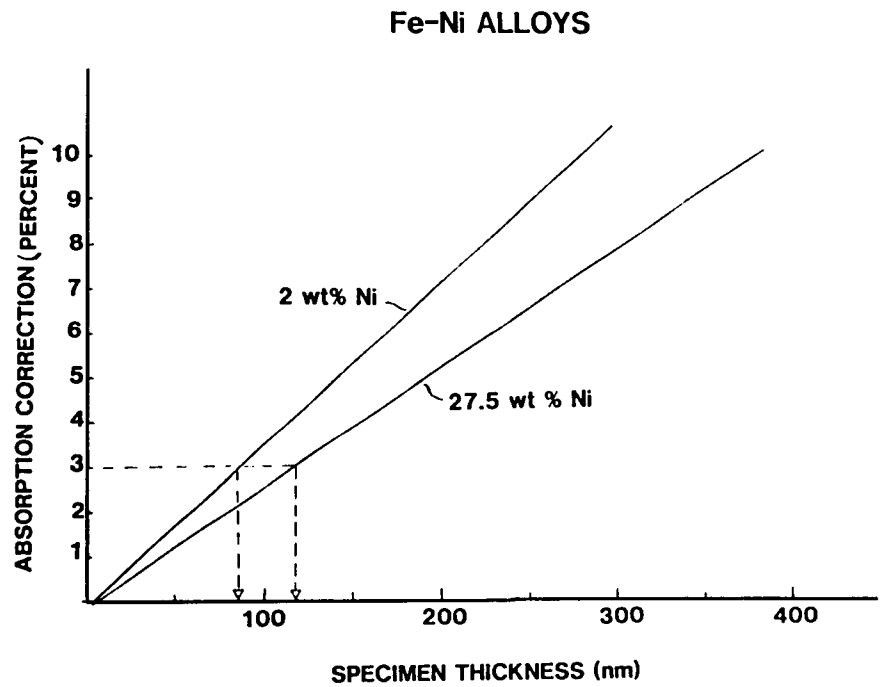

Fig. 8: Percent absorption correction as a function of specimen thickness in Fe-2 wt% Ni and Fe-27.5 wt% Ni alloys.

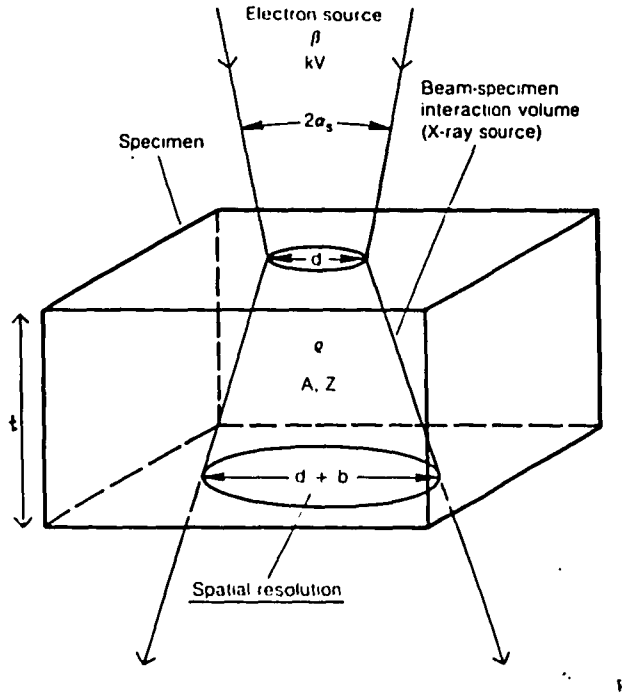

Fig. 9: Schematic of beam broadening in a thin film during AEM. Reference Williams (1984).

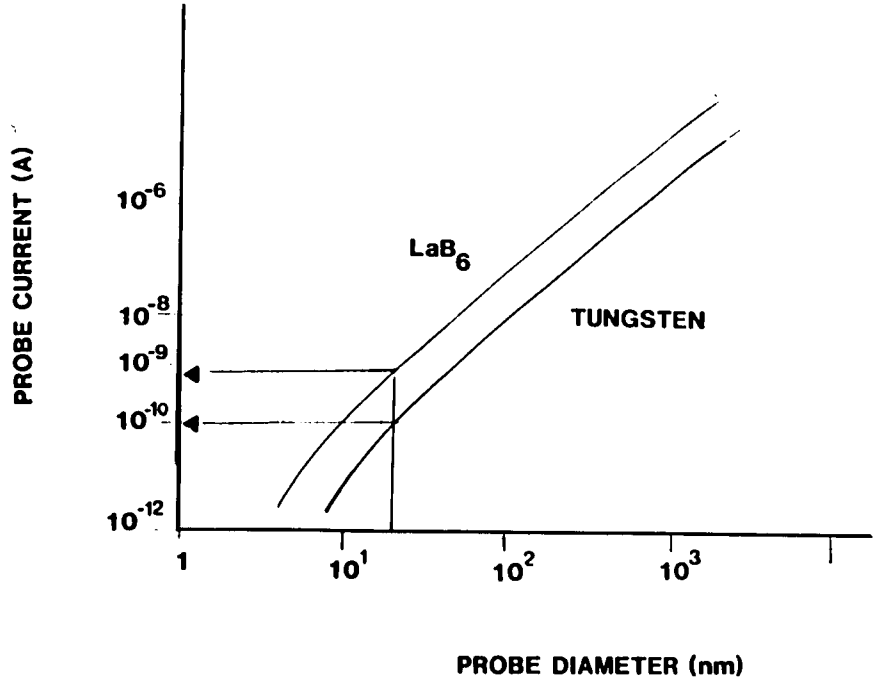

Fig. 10: Typical probe current variation at the specimen with probe diameter for LaB_6 and tungsten electron sources. Reference Zaluzec (1979).

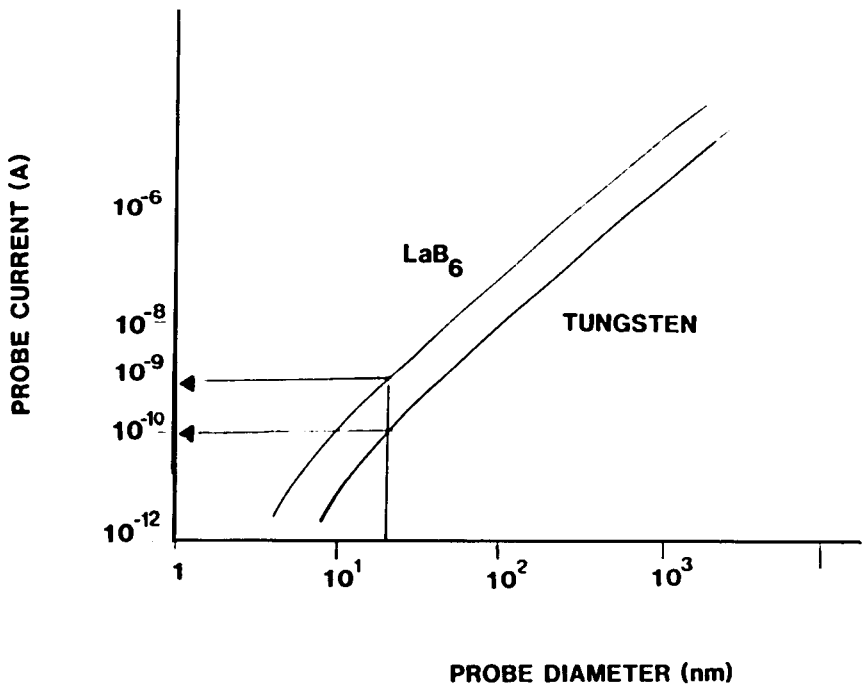

Fig. 10: Typical probe current variation at the specimen with probe diameter for LaB_6 and tungsten electron sources. Reference Zaluzec (1979).

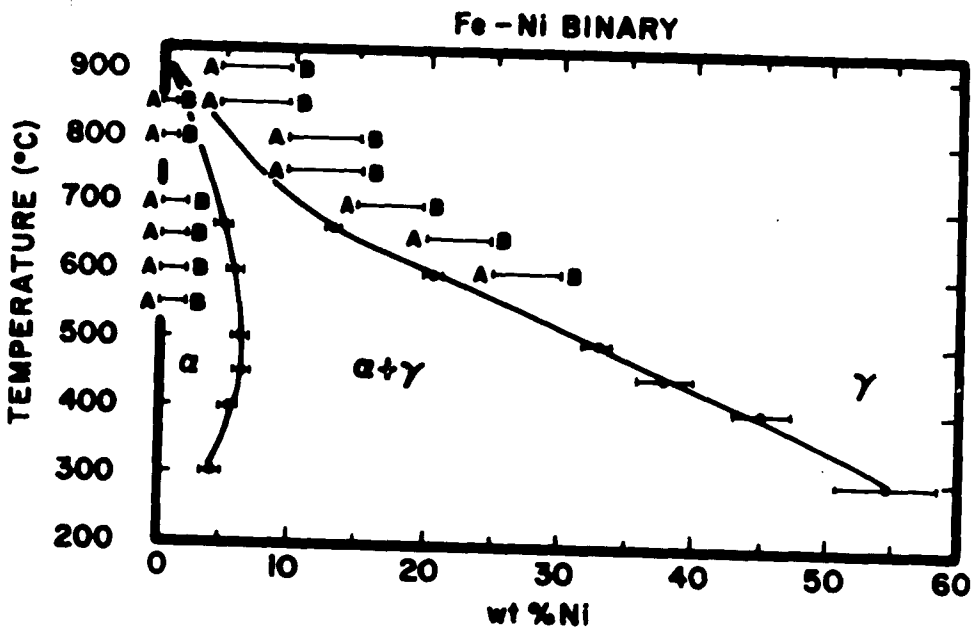

Fig. 11: Fe-Ni phase diagram below 900°C, as determined by Romig and Goldstein (1981). End member compositions A and B of diffusion couples in α and γ are given. Note variation of A and B in γ with temperature.

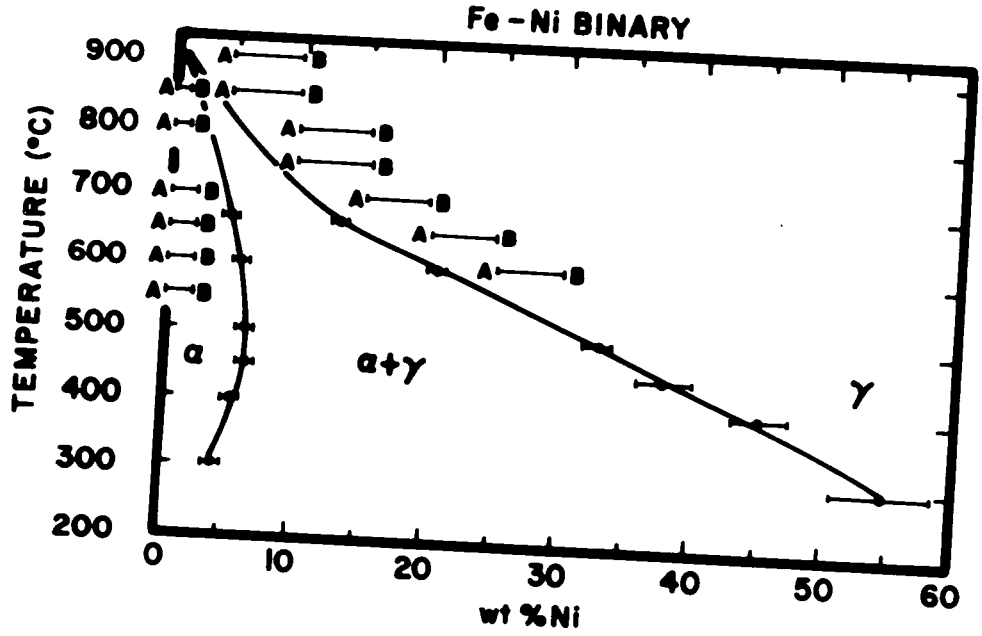

Fig. 11: Fe-Ni phase diagram below 900°C, as determined by Romig and Goldstein (1981). End member compositions A and B of diffusion couples in α and γ are given. Note variation of A and B in γ with temperature.

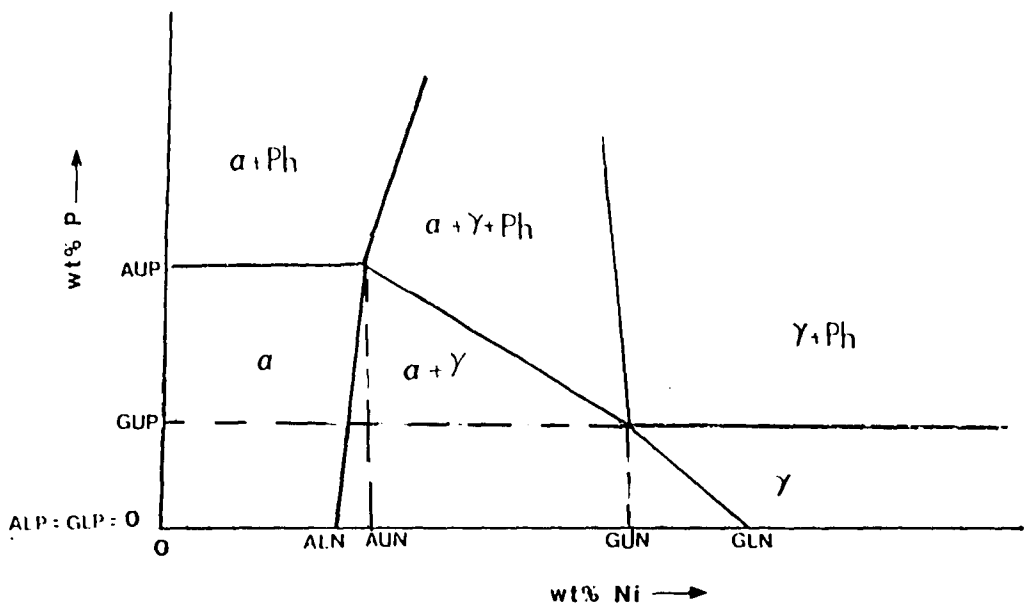

Fig. 12: Schematic of Fe-Ni-P isotherm with nomenclature proposed by Moren and Goldstein. Reference Narayan (1983).

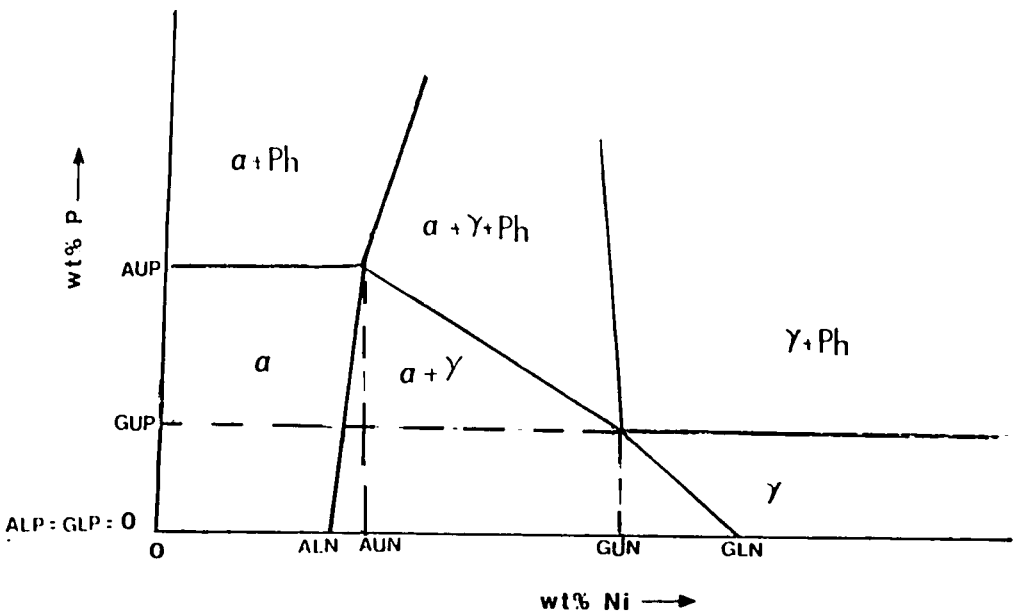

Fig. 12: Schematic of Fe-Ni-P isotherm with nomenclature proposed by Moren and Goldstein. Reference Narayan (1983).

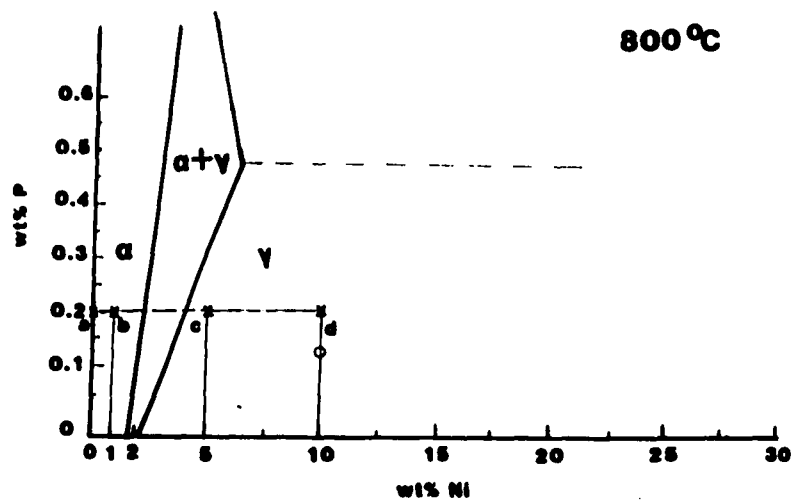

Fig. 13a: Fe-Ni-P isotherm at 800°C, a-b represent ferrite end member compositions, c-d represent the austenite end member compositions, (X) desired end member composition, (O) actual end member composition, if varying significantly from desired composition.

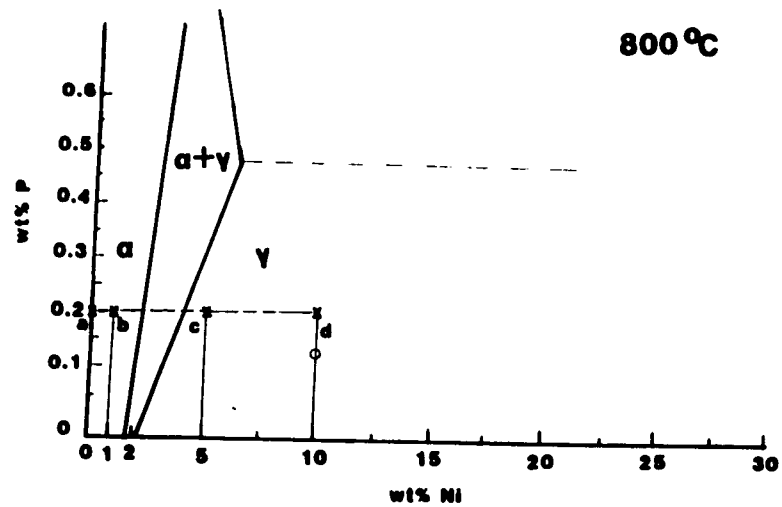

Fig. 13a: Fe-Ni-P isotherm at 800°C, a-b represent ferrite end member compositions, c-d represent the austenite end member compositions, (X) desired end member composition, (O) actual end member composition, if varying significantly from desired composition.

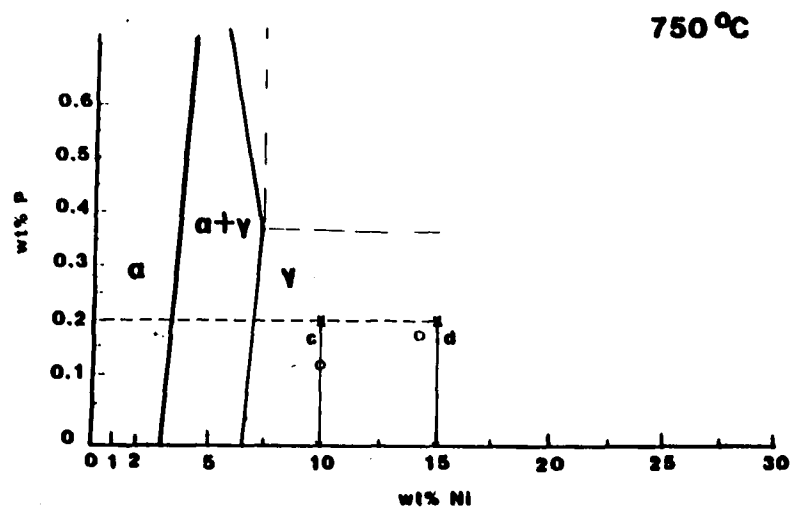

Fig. 13b: Fe-Ni-P isotherm at 750°C, a-b represent ferrite end member compositions, c-d represent the austenite end member compositions, (X) desired end member composition, (O) actual end member composition, if varying significantly from desired composition.

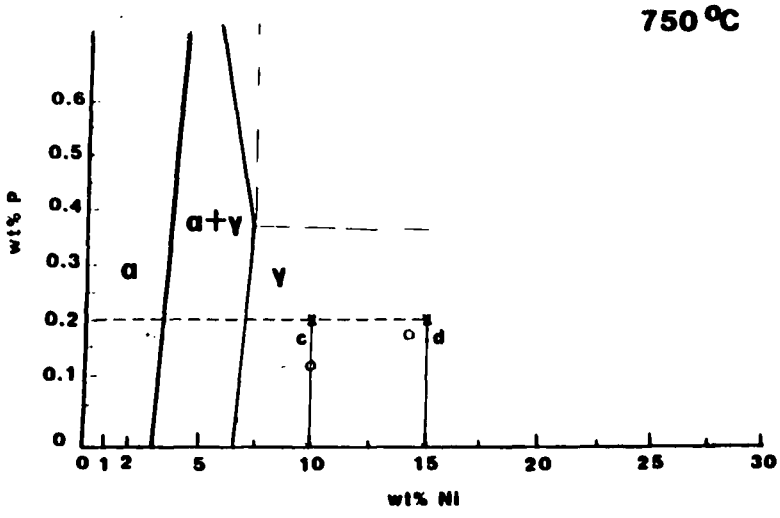

Fig. 13b: Fe-Ni-P isotherm at 750°C, a-b represent ferrite end member compositions, c-d represent the austenite end member compositions, (X) desired end member composition, (O) actual end member composition, if varying significantly from desired composition.

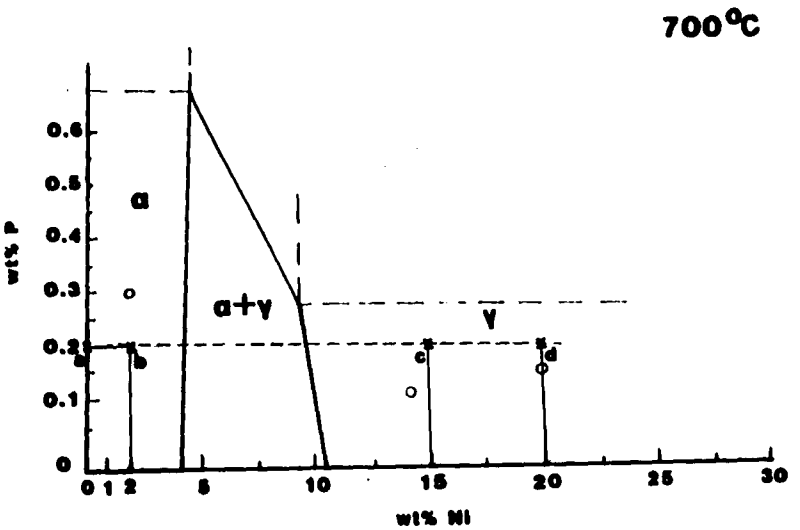

Fig. 13c: Fe-Ni-P isotherm at 700°C, a-b represent ferrite end member compositions, c-d represent the austenite end member compositions, (X) desired end member composition, (O) actual end member composition, if varying significantly from desired composition.

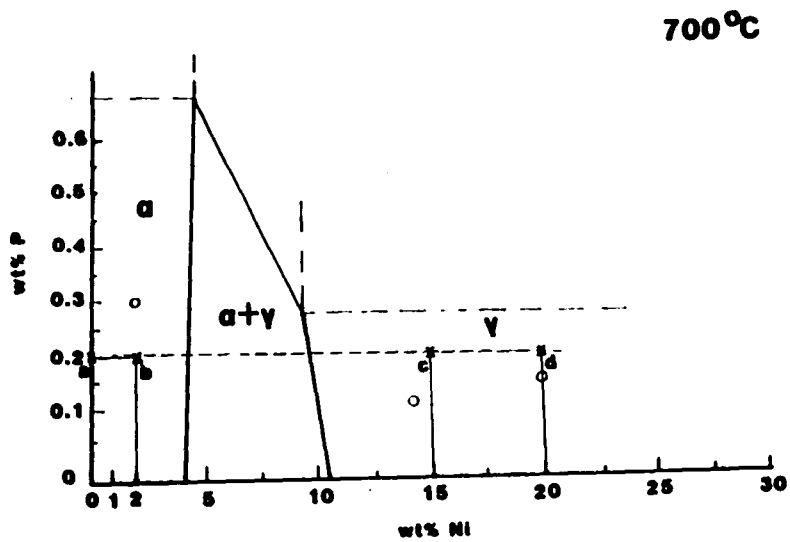

Fig. 13c: Fe-Ni-P isotherm at 700°C, a-b represent ferrite end member compositions, c-d represent the austenite end member compositions, (X) desired end member composition, (O) actual end member composition, if varying significantly from desired composition.

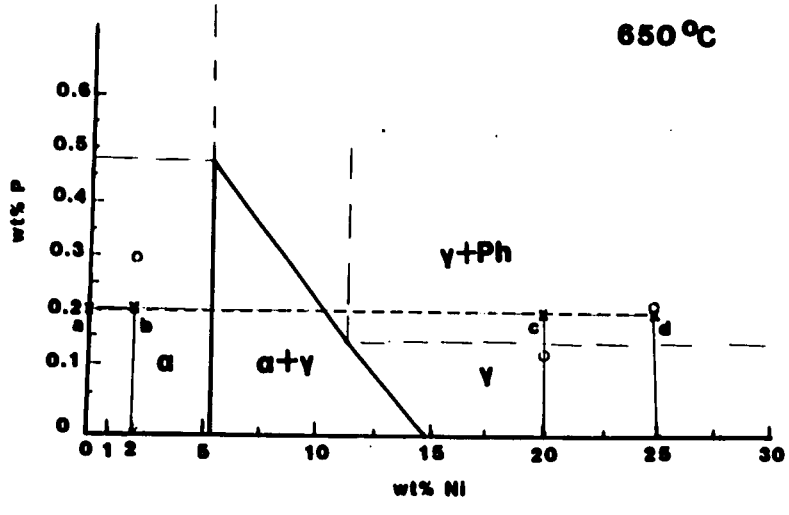

Fig. 13d: Fe-Ni-P isotherm at 650°C, a-b represent ferrite end member compositions, c-d represent the austenite end member compositions, (X) desired end member composition, (O) actual end member composition, if varying significantly from desired composition.

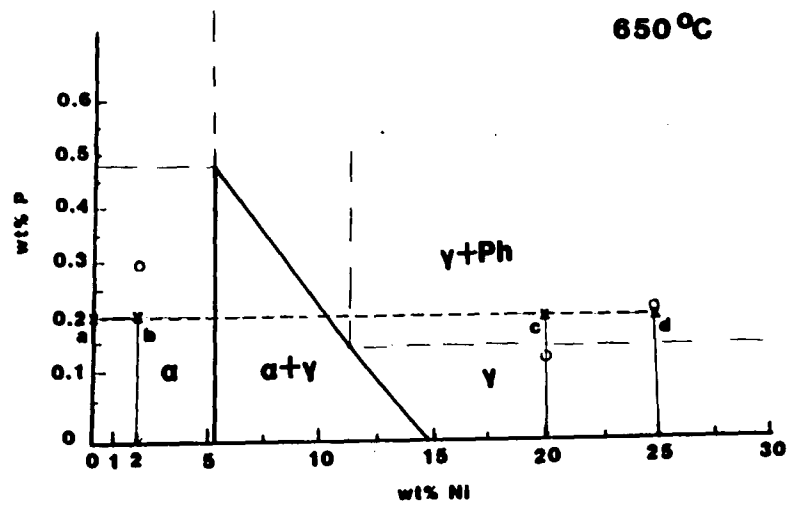

Fig. 13d: Fe-Ni-P isotherm at 650°C, a-b represent ferrite end member compositions, c-d represent the austenite end member compositions, (X) desired end member composition, (O) actual end member composition, if varying significantly from desired composition.

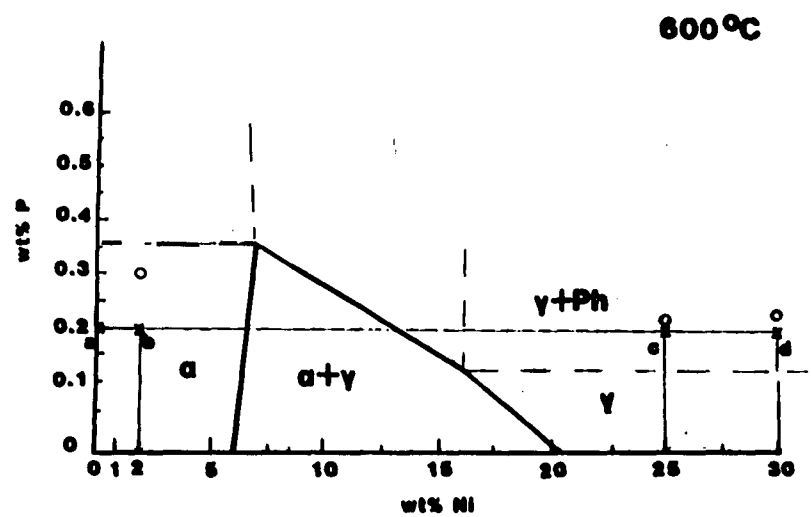

Fig. 13e: Fe-Ni-P isotherm at 600°C, a-b represent ferrite end member compositions, c-d represent the austenite end member compositions, (X) desired end member composition, (O) actual end member composition, if varying significantly from desired composition.

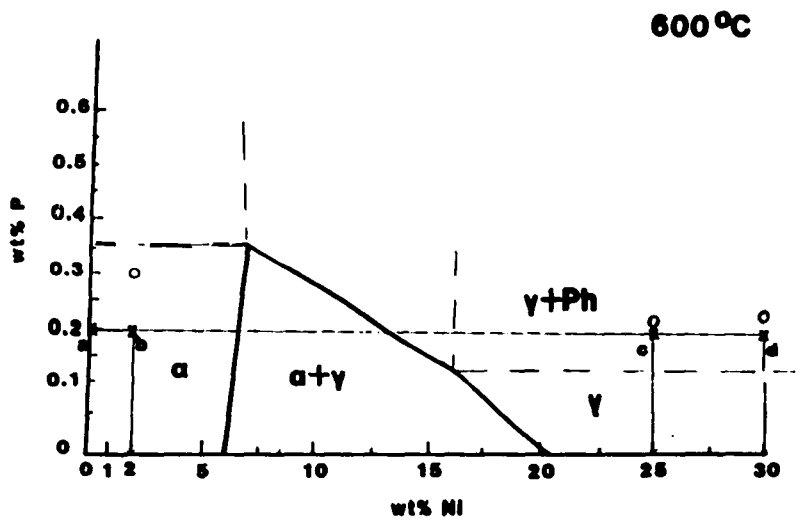

Fig. 13e: Fe-Ni-P isotherm at 600°C, a-b represent ferrite end member compositions, c-d represent the austenite end member compositions, (X) desired end member composition, (O) actual end member composition, if varying significantly from desired composition.

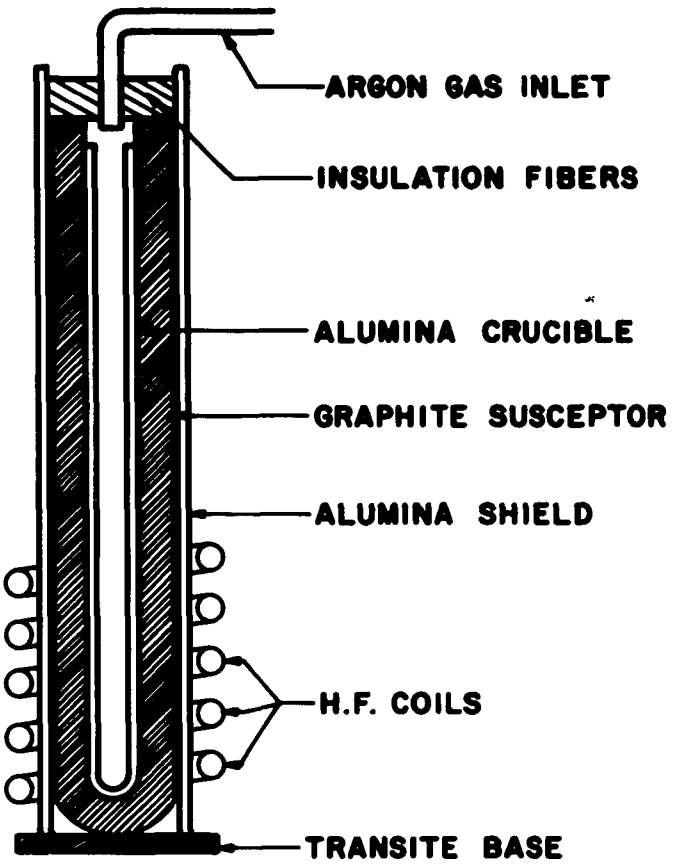

Fig. 14: Schematic representation of the set-up used to melt the Fe-Ni and Fe-Ni-P alloys.

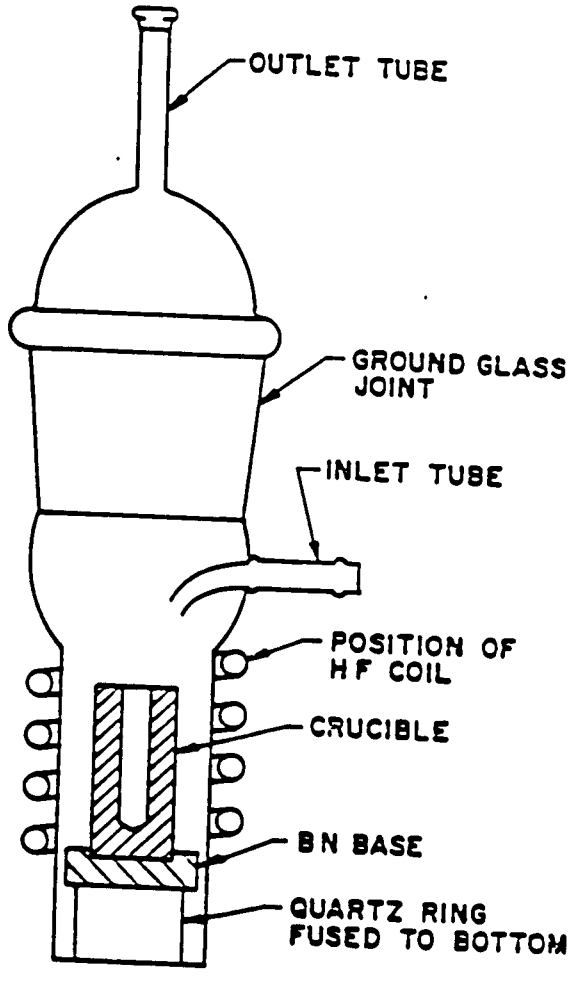

Fig. 15: Schematic representation of the set-up used to remelt the Fe-Ni and the Fe-Ni-P alloys. Reference Romig (1980).

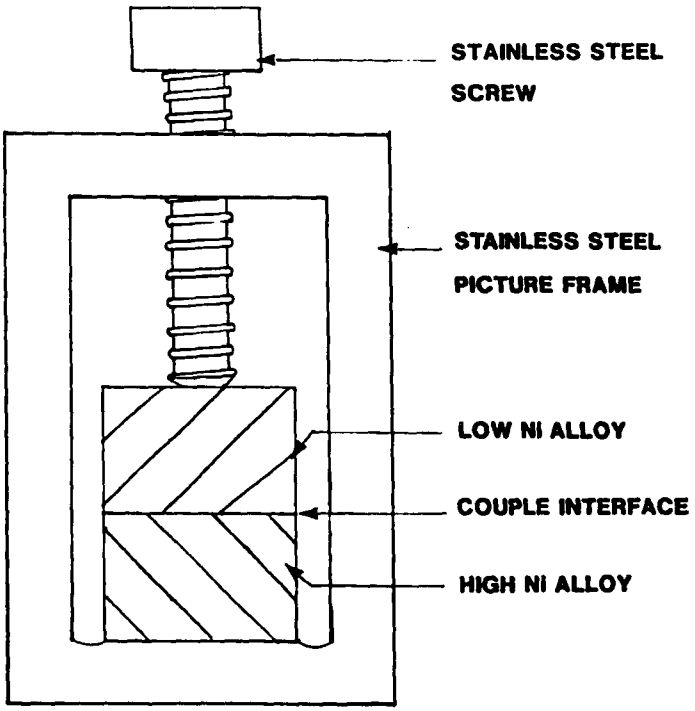

Fig. 16: Schematic representation of a diffusion clamp.

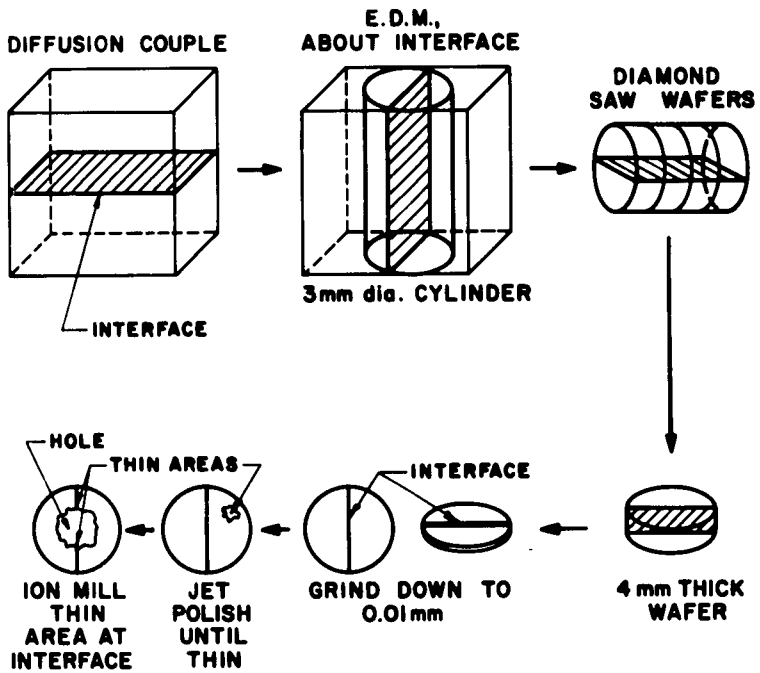

Fig. 17: Schematic of specimen preparation for AEM starting with a bonded diffusion couple. Note location of bond interface during the various stages of specimen preparation.

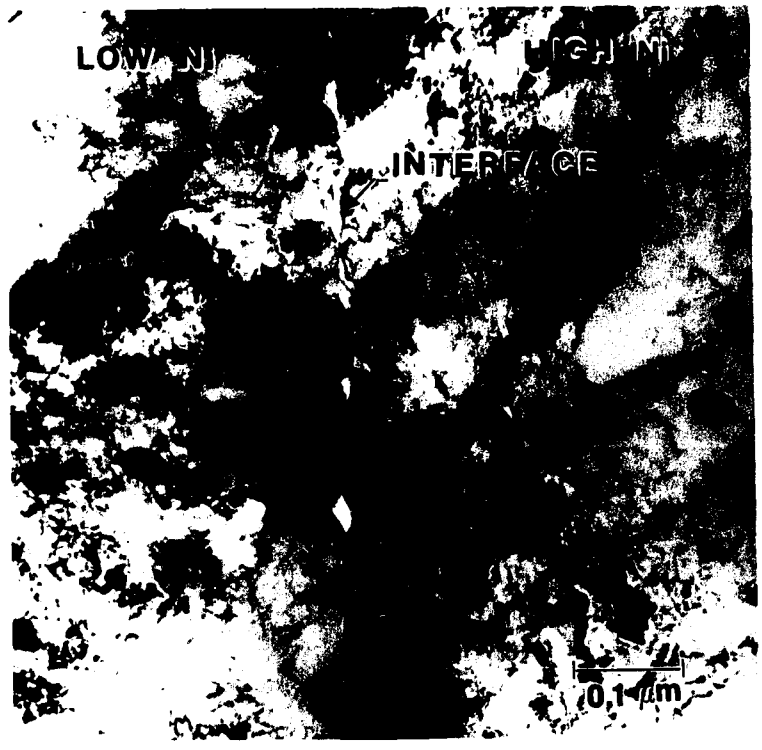

Fig. 18: TEM photomicrograph of a diffusion couple's bond interface with contamination spots indicating emplacement of point analysis during the generation of a Ni concentration profile. Note the smallest step size between points is 50 nm.

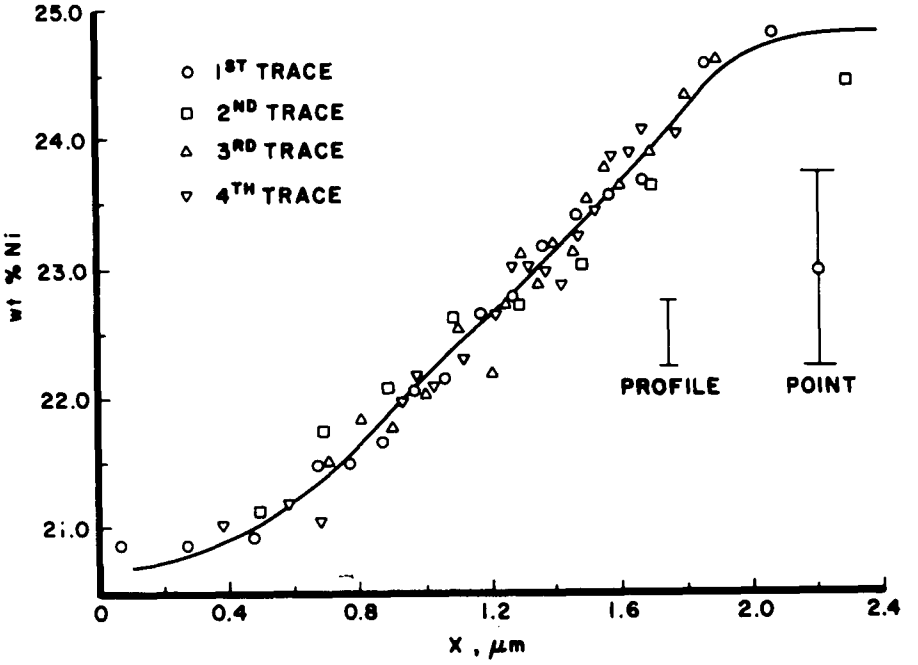

Fig. 19: Experimental Ni concentration gradient from F20NP-F25NP ternary γ couple diffused at 650°C for 121 days. Error bars for individual points and for the best fit profile are given. 4 traces were obtained from the couple.

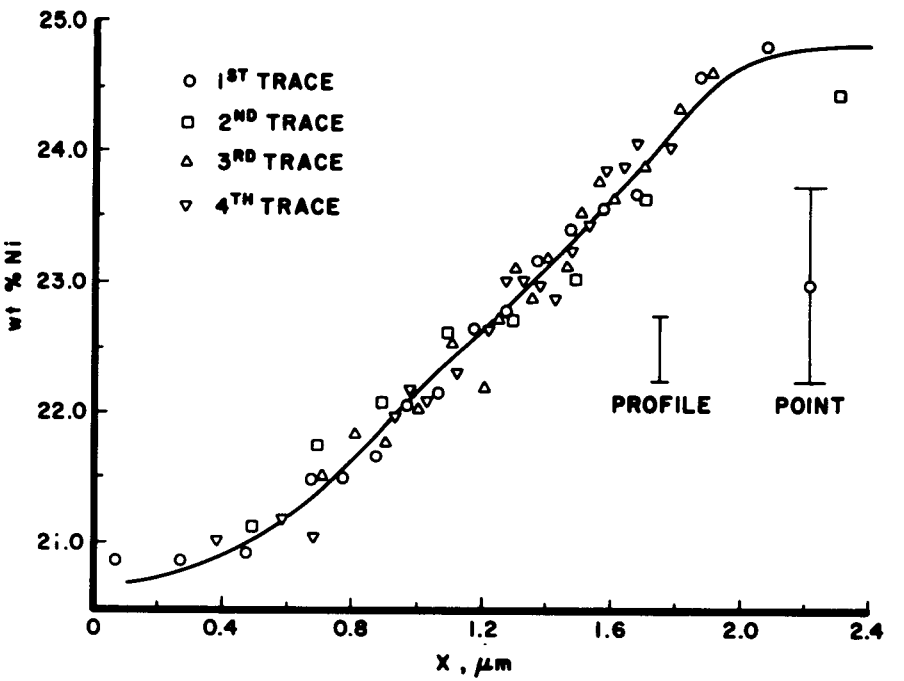

Fig. 19: Experimental Ni concentration gradient from F20NP-F25NP ternary γ couple diffused at 650°C for 121 days. Error bars for individual points and for the best fit profile are given. 4 traces were obtained from the couple.

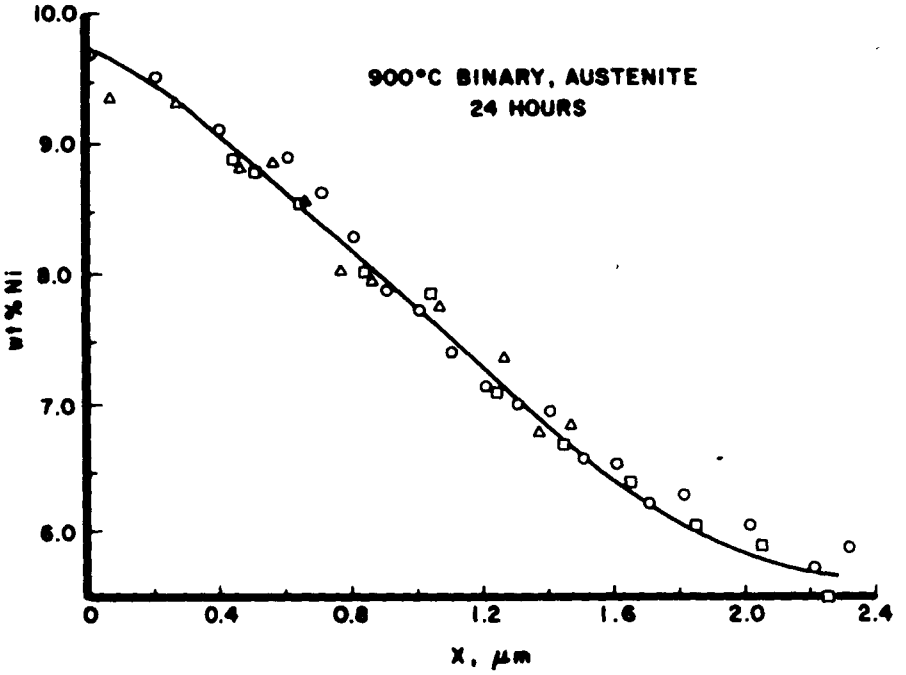

Fig. 20: Experimental Ni concentration gradient for F5N-F10N binary γ couple diffused at 911°C for 24 hrs. 3 traces were obtained from the couple.

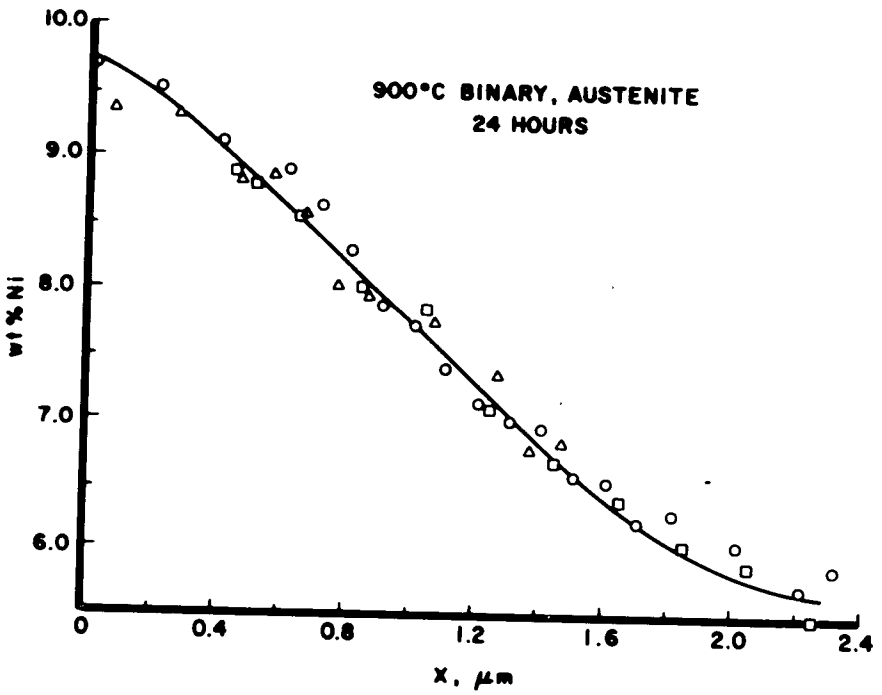

Fig. 20: Experimental Ni concentration gradient for F5N-F10N binary γ couple diffused at 911°C for 24 hrs. 3 traces were obtained from the couple.

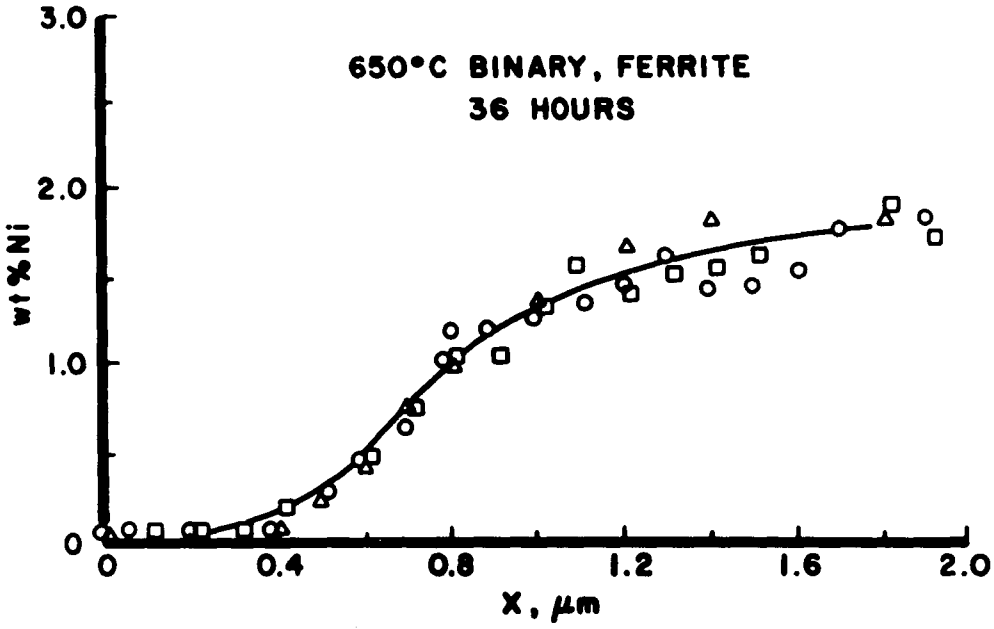

Fig. 21: Experimental Ni concentration gradient for F-F2N binary α couple diffused at 654°C for 36 hours. 3 traces were obtained during analysis.

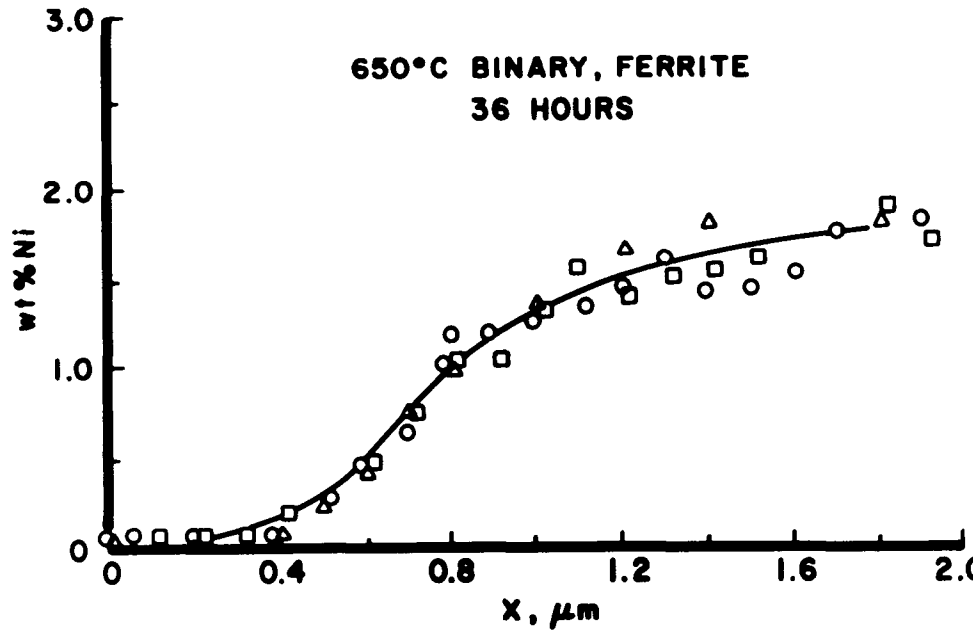

Fig. 21: Experimental Ni concentration gradient for F-F2N binary α couple diffused at 654°C for 36 hours. 3 traces were obtained during analysis.

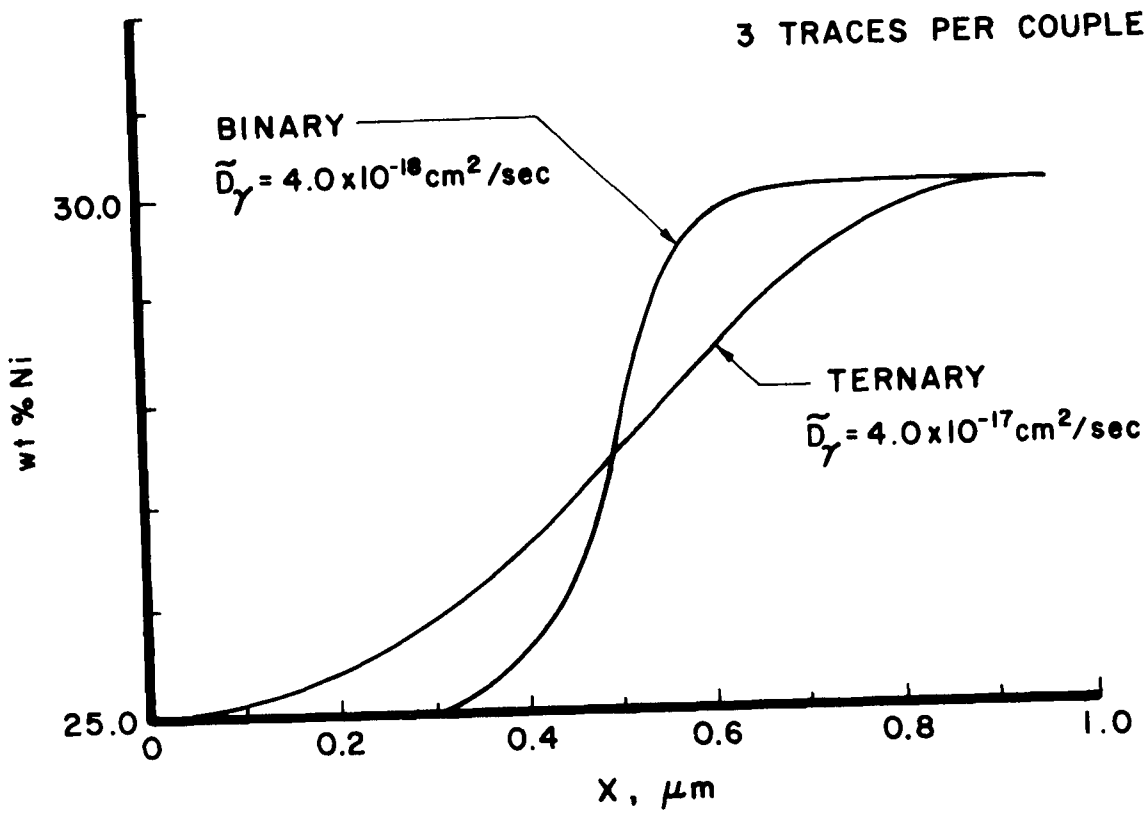

Fig. 22: Comparison between the binary and ternary γ couples F25N-F30N and F25NP-F30NP diffused together at 610°C for 62 days. The binary diffusion distance was ~0.4 μm and the ternary diffusion distance was ~0.9 μm. The curves were adjusted to compensate for differences in the end member compositions of the binary and the ternary couple.

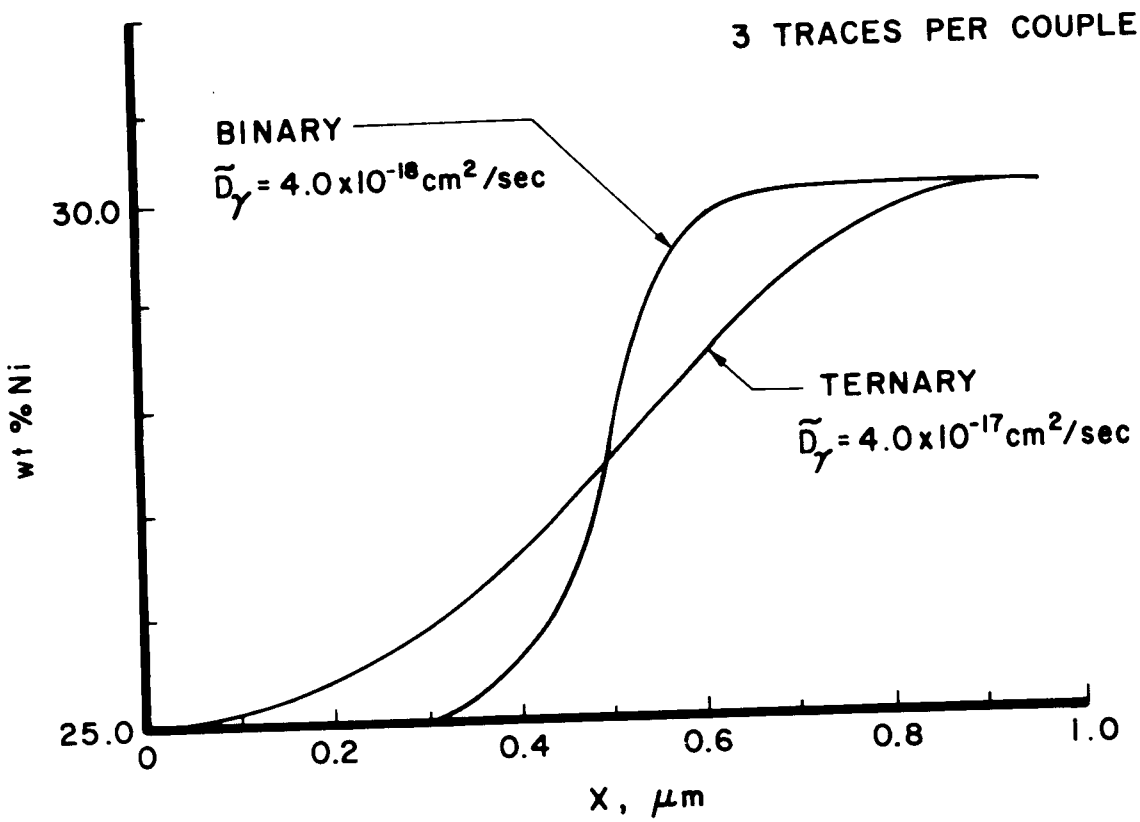

Fig. 22: Comparison between the binary and ternary γ couples F25N-F30N and F25NP-F30NP diffused together at 610°C for 62 days. The binary diffusion distance was ~0.4 μm and the ternary diffusion distance was ~0.9 μm. The curves were adjusted to compensate for differences in the end member compositions of the binary and the ternary couple.

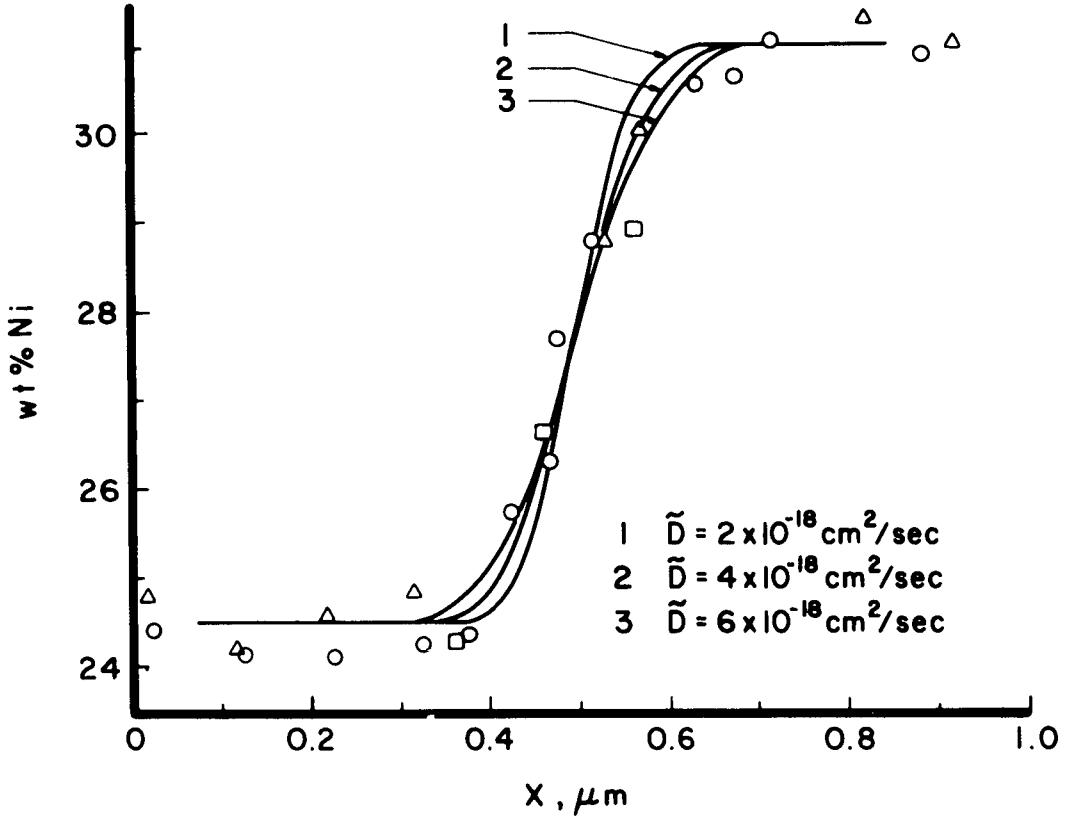

Fig. 23: Experimental Ni concentration gradient for F25N-F30 N binary γ couple diffused at 610°C for 2 months. Grube solutions using selected diffusivities between 2×10^{-18} cm^2/sec and 6×10^{-18} cm^2/sec were calculated.

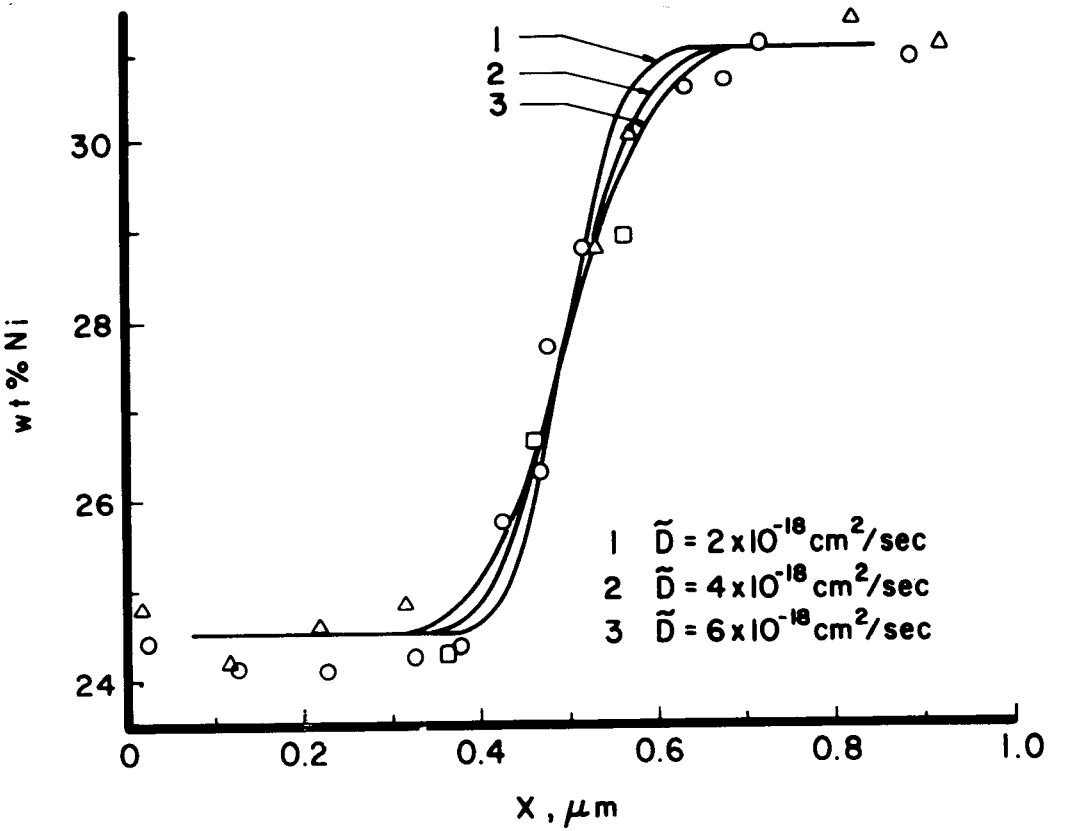

Fig. 23: Experimental Ni concentration gradient for F25N-F30 N binary γ couple diffused at 610°C for 2 months. Grube solutions using selected diffusivities between 2×10^{-18} cm^2/sec and 6×10^{-18} cm^2/sec were calculated.

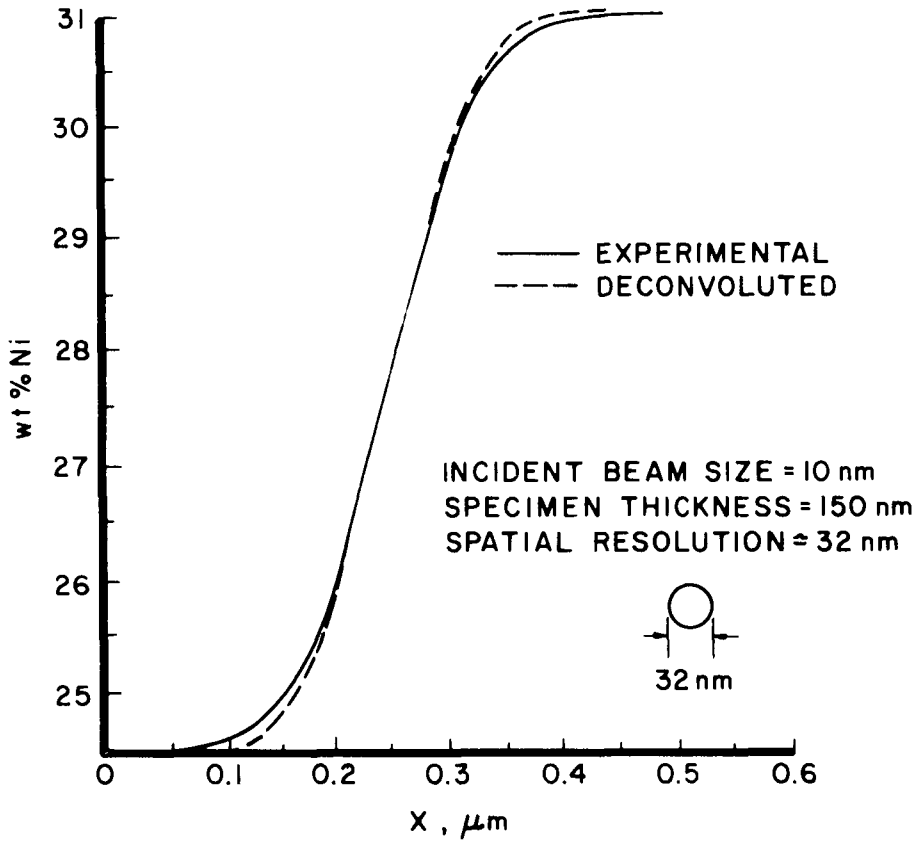

Fig. 24: Profile convolution of an assumed composition gradient using the F25N-F30N binary γ couple diffused at 610°C. $\tilde{D} \simeq 4 \times 10^{-18}$ cm^2/sec. The deconvoluted curve is the assumed composition gradient. The experimental curve is the calculated composition gradient which includes the effect of beam broadening.

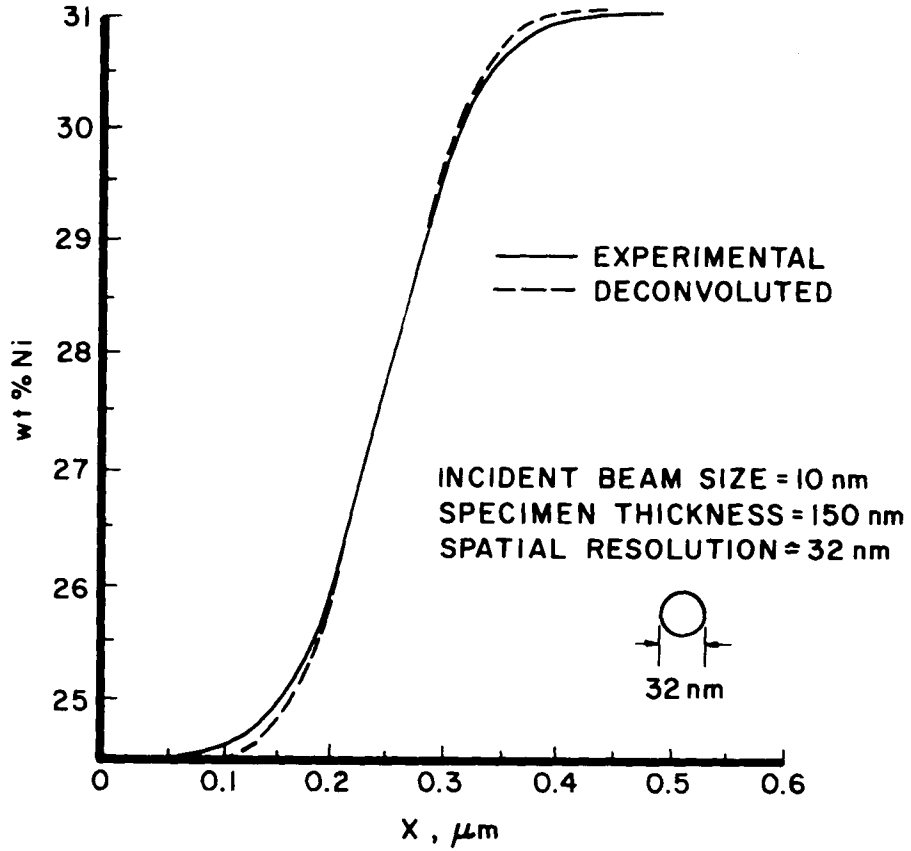

Fig. 24: Profile convolution of an assumed composition gradient using the F25N-F30N binary γ couple diffused at 610°C. $\tilde{D} \simeq 4 \times 10^{-18}$ cm^2/sec. The deconvoluted curve is the assumed composition gradient. The experimental curve is the calculated composition gradient which includes the effect of beam broadening.

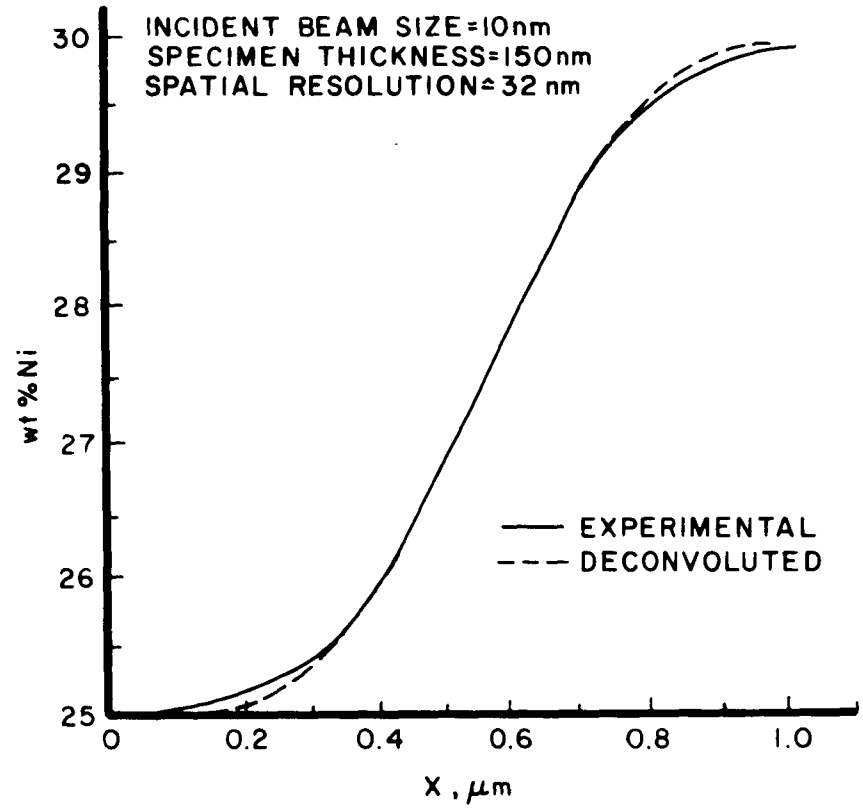

Fig. 25: Profile convolution of an assumed composition gradient using F25NP-F30NP ternary γ couple diffused at 610°C. ($\tilde{D} \simeq 4 \times 10^{-17}$ cm^2/sec.) This concentration gradient is more representative of the composition profiles measured in this study. The deconvoluted curve is the assumed composition gradient. The experimental curve is the calculated composition gradient which includes the effect of beam broadening.

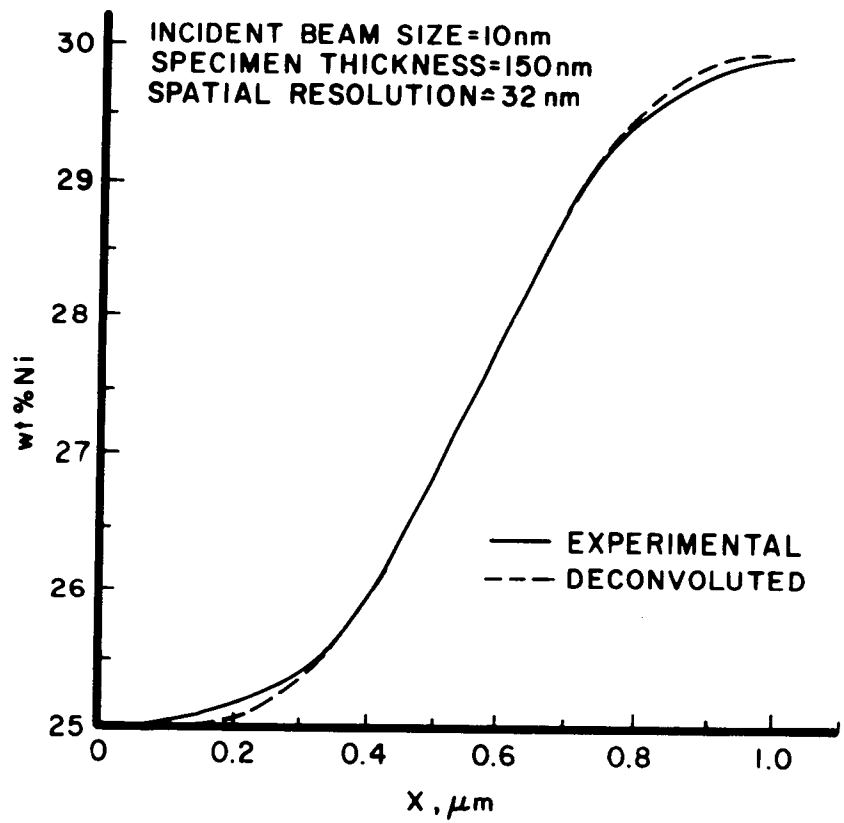

Fig. 25: Profile convolution of an assumed composition gradient using F25NP-F30NP ternary γ couple diffused at 610°C. ($\tilde{D} \simeq 4 \times 10^{-17}$ cm^2/sec.) This concentration gradient is more representative of the composition profiles measured in this study. The deconvoluted curve is the assumed composition gradient. The experimental curve is the calculated composition gradient which includes the effect of beam broadening.

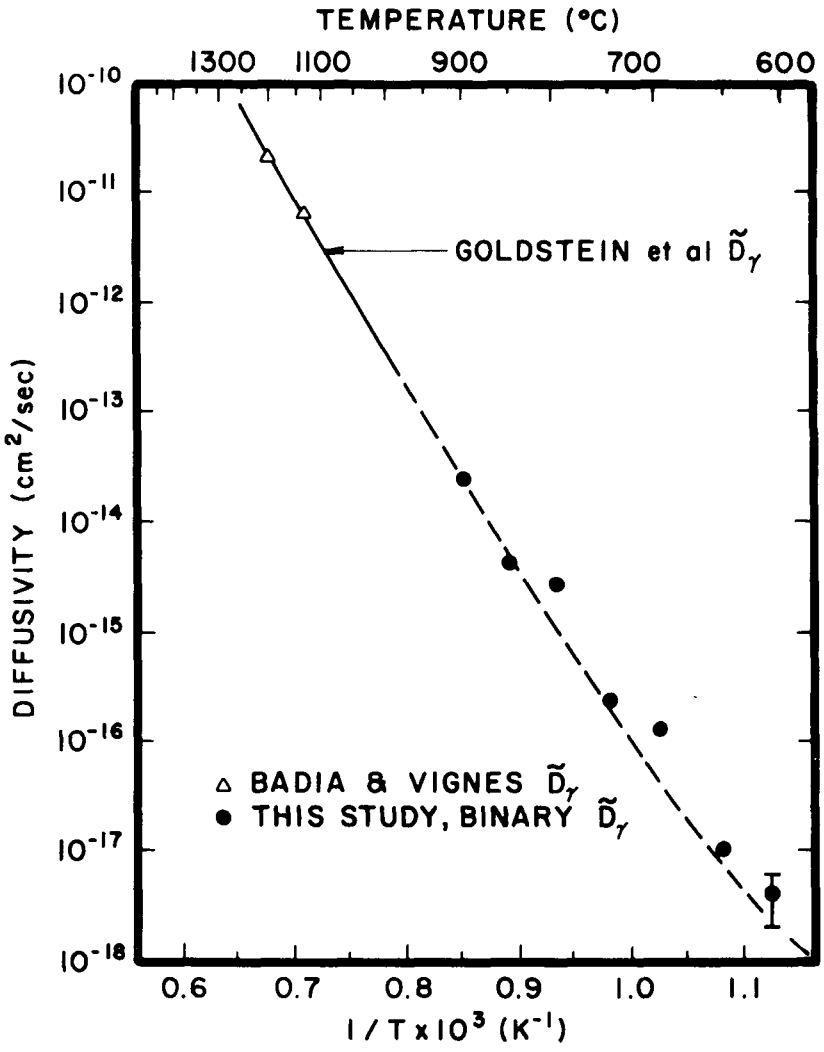

Fig. 26: Experimental results of binary γ interdiffusion coefficient as a function of temperature. Range 900°C to 610°C. The error bars on D_γ binary at 610°C indicate the possible range of $\tilde{D}_\gamma$ values at that temperature.

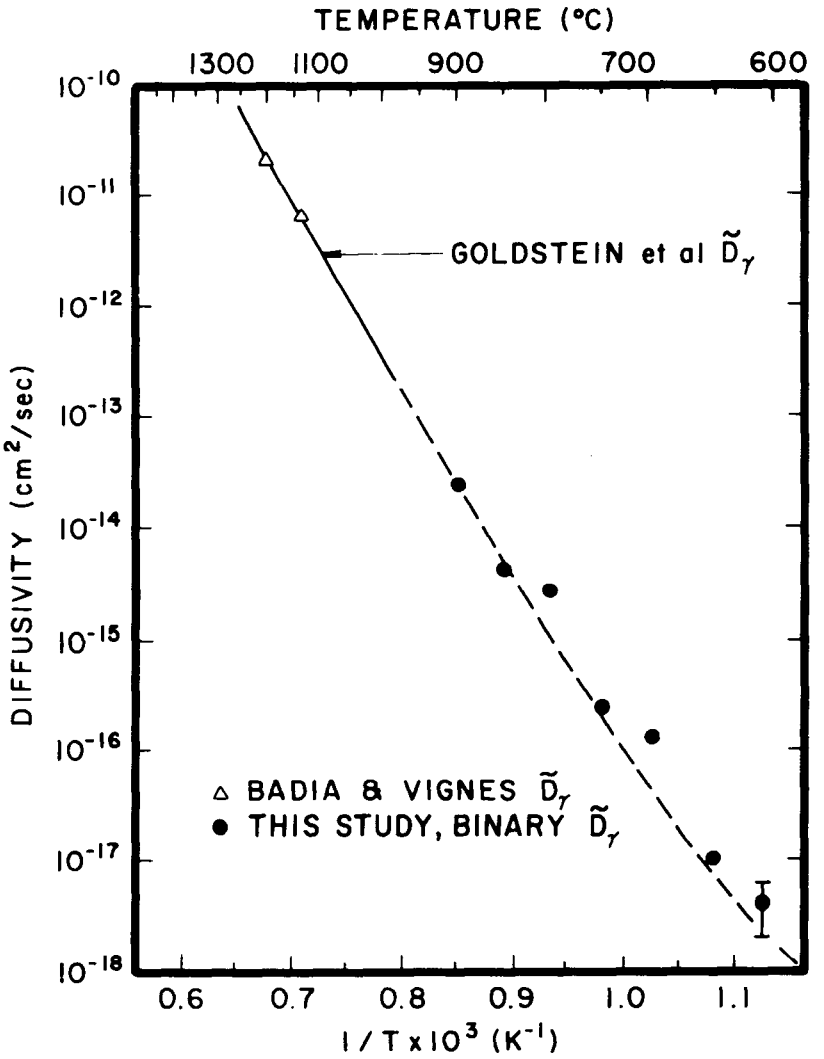

Fig. 26: Experimental results of binary γ interdiffusion coefficient as a function of temperature. Range 900°C to 610°C. The error bars on $\tilde{D}_\gamma$ binary at 610°C indicate the possible range of $\tilde{D}_\gamma$ values at that temperature.

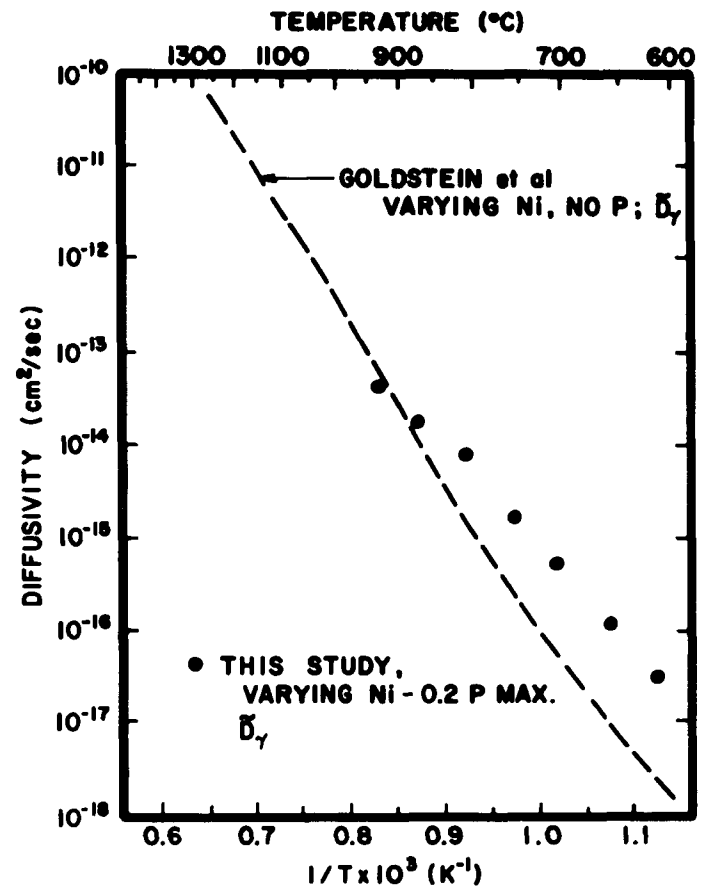

Fig. 27: Experimental results of ternary γ interdiffusion coefficient as a function of temperature.

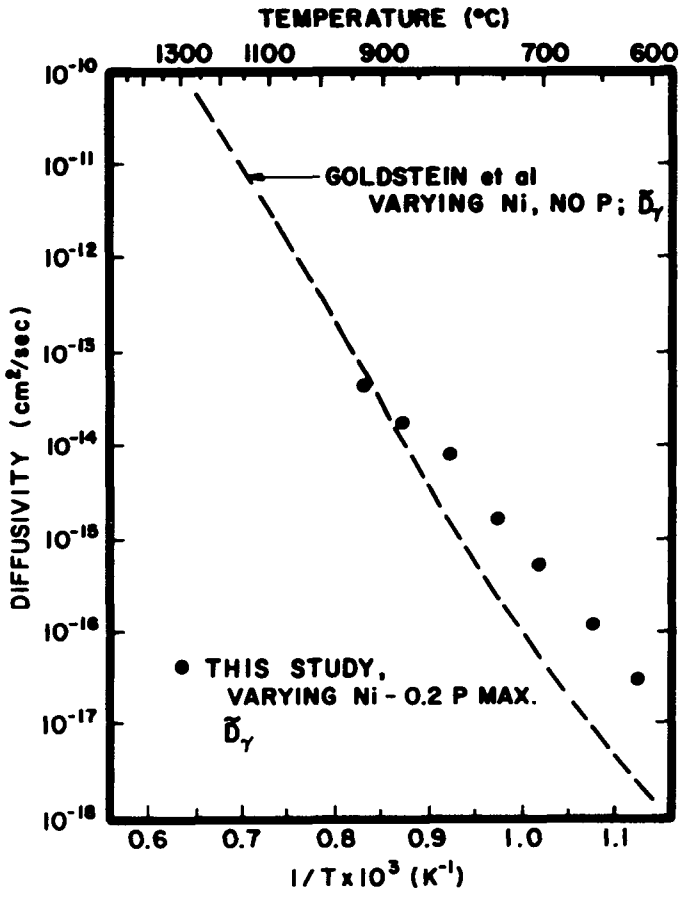

Fig. 27: Experimental results of ternary γ interdiffusion coefficient as a function of temperature.

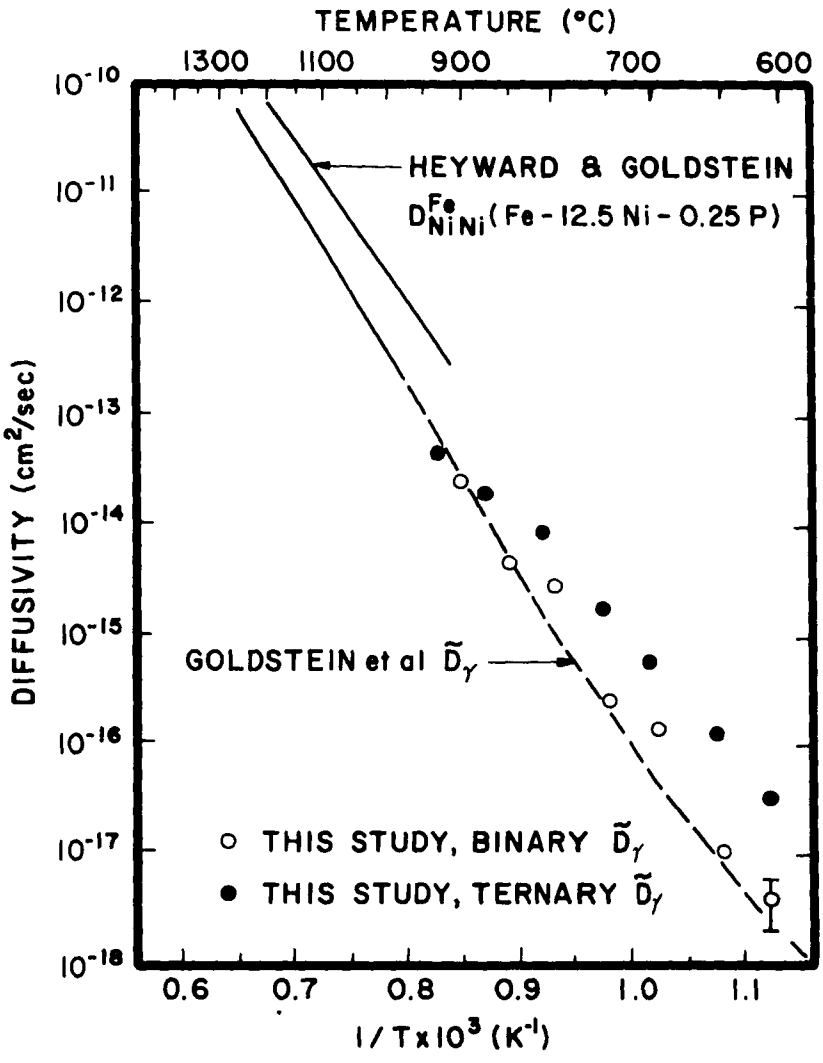

Fig. 28: Comparison between experimental binary and ternary interdiffusion coefficients in γ.

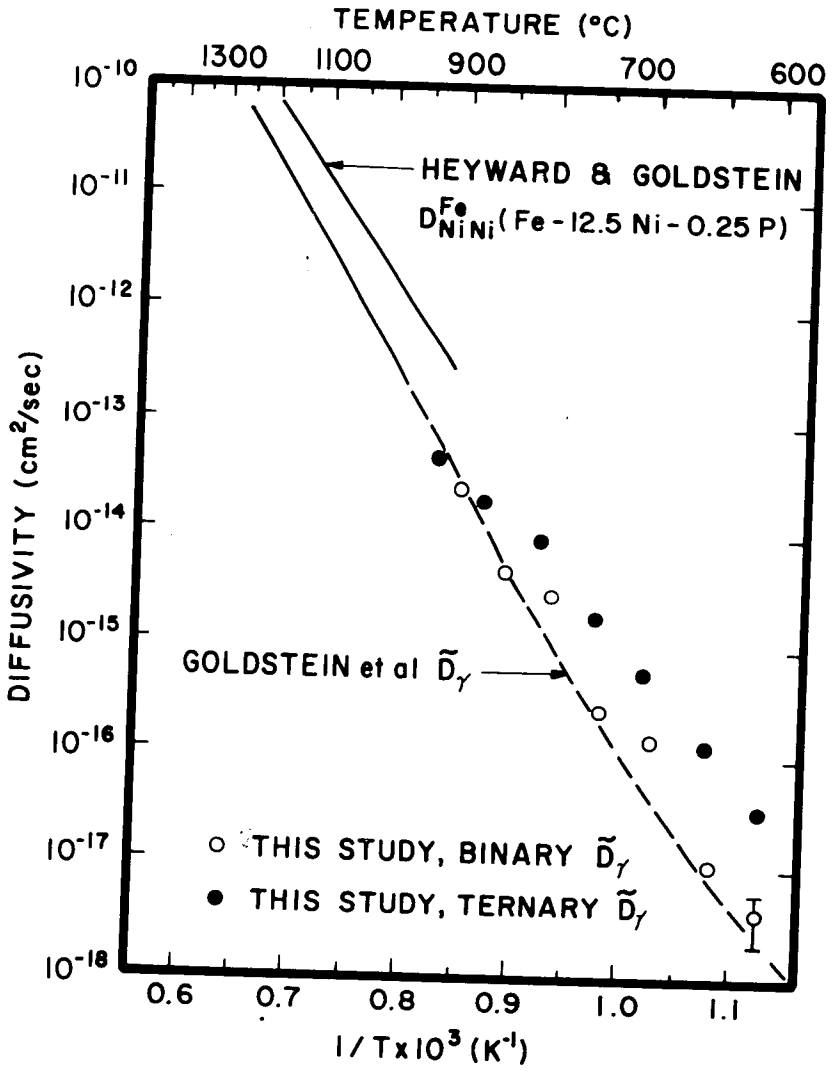

Fig. 28: Comparison between experimental binary and ternary interdiffusion coefficients in γ.

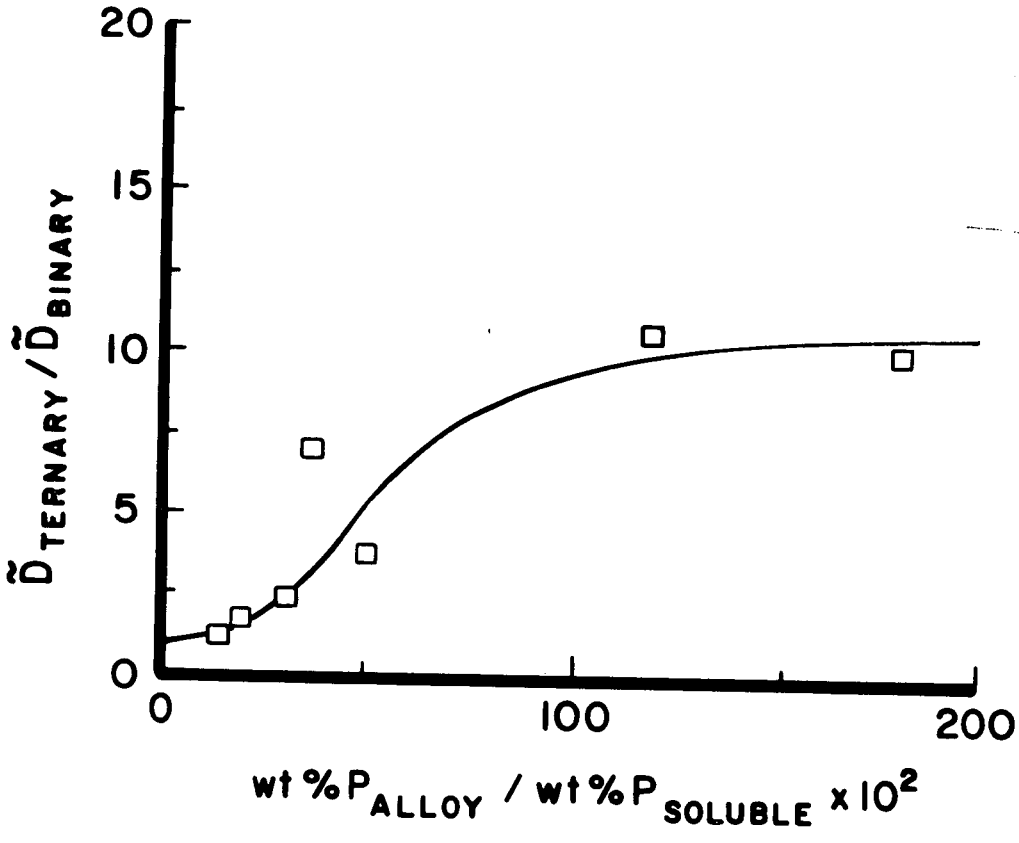

Fig. 29: Ratios of the experimental ternary interdiffusion coefficient to the binary coefficient in γ as a function of the ratio of the average wt% P in the ternary alloy to the wt% P soluble in the Fe-Ni matrix at a given temperature.

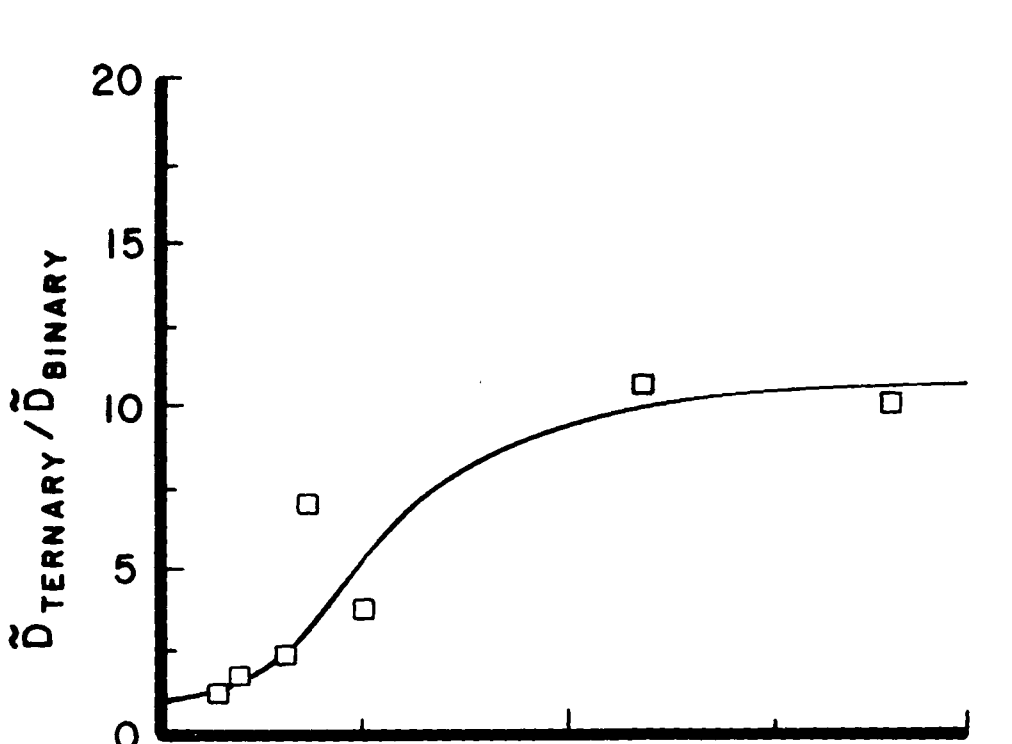

Fig. 29: Ratios of the experimental ternary interdiffusion coefficient to the binary coefficient in γ as a function of the ratio of the average wt% P in the ternary alloy to the wt% P soluble in the Fe-Ni matrix at a given temperature.

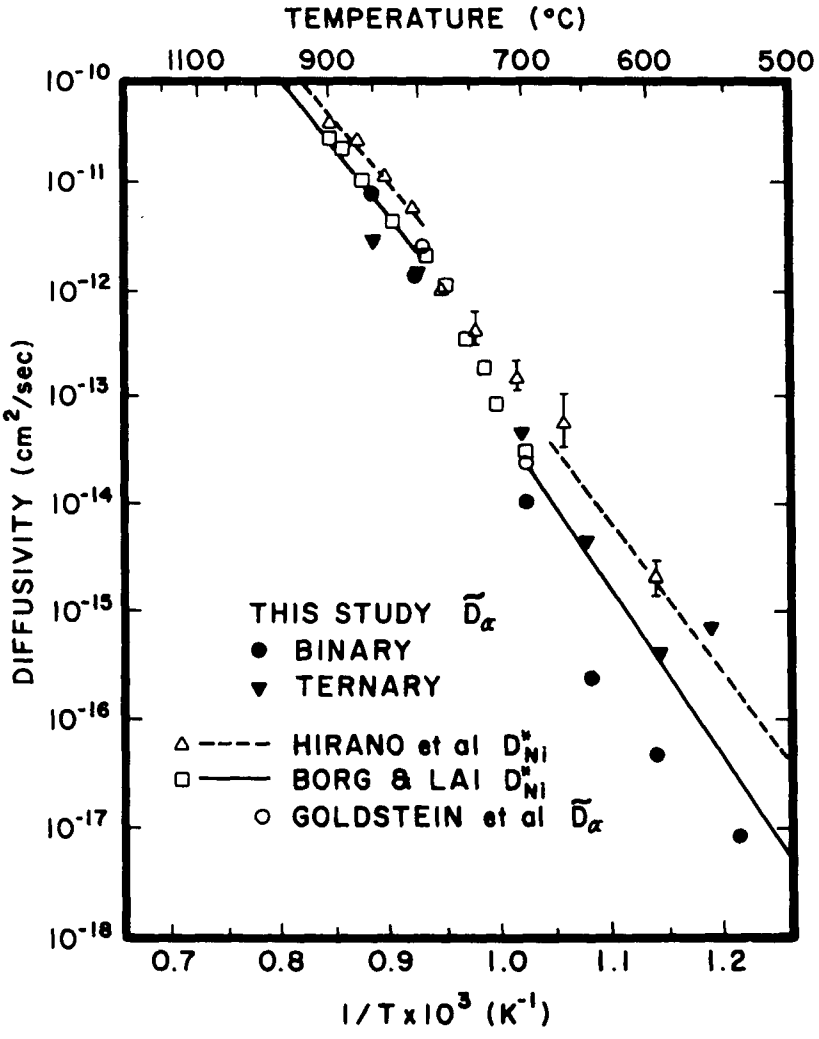

Fig. 30: Experimental results of binary and ternary α interdiffusion coefficient. Note the binary interdiffusion coefficient in ferromagnetic α is on the average an order of magnitude below the extrapolated value of Borg and Lai while the ternary coefficient follows Borg and Lai's values within experimental error.

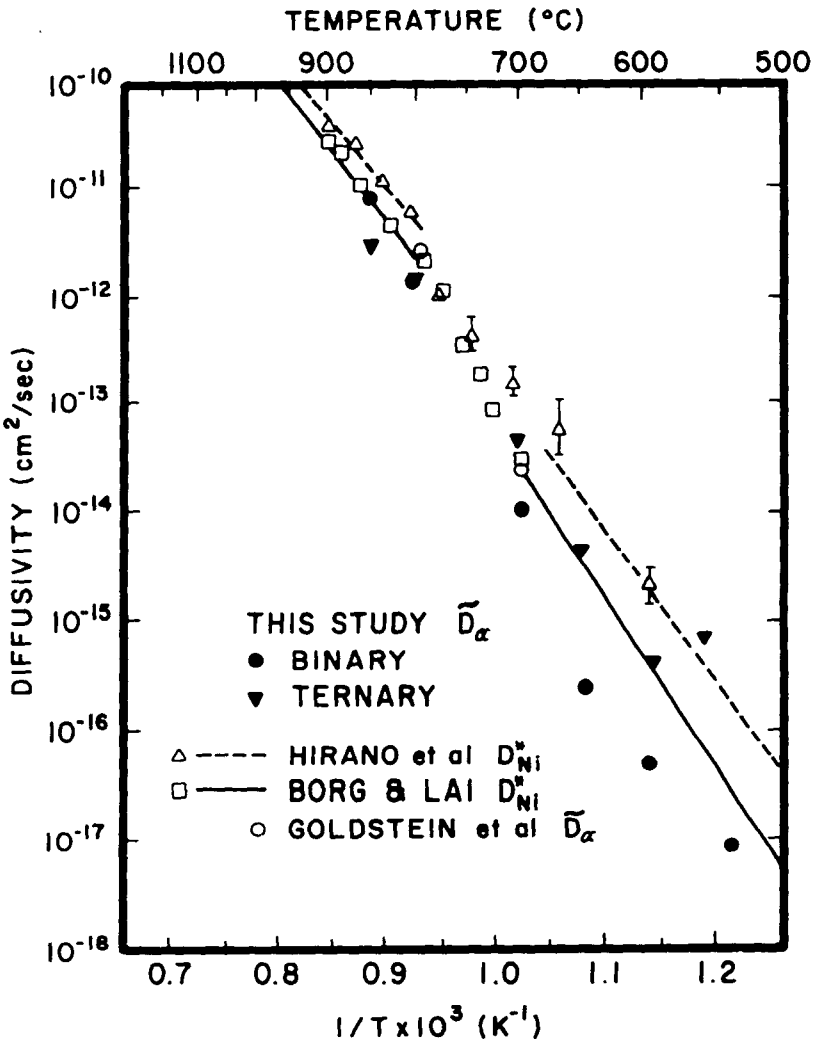

Fig. 30: Experimental results of binary and ternary α interdiffusion coefficient. Note the binary interdiffusion coefficient in ferromagnetic α is on the average an order of magnitude below the extrapolated value of Borg and Lai while the ternary coefficient follows Borg and Lai's values within experimental error.

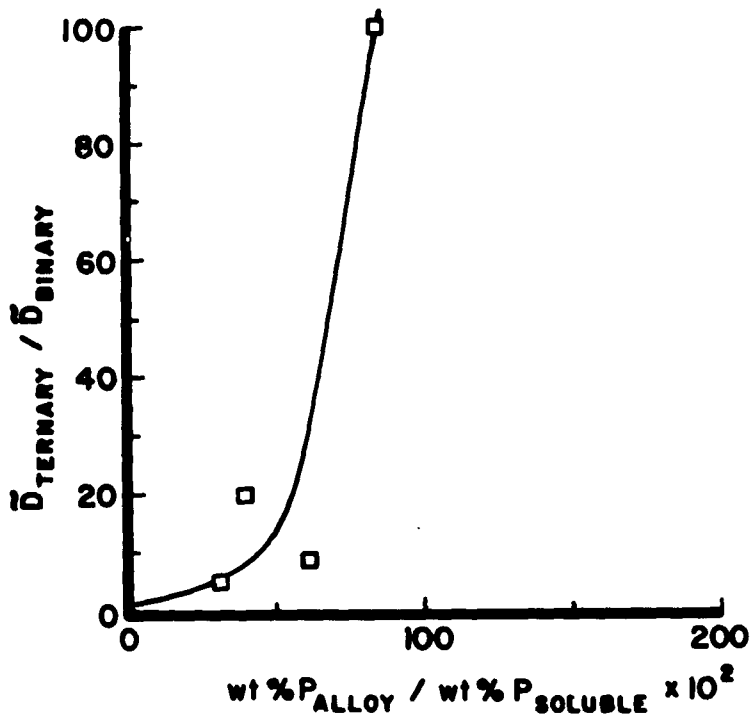

Fig. 31: Ratios of the experimental ternary interdiffusion coefficient to the binary coefficient in α as a function of the ratio of the average wt% P in the ternary alloy to the wt% P soluble in the Fe-Ni matrix at a given temperature.

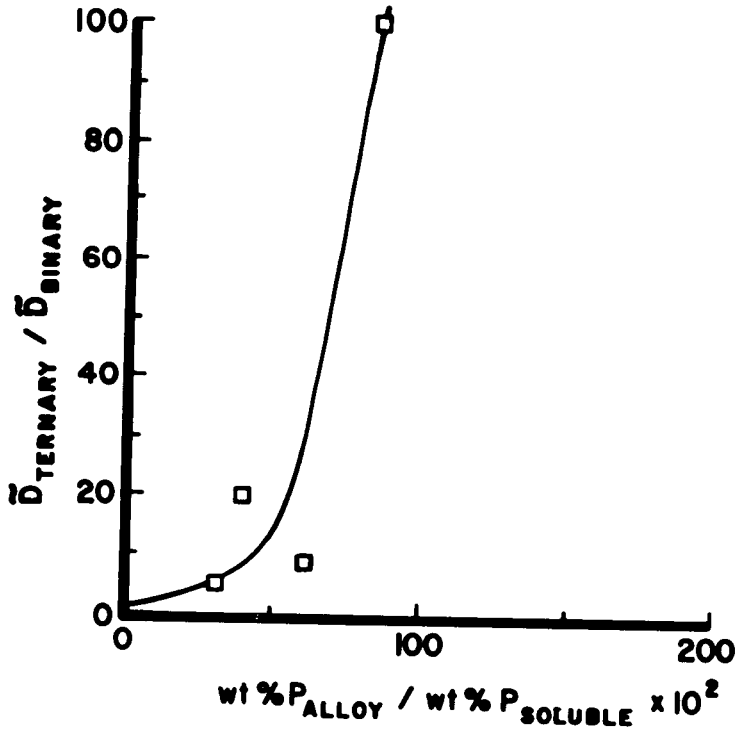

Fig. 31: Ratios of the experimental ternary interdiffusion coefficient to the binary coefficient in α as a function of the ratio of the average wt% P in the ternary alloy to the wt% P soluble in the Fe-Ni matrix at a given temperature.

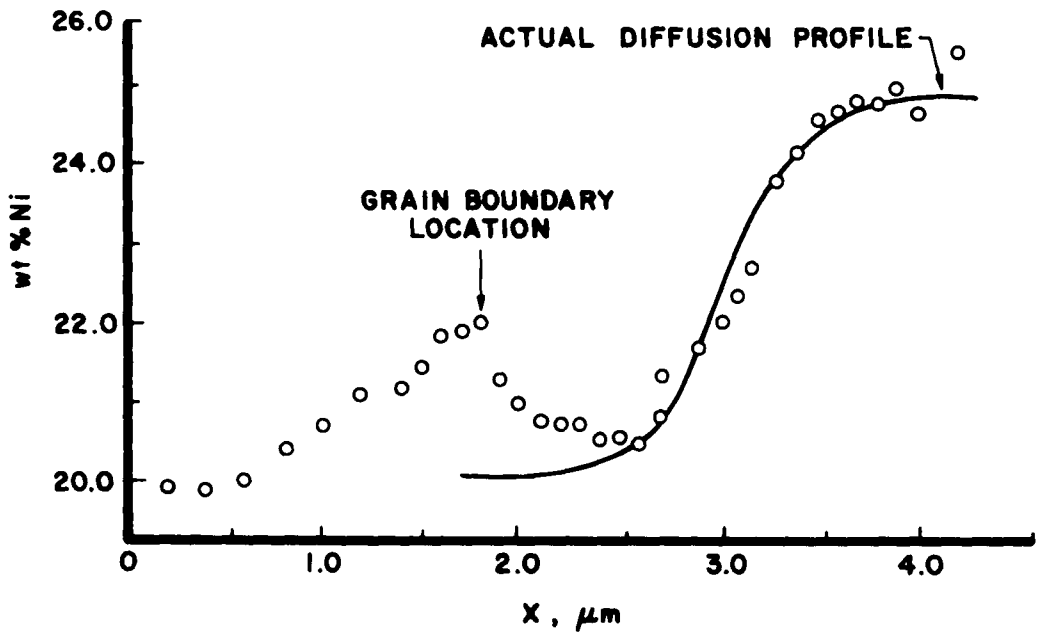

Fig. 32: Example of grain boundary diffusion compared to volume diffusion in 650°C ternary austenite sample diffused for 4 months.

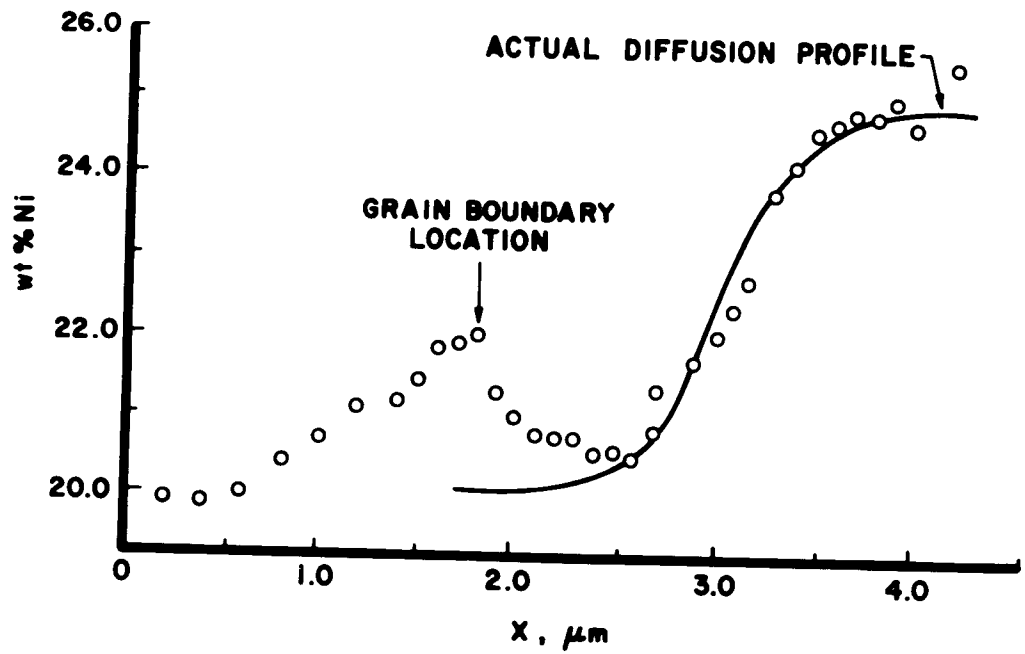

Fig. 32: Example of grain boundary diffusion compared to volume diffusion in 650°C ternary austenite sample diffused for 4 months.

REFERENCES

Badia, M. and Vignes, A. (1967), "Diffusion dans le Systeme Fe-Ni," C. R. Acad. Sci. Paris, vol. 264, p. 1528-1531.

Badia, M. and Vignes, A. (1969), "Diffusion du Fe, du Ni et du Co dans les metaux de transition du groupe de Fe," Acta Met., vol. 17 p. 177-187.

Bakker, H., Backus, J. and Waals, F. (1971), "A Curvature in the Arrhenius Plot for Diffusion of Fe in Single Crystals of Ni between 1200 and 1400°C," Phys. Stat. Sol.(b), vol. 45, p. 633-638.

Balakir, E. A., Zotov, Yu. P., Malysheva, E. B. and Panchishnyy, V. I. (1974), "Study of Mutual Diffusion in the Fe-Ni System," Aka. Nauk. SSR Izvestiia Metally, vol. 5, p. 198-200.

Borg, R. J. and Lai, D. Y. F. (1963), "Diffusion of Au, Ni, Co in α-Fe: Study of the Effect of Ferromagnetism upon Diffusion," Acta Met., vol. 11, p. 861-866.

Borovskiy, I. B., Marchukova, I. D., and Ugaste, Y. U. (1967), "Local X-ray Spectroanalysis of Mutual Diffusion in Binary Systems Forming a Continuous Series of Solid Solutions: II The Systems Fe-Ni, Ni-Co, Ni-Pt and Co-Pt," Fiz. Metal. Metalloved, vol. 24, p. 436-441.

Bruggeman, G. A. and Roberts, J. A. (1975), "Diffusion of Sb in α-Fe," Metall. Trans. A., vol. 6A, p. 755-760.

Buchwald, V. F. (1975), "Handbook of Iron Meteorites, Their History, Distribution, Composition and Structure," vol. 1, University of California Press.

Cliff, G. and Lorimer, G. W. (1975), "The Quantitative Analysis of Thin Specimens," J. Micros., vol. 103, p. 203-207.

Doan, A. S. and Goldstein, J. I. (1970), "Ternary Phase Diagram, Fe-Ni-P," Met. Trans. vol. 1, p. 1759-1767.

Doig, P. and Flewitt, P. E. J. (1982), "The Detection of Monolayer Grain Boundary Segregation in Steels using STEM-EDS X-ray Microanalysis," Metall. Trans. A., vol. 13A, p. 1397-1403.

Erhart, H. and Paju, M. (1983), "Phosphorus Segregation in Austenite," Scripta Met., vol. 17, p. 171-174.

Fisher, J. C. (1951), "Calculation of Diffusion in Grain Boundaries," J. of App. Phys., vol. 22, p. 74-77.

Frantsevich, I. N., Kalinovich, D. F., Kovenskii, I. I. and Smolin, M. D. (1969), "Electrotransport and Diffusion in Mo-W and Fe-Ni Alloys over Wide Ranges of Temperatures," J. Phys. Chem. Sol., vol. 30, p. 947-957.

Ganessan, V., Seetharaman, V. and Raghunathan, V. S. (1984), "Interdiffusion in the Fe-Ni System," Mat. Letters, vol. 2, No. 4A p. 257-262.

Garmong, G., Paton, N. E. and Argon, A. S. (1975), "Attainment of Full Interfacial Contact During Diffusion Bonding," Metall. Trans. A, vol. 6A, p. 1269-1279.

Glitz, R., Notis, M. and Goldstein, J. I. (1982), "AEM Study of Early Stage Growth of Ni_3Al," Met. Trans. A, vol. 13A, p. 1921-1926.

Goldstein, J. I. and Axon, H. J. (1973), "The Widmanstatten Figure in Fe Meteorites," Naturwissenschaften, vol. 60, Pub. Springer-Verlag, p. 313-321.

Goldstein, J. I., Costley, J. L., Lorimer, G. W. and Reed, S. J. B. (1977), "Quantitative X-ray Analysis in the Electron Microscope," Scanning Electron Microscopy/1977, vol. 1, Proceedings of Workshop on Analytical Electron Microscopy, ITT Research Institute, Chicago.

Goldstein, J. I., Hanneman, J. J. and Ogilvie, R. E. (1965), "Diffusion in Fe-Ni System at 1 atm and 40 kbar Pressure," Trans. AIME, vol. 233, p. 812-820.

Goldstein, J. I., Newbury, D. E., Echlin, P., Joy, D. C., Fiori, C. and Lifshin, E. (1981), Scanning Electron Microscopy and X-ray Microanalysis," Pub. Plenum Press, New York.

Goldstein, J. I. and Short, J. M. (1967), "Iron Meteorites, Thermal History and Parent Bodies," Geo. Chem. et Cosmochim. Acta, vol. 31, p. 1733-1770.

Guiraldenq, P, (1962), "Influence des impuretes et de la structure frittee sur les coefficients de diffusion en volume et aux joints des grains du Fe dans le Ni," C. R. Acad. Sci., Paris, p. 1994-1996.

Gruzin, P. L. and Mural, V. V. (1963), "Radiometric Study of P Diffusion in Fe," Fiz. Metal. Metalloved., vol. 16, p. 551-556.

Gruzin, P. L. and Mural, V. V. (1964), "Effect of Alloying Upon Diffusion of P in Fe," Fiz. Metal. Metalloved, vol. 17, p. 384-389.

Hanatate, Y., Majima, K and Mitani, H. (1978), "Grain Boundary Diffusion of Ni in γ Fe," Trans. J.I.M., vol. 19, p. 669-673.

Hancock, G. F. and Leak, G. M. (1967), "Diffusion of Ni in Binary Fe-Ni Alloys of Fe with Ni, Mg and Cr," Met. Sc. J., vol. 1, p. 33-36.

Helfmeier, H. U. (1974), "Influence of Solute Atoms on Diffusion of Cu and Ni," Z. Metallkde., vol. 3, p. 238-241.

Henry, G. and Cizeron, G. (1978), "Diffusion du nickel dans des alliages Fe-Ni de structure C.F.C.--comparaison avec la diffusion dans des systemes de meme symetrie," Ann. Chim. Fran., vol. 3, p. 167-176.

Heumann, T. and Kottman, A. (1953), "Uber den Ablauf der Diffusions-vorgange in Substitutionsmischkristallen," Z. Metallkde., vol. 44, p. 139-154.

Heyward, T. R. (1973), M.S. Thesis, Lehigh University.

Heyward, T. R. and Goldstein, J. I. (1973), "Ternary Diffusion in the Alpha and Gamma Phases of the Fe-Ni-P Systems," Metall. Trans., vol. 4, p. 2335-2342.

Hirano, K, Cohen, M. and Averbach, B. L. (1961), "Diffusion of Ni into Fe," Acta Met., vol. 9, p. 440-445.

Hoshino, K., Iijima, Y. and Hirano, K. (1982), "Solute Enhancement of Self Diffusion of Cu in Cu-Sn, Cu-In and Cu-Sb Dilute Alloys," Acta Met., vol. 30, p. 265-271.

Joy, D. C. and Maher, D. M. (1977), Scanning Electron Microscopy/1977, ed. O. Johari, IIT Research Institute, Chicago, IL.

Krishtal, M. A., Mokrov, A. P. and Stepanova, O. V. (1967), "Boundary and Volume Diffusion of Ni in Fe," Fiz. Metal. Metalloved, vol. 24, no. 4, p. 688-692.

Lange, W., Hassner, A. and Mischer, G. (1964), "Messung der Korngrenzendiffusion von Ni-63 in Ni und γ-Fe," Phys. Stat. Sol., 5, p. 63-71.

Levasseur, J. and Philibert, J. (1967), "Determination des coefficients de diffusion intrinseques par mesure de l'effet Kirkendall dans le systeme Fe-Ni," C. R. Acad. Sci Paris, Series C, vol. 264, p. 380-383.

Lorimer, G. W., Cliff, G. and Clark, J. N. (1976), "Developments in Electron Microscopy and Analysis," ed. J. A. Venables, Pub. The Academic Press, London.

MacEwan, J. R., MacEwan, J. U. and Yaffe, L. (1959), "Diffusion of N^* in Fe, Co, Ni and Two Fe-Ni Alloys," Can. J. Chem., vol. 37, p. 1629-1636.

Marchukova, I. D. (1966), "Interdiffusion in Some Binary Systems Forming Continuous Series of Solid Solutions," Aka. Nauk. Ukrain. SSR Publishers, V. N. Svechnikov ed., "Diffusion Processes in Metals.

Matsuyama, T., Hosokawa, H. and Suto, H. (1983), "Tracer Diffusion of P in Fe and Fe Alloys," Trans. JIM, vol. 24, p. 589-594.

Metals Handbook (1973), "Metallography, Structures and Phase Diagrams," vol. 8, American Society for Metals, Cleveland, OH.

Michael, J. R. (1984), Ph.D. Dissertation, Lehigh University.

Million, B., Ruzickova, J., Velisek, J. and Vestral, J. (1981), "Diffusion Processes in Fe-Ni System," Matl. Sci. & Eng., vol. 50, p. 43-52.

Moren, A. E. and Goldstein, J. I. (1978), "Cooling Rate Variations in Fe Meteorites," Earth & Planet. Sci. Letters, vol. 40, p. 151-161.

Moren, A. E. and Goldstein, J. I. (1979), "Cooling Rates Determined from Fe-Ni-P Model," Earth & Planet. Sci. Letters, vol. 43, p. 182-196.

Nakagawa, Y., Tanji, Y., Morita, H., Hiroyoshi, H. and Fujimori, H. (1979), "Virtual Miscibility Gap and Interdiffusion Coefficient in Fe-Ni Invar Alloys," J. of Magn. & Magn. Matls., vol. 10, p. 145-151.

Narayan, C. (1983), Ph.D. Dissertation, Lehigh University.

Narayan, C. and Goldstein, J. I. (1983), "Low Temperature Diffusivity Measurements in Fe-Ni System using STEM Techniques," Metall. Trans., 14A, p. 2437-2439.

Nockolds, C., Nasir, M. J., Cliff, G. and Lorimer, G. W. (1979), Electron Microscopy and Analysis, 1979, p. 417, T. Mulvey, ed., Pub. The Institute of Physics, Bristol and London.

Reed, S. J. B. (1982), "The single-scattering model and spatial resolution in x-ray analysis of thin foils," Ultramicroscopy, vol. 7, p. 405-410.

Reed-Hill, R. E. (1973), Physical Metallurgy Principles, D. Van Nostrand Co., New York, p. 480.

Reuter, K. J., Williams, D. B. and Goldstein, J. I. (1984), "Micro-analysis and Microdiffraction of Two Phase Regions in the Metallic Phase of the Estherville Meteorite," to be published in the 4th AEM Workshop, D. B. Williams, and D. C. Joy eds., San Francisco Press.

Romig, A. D. (1979), Ph.D. Dissertation, Lehigh University.

Romig, A. D. and Goldstein, J. I. (1980), "Determination of Fe-Ni and Fe-Ni-P Phase Diagram," Metall. Trans. A., vol. 11A, p.1151-1159.

Romig, A. D. and Goldstein, J. I. (1981), "The Diffusivity of Ni in Fe-Ni and Fe-Ni-P Martensites," Metall. Trans., vol. 12A, p. 243-251.

Shewmon, P. G. (1963), Diffusion in Solids, McGraw-Hill Book Co.

Tavadze, F. N., Bernshtein, M. L., Jugeli, K. J. and Surmava, B. M. (1973), "Deformation on Diffusion in Fe-Ni," Bull. Aca. Sc. Geogian. SSR, vol. 69, No. 2, p. 389-392.

Ustad, T. and Sorum, H. (1973), "Interdiffusion in Fe-Ni, Ni-Co and Fe-Co System," Phys. Stat. Sol.(a), vol. 20, p. 285-294.

Vignes, A. and Sabatier, J. P. (1969), "Ternary Diffusion in Fe-Co-Ni Alloys," Trans. AIME, vol. 245, p. 1969-1795.

Walsoe de Reca, E. and Pampillo, C. (1967), "Self Diffusion of Ni in Ni-Fe Alloys," Acta. Met., vol. 15, p. 1263-1268.

Wanin, M. and Kohn, A. (1968), "Determination par des techniques de traceur des coefficients de diffusion du Fe et du Ni dans des alliages Fe-Ni et du Fe et du Co dans des alliages Fe-Co," C. R. Acad. Sci. Paris, vol. 267c, p. 1558-1561.

Wasson, J. T. and Willis, J. (1978), "Cooling Rates of Group IVA Iron Meteorites," Earth and Plan. Sci. Letters, vol. 40, p. 1978.

Wells, C. and Mehl, R. F. (1941), "Rate of Diffusion of Ni in γ-Fe in Low-C and High-C Ni Steels," Trans. AIME, vol. 143, p. 329-339.

Williams, D. B. (1984), "Practical Analytical Electron Microscopy in Materials Science," Philips Electronic Optics Publishing Group, Mahwah, NJ.

Wood, J., Williams, D. B. and Goldstein, J. I. (1981), "Determination of Cliff-Lorimer k Factor for Philips EM400T," Quantitative Microanalysis with High Spatial Resolution, G. W. Lorimer, M. H. Jacobs and P. Doig eds., The Metals Society London, p. 24-29.

Wood, J., Williams, D. B. and Goldstein, J. I. (1984), "k_{AFe} Factor Determination," J. Micros., vol. 255, p. 255-275.

Zaluzec, N. (1977), "Quantitative X-ray Microanalysis Instrumental Considerations and Applications to Materials Science," Introduction to Analytical Electron Microscopy, J. J. Hren, J. I. Goldstein and D. C. Joy, eds., Plenum, New York.

Zemskiy, S. V., L'vov, V. S. and Makashova, L. S. (1976), "Self Diffusion of Ni in Fe-Ni Alloys," Fiz. Metal. Metalloved, vol. 41, No. 4, p. 775-781.

APPENDIX #1

References for Fe-Ni and Fe-Ni-P Diffusion in Austenite

(Note the exact references are given under REFERENCE section)

1. M. Badia and A. Vignes (1967).
2. M. Badia and A. Vignes (1969).
3. H. Bakker, J. Backus and F. Waals (1971).
4. E. Balakir, Yu. Zotov, E. Malysheva and V. Panchishnyy (1974).
5. I. Borovskiy, I. Marchukova and Y. Ugaste (1967).
6. I. Frantsevich, D. Kalinovich, I. Kovenskii and M. Smolin (1969).
7. V. Ganessan, V. Seetharaman and V. Raghunathan (1984).
8. J. Goldstein, R. Hanneman and R. Ogilvie (1965).
9. P. Guiraldenq (1962).
10. G. Hancock and G. Leak (1967).
11. Y. Hanatate, K. Majima and H. Matani (1978).
12. G. Henry and G. Cizeron (1978).
13. T. Heumann and A. Kottman (1953).
14. T. Heyward and J. Goldstein (1973).
15. K. Hirano, M. Cohen and B. Averbach (1961).
16. M. Krishtal, A. Mokrov and O. Stepanova (1967).
17. W. Lange, A. Hassner and G. Mischer (1964).
18. J. Levasseur and J. Philibert (19667).
19. J. MacEwan, J. MacEwan and L. Yaffe (1959).
20. I. Marchukova (1966).
21. B. Million, J. Ruzickova, J. Velisek and J. Vestral (1981).

22. Y. Nakagawa, Y. Tanji, H. Morita, H. Hiroyoshi and H. Fujimori (1979).

23. C. Narayan and J. Goldstein (1983).

24. A. Romig and J. Goldstein (1981).

25. F. Tavadze, M. Bernshtein, K. Jugeli, B. M. Surmava (1973).

26. T. Ustad and H. Sorum (1973).

27. E. Walsoe de Reca and C. Pampillo (1967).

28. M. Wanin and A. Kohn (1968).

29. C. Wells and R. Mehl (1941).

30. S. Zemskiy, V. L'Vov and L. Makashova (1976).

VITA

Douglas Clarke Dean III was born to Joan and Doug Dean in Bridgeport, Connecticut on August 14, 1959. He received his high school diploma from St. Aspais de Fontainebleau, France in June 1978. He received a Bachelor of Science in Metallurgy and Material Science from Lehigh University in June 1982.